

TALLINN UNIVERSITY OF TECHNOLOGY
DOCTORAL THESIS
39/2019

**Electrospinning of Nanofibrous
Composites with Cellulose Acetate, Ionic
Liquids and Graphene Oxide**

KASHIF JAVED



TALLINN UNIVERSITY OF TECHNOLOGY

School of Engineering

Department of Materials and Environmental Technology

This dissertation was accepted for the defence of the degree 29/05/2019

Supervisor:

Professor Andres Krumme
School of Engineering
Tallinn University of Technology
Tallinn, Estonia

Opponents:

Professor Eero Kontturi
Department of Bioproducts and Biosystems
Aalto University
Helsinki, Finland

Dr. Martin Järvekülg
Institute of Physics
Tartu University
Tartu, Estonia

Defence of the thesis: 27/06/2019, Tallinn

Declaration:

Hereby I declare that this doctoral thesis, my original investigation and achievement, submitted for the doctoral degree at Tallinn University of Technology has not been submitted for doctoral or equivalent academic degree.

Kashif Javed

signature



European Union
European Regional
Development Fund



Investing
in your future



Copyright: Kashif Javed, 2019

ISSN 2585-6898 (publication)

ISBN 978-9949-83-458-7 (publication)

ISSN 2585-6901 (PDF)

ISBN 978-9949-83-459-4 (PDF)

TALLINNA TEHNIKAÜLIKOOL
DOKTORITÖÖ
39/2019

**Tselluloosatsetaadi, ionsete vedelike
ja grafeenoksiidi nanokiuliste
komposiitide elektroketrus**

KASHIF JAVED



Contents

List of Publications	6
Author's Contribution to the Publications	7
Introduction	8
Abbreviations	10
1 Literature review	11
1.1 Introduction	11
1.2 Introduction of electrospinning	11
1.3 Properties of cellulose acetate.....	12
1.4 Ionic liquid a solvent for cellulose dissolution	12
2 Graphite, graphene oxide and graphene	14
2.1 Graphene as nanofiller for electrospinning	15
2.1.1 Electrospinning of conductive nanofibers by graphene.....	16
2.1.2 Electrospinning of cellulose acetate and GO	19
2.2 The aim of the study	21
3 Experimental	22
3.1 Materials	22
3.2 Methods.....	22
3.2.1 Preparation of CA, CA-[BMIM]Cl and [BMIM]Cl-GO blends.....	22
3.2.2 Preparation of CA-[BMIM]Cl and CA-[BMIM]Cl-rGO nanofibers	23
3.2.3 Characterizations of the nanofibers.....	24
4 Results and discussion.....	25
4.1 Influence of [BMIM]Cl on the CA electrospun nanofibers	25
4.1.1 Influence of [BMIM]Cl on the CA solution's viscosity and conductivity.....	25
4.1.2 Influence of [BMIM]Cl on the morphology of CA nanofibers	25
4.2 Influence of GO on the electrospun nanofibers.....	28
4.2.1 Influence of GO on the morphology and conductivity of the hybrid nanofibers...	28
4.3 Structure of GO in the nanofibers before and after reduction	29
4.3.1 Chemical bonds and interactions within the nanofibers	32
4.4 Thermal analysis of the hybrid nanofibers.....	35
Conclusions	37
References	38
Acknowledgements.....	46
Abstract.....	47
Lühikokkuvõte.....	48
Appendix A	49
Appendix B	91
Curriculum vitae.....	95
Elulookirjeldus.....	96

List of Publications

The list of author's publications, the thesis has been prepared on the basis of these publications:

- I **Javed, K.;** Krumme, A.; Viirsalu, M.; Krasnou, I.; Plamus, T.; Vassiljeva, V.; Tarasova, E.; Savest, N.; Mere, A.; Mikli, V.; Danilson, M.; Kaljuvee, T.; Lange, S.; Yuan, Q.; Topham, P. D.; Chen, C.-M. (2018). A method for producing conductive graphene biopolymer nanofibrous fabrics by exploitation of an ionic liquid dispersant in electrospinning. *Carbon*, 140, 148–156.
- II **Javed, K.;** Krumme, A.; Krasnou, I.; Mikli, V.; Viirsalu, M.; Plamus, T.; Vassiljeva, V.; Tarasova, E.; Savest, N.; Mendez, J. D. (2018). Impact of 1-butyl-3-methylimidazolium chloride on the electrospinning of cellulose acetate nanofibers. *Journal of Macromolecular Science, Part A*, 55 (2), 142–147. *Journal of Macromolecular Science, Part A*, 55, 142–147.
- III **Javed, K.;** Oolo, M.; Savest, N.; Krumme, A. (2018). A Review on Graphene-Based Electrospun Conductive Nanofibers, Supercapacitors, Anodes, and Cathodes for Lithium-Ion Batteries. *Critical Reviews in Solid State and Materials Sciences*, 1-17.

Author's Contribution to the Publications

Contribution to the papers in this thesis are:

- I The author participated in the preparation of CA/IL/GO solution, performed electrospinning, and developed the method to reduce CA/IL/GO nanofibers by hydrazine vapors. The author characterized the hybrid nanofibers, data analysis, and wrote the paper.
- II The author participated in solution preparation, electrospinning, characterisation of CA-[BMIM]Cl nanofibers, data analysis, and writing of the paper.
- III The author researched the literature on graphene based electrospun nanofibers and wrote the introduction and main sections of the article. The author compared the data with previous research and summarised it into tables.

Introduction

Synthetic polymers accumulating in the natural environment have been a threat to the earth. Efforts have been made to explore new biomaterials that can replace synthetic polymers, which could contribute to waste reduction and participate in energy efficiency and supply conservation. Advanced technologies focused around bio-based materials now have good reputations as they are less dependent on natural gas, coal, or oil. Biopolymers are the by-products of naturally-occurring materials such as wood, mushrooms, and crustacean's shells (Mohanty, Misra, & Drzal, 2002; Schiffman & Schauer, 2008). Bio-composites, referred to as "green composites," consist of biopolymers from renewable resources (Kaplan, 1998). Therefore, biopolymers are the ideal polymers to be used in wide range of industries such as textiles, medicine, pulp and paper, agriculture, coatings, and automobiles (Rezaei, Nasirpour, & Fathi, 2015). In general, nanofibers can be produced by bicomponent spinning, force spinning, melt blowing, or flash-spinning. Among these methods, electrospinning is an efficient fiber fabrication method used for the fabrication of micro and nanofibers (Bhardwaj & Kundu, 2010; Leach, Feng, Tuck, & Corey, 2011; Subbiah, Bhat, Tock, Parameswaran, & Ramkumar, 2005). Currently, conductive nanofibrous materials using electrospinning have been developed from a wide range of synthetic polymers as a matrix of polyaniline (PANI) and poly(vinyl pyrrolidone) (PVP), with graphene as a conductive additive (Z-M. Huang, Zhang, Kotaki, & Ramakrishna, 2003; Wahab et al., 2016). Electrospinning of biopolymers with carbon nanotubes or metal-based nano-powders could have specific applications including smart fabrics, nanosensors, and flexible electrode materials. Among these nanomaterials, graphene has received more interest from fiber scientists due to its multifunctional properties such as high specific surface area, electrical and thermal conductivity, and superior mechanical strength (Hu, Kulkarni, Choi, & Tsukruk, 2014). However, conductive nanofibers using biopolymers have been limited due to due to the disperability of graphene oxide (GO) and their inferior property profiles, compared to commercial thermoplastic polymers. The most widely used methods require complex processes, expensive materials, and pre-functionalizations. These methods have disadvantages such as a lack of uniformity and flexibility, which increase the cost of production. Electrospinning of biopolymers by incorporating graphene as a nanofiller (to obtain conductive nanofibers) is challenging because of the distinct processing conditions of biopolymers and graphene. There are three challenges to this approach: 1) disrupting the extensive hydrogen bonding in the biopolymer (cellulose is a linear polysaccharide consisting of repeated D-glucose units which forms strong inter- and intramolecular hydrogen bonds); 2) breaking the aggregation of the graphene source in nano-particles to prepare a uniform mixture for electrospinning; and 3) establishing appropriate interactions in the hybrid material to facilitate electron movement. Cellulose acetate, a derivative of cellulose (Brown, 1996; Feldman, 2015) has attracted considerable interest due to its biocompatibility, biodegradability, non-toxicity, and low cost. It has been widely used in various nanocomposite materials (Seifert, Hesse, Kabrelian, & Klemm, 2004; Suwantong & Supaphol, 2015). This thesis focuses on the electrospinning of cellulose acetate (CA), with graphene oxide as a nanofiller. The work also introduces the use of [BMIM]Cl ionic liquid to enhance the better dispersion of the nanofiller and serve as bridging components between the polymer and nanofiller.

Finally, this study also focuses on the reduction of graphene oxide to graphene using a chemical reduction method with hydrazine (N_2H_4), to restore the conductive networks of graphene, which are conductive nanofibers.

Abbreviations

GO	Graphene oxide
CA	Cellulose acetate
ILs	Ionic liquids
[BMIM]Cl	1-butyl-3-methylimidazolium chloride
[EMIM]Ac	1-methyl-3-methylimidazolium acetate
DMAc	Dimethylacetamide
rGO	Reduced graphene oxide
IL	Ionic liquid
GONRs	Graphene nano ribbons
GNSs	Graphene nanosheets
CNTs	Carbon nanotubes
MWNTs	Multiwalled carbon nanotubes
PAN	Polyacrylonitrile
DMF	Dimethylformamide
PVP	Polyvinyl pyrrolidone
PMMA	Polymethyl methacrylate
PVC	Polyvinyl chloride
PLGA	Poly lactic-co-glycolic acid
CNF	Carbon nanofibers
ACNF	Activated carbon nanofiber
GCNF	Graphene carbon nanofibers
ACF	Anisotropic conductive films
PANi	Polyaniline
AgNps	Silver nanoparticles
HCSA	Camphor-10-sulfonic acid
PEO	Poly(ethylene oxide)
G-PBASE	Graphene-1-Pyrenebutanoic acid-succinimidyl ester
PVA/ODA-MMT	Polyvinyl alcohol/Octadecylamine-modified montmorillonites
GO-g-[P(HEMA-g-PCL)]	Graphene-Poly(2-Hydroxyethyl methacrylate)-graft Poly(ϵ -caprolactone)
PI-GNR	Polyimide with graphene nanoribbon
GBEENS	Graphene based electroconductive electrospun nanofibers
PEO	Polyethylene oxide
XPS	X-ray photoelectron spectroscopy
XRD	X-ray diffraction
SEM	Scanning electron microscopy
FTIR	Fourier-transform infrared spectroscopy
TGA	Thermogravimetric analysis
wt%	Weight percent
S/cm	Siemens per cm
mS/cm	Millisiemens per cm

1 Literature review

1.1 Introduction

This research focuses on graphene oxide as a nanofiller for the electrospinning of a biopolymer, to create conductive nanofibers. This chapter presents the literature review of the following topics: electrospinning technique, properties of cellulose acetate (CA), graphene oxide (GO), and ionic liquids (IL) such as 1-butyl-3-methylimidazolium chloride ([BMIM][Cl]). The IL is used to disperse GO into the biopolymer and enhance the nanofibers' conductivity.

1.2 Introduction of electrospinning

Nanofibers can be produced by a number of methods such as drawings of different polymers, template synthesis of nanostructured polymer, phase separation, and self-assembly (Deka, 2010; Ramakrishna, 2005). However, a unique and versatile technique that produces micro and nanofibers through an electric field, called “electrospinning”, has become a ubiquitous method in the field of nanotechnology (Almecija, Blond, Sader, Coleman, & Boland, 2009; Jeong et al., 2007; Nain, Wong, Amon, & Sitti, 2006). The term electrospinning comes from electro static spinning, which was used more than 60 years ago. The first description of this method was patented in 1902 by J.F.Cooley, entitled as an “apparatus for electrically dispersing fluids.” In this patent (US 692631), Cooley designed an apparatus for producing the fibers from the composite fluids through an electrical discharge field (Cooley, 1902). In brief, electrospinning is a process whereby a charged jet of polymer solution is spun on a ground collector to produce nanofibers, as shown in Figure 1. This is an easy and robust way to produce nanofibers from huge quantities of different polymers including synthetic polymers, biopolymers, and blends of these polymers (Bhardwaj & Kundu, 2010; Ramakrishna, 2005; Schiffman & Schauer, 2008; Torres-Giner, Pérez-Masiá, & Lagaron, 2016). The rising popularity of this method has resulted in over 200 research institutes and universities studying the electrospinning process and producing different kinds of nanofibers (Bhardwaj & Kundu, 2010), in order to explore the potential in this technique.

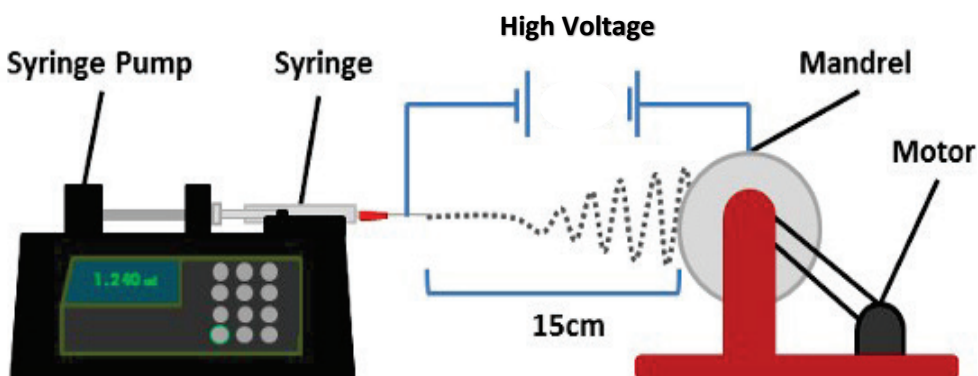


Figure 1. Scheme of typical electrospinning setup (Bridge et al., 2015).

The main components of the electrospinning process are (i) a syringe, (ii) a high voltage power supply and (iii) a counter electrode (rotatory collector).

1.3 Properties of cellulose acetate

Cellulose acetate was prepared by Paul Schutzenberger for first time in 1865. It is a renewable natural resource and a derivative of cellulose (an acetate ester of cellulose). Cellulose acetate attracted considerable interest from researchers because of its biocompatibility, biodegradability, nontoxicity, and low cost (Seifert et al., 2004). Cellulose acetate partially or completely acetylated (COCH₃) hydroxyl groups with molecular weights ranging from 30,000 to 60,000, as well as varying acetyl levels (29-44.8%) and chain lengths. Due to the polar hydroxyl groups, it has a tendency to form hydrogen bonds with other hydroxyl groups on adjacent chains. The chemical structure of CA is presented in Figure 2.

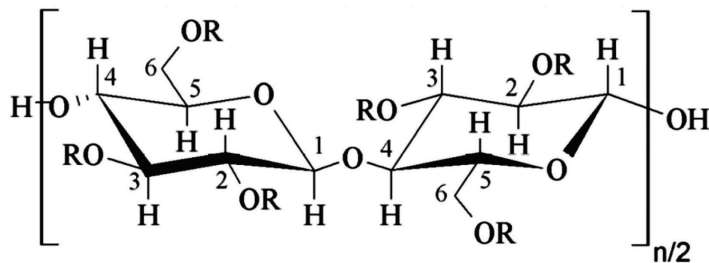


Figure 2. Chemical structure of cellulose esters where H, 1 represents R groups (Van de Ven, 2013).

Cellulose acetate granules are a high-performance thermoplastic with a unique combination of properties. This makes CA the material of choice for many applications. It is soluble in acetone, esters, acids, and strong mineral bases, and chemically degrades with oxidizing salts. To create CA nanofibers, electrospun CA must be successfully established in a solvent mixture of 2:1 acetone (AC) and dimethylacetamide (DMAc) (Puls, Wilson, Hölter, & Environment, 2011; Tungprapa et al., 2007). CA electrospun nanofibers been attracted significant attention in science and technology due to their high surface ratio (area-to-mass). CA electrospun nanofibers have high porosity with outstanding pore interconnectivity, and flexibility with reasonable strength, and can thus be excellent nanocomposites for advanced applications (Lee, Nishino, Sohn, Lee, & Kim, 2018).

1.4 Ionic liquid a solvent for cellulose dissolution

The phrase 'ionic liquid' was to refer to ambient temperature liquid salts. The most useful and realistic definition of an IL is "a liquid comprised entirely of ions". Ionic liquids are the organic salts which exist in the liquid state below 100°C, preferably at room temperature. They offer chemical and thermal stability, non-flammability, and immeasurably low vapor pressure (Marsh, Boxall, & Lichtenthaler, 2004; Swatloski, Spear, Holbrey, & Rogers, 2002). Choosing an appropriate dispersing agent is therefore the key to formulating spinnable mixtures to fabricate hybrid biopolymer nanofibers. Ionic liquids are an interesting class of reagents that can be used as dispersing agents because of their novel dissolution ability. They have the potential to play more functional roles such as stabilizers, compatibilizers, modifiers, and additives in the fabrication of polymer composites that contain carbon nanotubes or graphene sheets (R. Peng, Wang, Tang, Yang, & Xie, 2013).

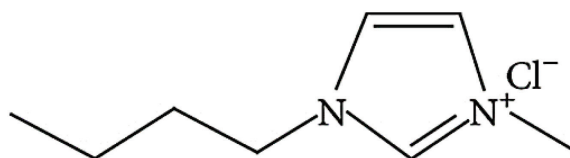


Figure 3. Molecular representation of [BMIM]Cl (Puerto, Cuesta, Sanchez-Cortes, Garcia-Ramos, & Domingo, 2013).

1-butyl-3-methylimidazolium chloride is a hydrophilic IL which is most widely used for dissolving cellulose and its derivatives. It can dissolve cellulose at high concentrations (10%–25%) (Arends, Gamez, & Sheldon, 2006). A molecular representation of [BMIM]Cl is presented in Figure 3.

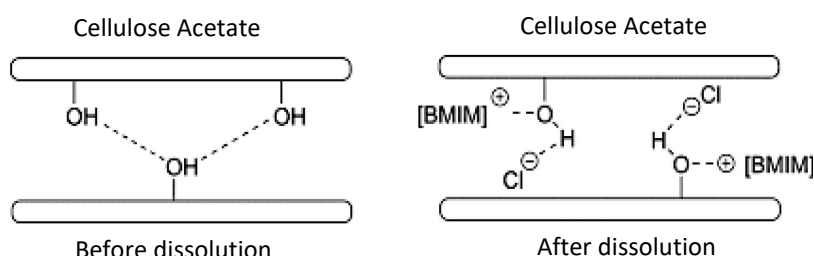


Figure 4. A proposed chemical interaction of [BMIM]Cl reproduced from the ref. (Arends et al., 2006).

Imidazolium chloride-based ILs demonstrate an outstanding dissolving capacity for many biopolymers such as cellulose, CA, chitin, wool, and chitosan. The ILs' high chloride concentration breaks the extensive hydrogen-bonding network of these biopolymers, in order to enable successful electrospinning. A study has proven that with the coordination of the cation and anion of [BMIM]Cl, OH groups on the glucose and the structure units of cellulose form a H-bond (Kaszyńska, Rachocki, Bielejewski, & Tritt-Goc, 2017). A proposed chemical interaction of [BMIM]Cl with CA is illustrated in Figure 4. In such ILs, graphene oxide sheets can be effectively exfoliated, stabilized, and reduced by chemical and thermal treatment methods. Peng et.al successfully fabricated graphene-cellulose nanocomposite films with casting methods, by exploiting imidazolium chloride-based ILs (H. Peng, Meng, Niu, & Lu, 2012). These cast films demonstrated conductivities up to 3.2×10^{-2} S/cm, thus demonstrating the viability of an approach for ionic liquid-biopolymer conductive nanocomposites with graphene. Furthermore, using IL 1-butyl-3-methylimidazolium chloride ([BMIM]Cl, 20%) in the production of electrospun hybrid carbon nanotube nanofibers with styrene-acrylonitrile resin demonstrated a significant increase in the conductivity of samples containing 3 wt% carbon nanotubes, from 1.08×10^{-6} S/cm to 5.9×10^{-6} S/cm (Gudkova et al., 2015). However, the fabrication of electrospun graphene-biopolymer conductive nanofibers remains a significant challenge.

2 Graphite, graphene oxide and graphene

The graphene family includes graphite, graphene oxide and reduced graphene oxide (rGO). Graphite is one of the three naturally occurring allotropes of carbon. It has a layered structure (as shown in Figure 5), and a single layer of graphite is called a “graphene”. When the single layer of graphite contains some oxygen functionalities, then it is referred to as “graphene oxide”. Reduced graphene oxide is prepared from the reduction of graphene oxide (although a few oxygen functionalities will remain) through thermal, chemical, or ultraviolet means.

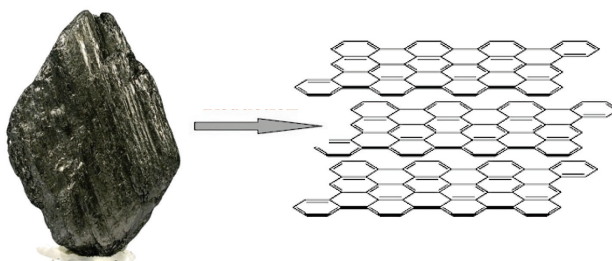


Figure 5. Graphite (rock) and its layered structure.

Graphene is a one atom-thick sheet of carbon atoms in a honeycomb crystal lattice (hexagons). Graphene is the building-block of graphite (used in pencil tips) and has many versatile properties. Graphite oxide was first prepared by Oxford chemist Brodie in 1859 (Brodie, 1859), who treated graphite with a mixture of potassium chlorate and fuming nitric acid. In 1957, Hummers and Offeman developed a safer, quicker, and more efficient process, using a mixture of H_2SO_4 , sodium nitrate $NaNO_3$, and potassium permanganate $KMnO_4$. This method is still widely used to synthesise GO (Hummers & Offeman, 1958). The structures of the graphene family are presented in Figure 6.

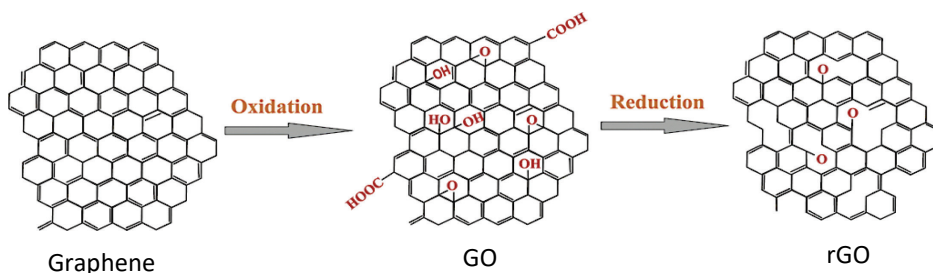


Figure 6. Graphene, graphene oxide and reduced graphene (Priyadarsini, Mohanty, Mukherjee, Basu, & Mishra, 2018).

The word “graphene” referred to a world-first 2-dimensional sheet-like lightweight material (Geim & Novoselov, 2007; Novoselov et al., 2012). Graphene has several properties such as conductivity, specific capacitance, photocatalytic activity, hydrophobicity, antibacterial functions, and high mechanical strength, which make it far superior to other nanomaterials (Soldano, Mahmood, & Dujardin, 2010). As a conductor, it performs as well as copper. Due to the presence of the oxygen functionalities in GO, it can easily disperse in water and other organic solvents together with different polymer matrixes, which can improve the electrical and mechanical properties of the polymers.

However, GO is often described as a poor electrical conductor and it behaves like an electrical insulator, due to the disruption of its sp^2 bonding networks. To restore the honeycomb hexagonal lattice and graphene's electrical conductivity, the GO has to be reduced once most of the oxygen groups are removed. It is worth noting that the rGO produced is more difficult to disperse, due to its tendency to create aggregates.

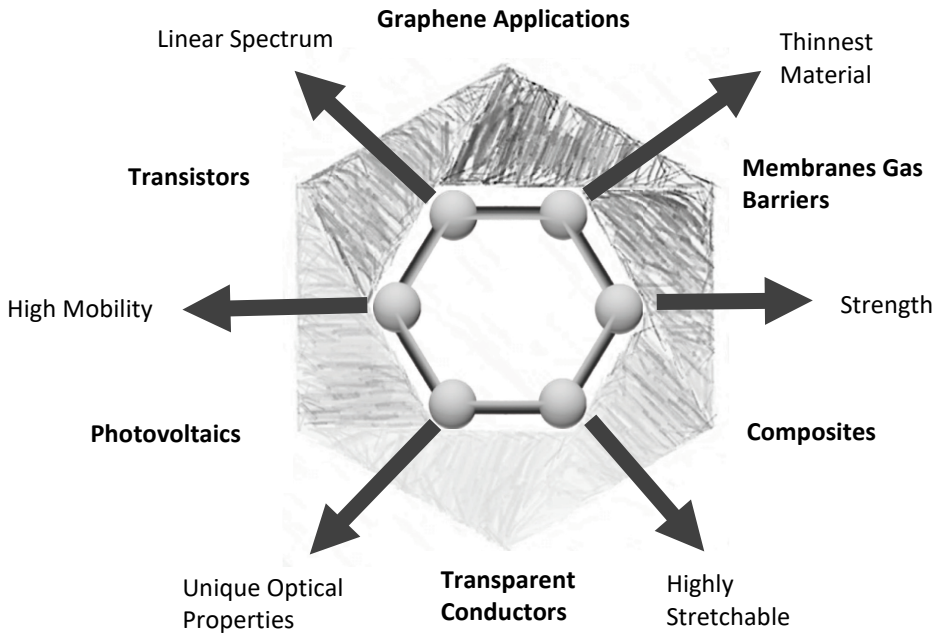


Figure 7. Properties and applications of graphene in different fields (same as Figure 5 in Article III).

Graphene is a one atom-thick sheet of carbon atoms tightly packed into hexagonal structures. It looks like a honeycomb lattice, as illustrated in Figure 7. It is the strongest and thinnest material known to man, 100-300 times stronger than steel and weighing approximately 0.77 milligrams for every $1m^2$ (H. S. Dong & Qi, 2015). It has been over 13 years since Andre Geim and Konstantin Novoselov, two innovative scientists, won the Nobel prize for the discovery of the wonder material “graphene”. Their discovery triggered a sharp rise in graphene research (Geim, 2009; Geim & Novoselov, 2007; Novoselov et al., 2004).

2.1 Graphene as nanofiller for electrospinning

Graphene is a promising candidate to act as a nanofiller in electrospinning, given its many multifunctional properties such as mechanical, electrical, and morphological enhancement, which can achieve the nanofibers' desired diameters or porosity. These characteristics of graphene make it a strong nanofiller candidate to potentially revolutionized as a promising candidate in nanocomposites. Since graphene was discovered, many types of synthetic and natural polymers have been electrospun by this novel nanofiller, which can remarkably stimulate the spinning process and dramatically enhance the properties of electrospun nanofibers such as their mechanical strength, hydrophilicity, conductivity, and thermal stability (An, Ma, Liu, & Wang, 2013;

Ardeshirzadeh, Anaraki, Irani, Rad, & Shamshiri, 2015; Q. Bao et al., 2010; Ding et al., 2015; Pant et al., 2012; Pant et al., 2015; Qi et al., 2013; Ramazani & Karimi, 2016; Shin et al., 2015; Song et al., 2015; Tan, Gan, Hu, Zhu, & Han, 2015; C. Wang, Li, Ding, Xie, & Jiang, 2013; Y. Wang et al., 2015; Xu, Zhang, & Kim, 2014; Yoon et al., 2011; C. Zhang et al., 2016). Adding graphene in an electrospinning solution to create conductive nanofibers is a crucial step, which determines the nanofibers' flexibility, chemical affinity, stability, and functionality. It consists of two steps: 1) incorporation of GO sheets into the polymeric solution by melt mixing, solution blending, or in-situ polymerization of a polymeric matrix; and 2) reduction of GO electrospun nanofibers either by chemical methods or annealing under high temperatures, which are referred-to as rGO nanofibers. GO is naturally a poor electrical conductor (less than a micro S/m) but when treated with strong reducing agents or under high temperatures, most of the conjugated structures of graphene will be restored by the removal of oxygen-containing functionalities. However, there are the methods (Q. Dong et al., 2014; Lavanya, Satheesh, Dutta, Victor Jaya, & Fukata, 2014) in which reduced graphene can be electrospun directly with the polymers. Nevertheless, these methods lead to inhomogeneous dispersions, which might present challenges and difficulties in the continuous electrospinning processes.

2.1.1 Electrospinning of conductive nanofibers by graphene

There have been significant advances in graphene-based electro-conductive electrospun nanofibers (GBEENs), especially in the field of electronics. Compared to traditional metallic wires, GBEENs are popular materials due to their remarkable properties, such as being lightweight, good mechanical properties, high electrical conductivity, and environmental stability. The matrixes for developing GBEENs nanofibers with polymers such as polyacrylonitrile (PAN), polyvinyl alcohol (PVA), PVC (polyvinyl chloride) nylon, polymethyl methacrylate (PMMA), poly lactic-co-glycolic acid (PLGA), and poly(vinyl acetate) (PVAc) have been reported in the data provided in Table 1 which described electrospinning components, reduction methods, and conductivities.

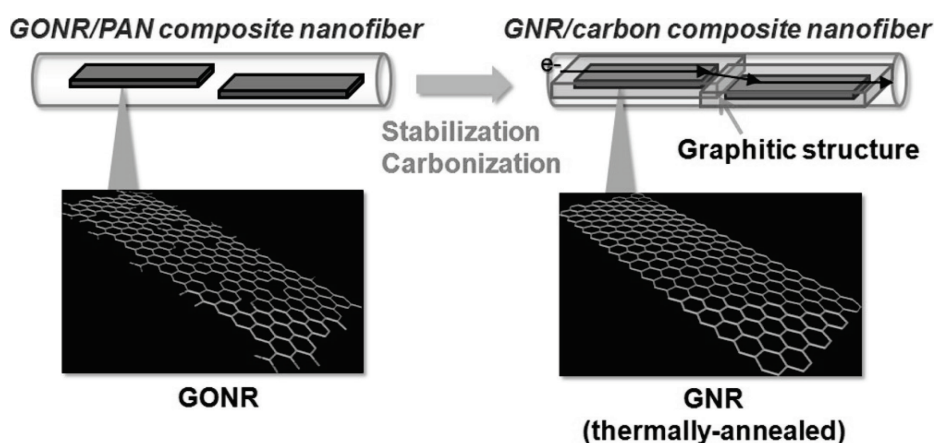


Figure 8. Schematic structures of the GO/PAN nanofiber before and after carbonization (As adapted from Article III as Figure 7).

H. Matsumoto (Matsumoto et al., 2013) reported the interaction of graphene with PAN. Matsumoto et al. prepared graphene nano ribbons (GONRs) by unzipping the multiwalled carbon nanotubes (MWNTs) with the oxidation process, followed by

electrospinning the MWNTs with GONRs in PAN/DMF solutions. The reported conductivity of the substance is presented in the Table 1.

The nanofibers' conductivity is heavily dependent on the reduction strategy, and on the sheet-to-sheet interdependence inside the fibers. This phenomena is explained well by the same study (Matsumoto et al., 2013). The schematic graphitic structure of graphene sheets inside nanofibers is illustrated in Figure 8. The governing parameter for the properties of GBEENs is the interaction with the polymer matrix. This influence was highlighted in the schematic interactions of PVP and PVA with graphene sheets, as reported in Figure 9a. (Y. Wang et al., 2015). Table 1 illustrated that the fibers treated under high temperatures had significantly improved conductivity, in comparison with the nanofibers reduced by chemical methods. This difference might have been due to the removal of significant amounts of oxygen from the GO's surface i.e. attached to the interior of an aromatic domain in graphene oxide by restoring sp^2 graphene networks. This significantly improved the conductivity of the nanofibers by the thermal reduction process.

The main challenges for obtaining graphene-based electrospun nanofibers are improving the dispersion, alignment, and appropriate loadings of GO within the polymer matrix. This phenomenon is explained by the SEM images of H. Matsumoto's study. Nanofibers with lower wt% (i.e. 0.5 wt%) fractions of GONRs were distributed more homogeneously than the fractions with higher amounts (5 wt%) of GONRs, where the agglomeration phenomenon with the excessive addition of graphene. Loaded-down graphene, which is a better contributing factor, has created smooth structural formations of nanofibers (Figure 9b). Besides thermal reduction, several attempts have been made in the chemical reduction of GBEENs. Yao Wan et al. described the chemical reduction of GBEENs for the recovery of conductive networks of graphene. A novel composite network of GO sheets within PAN and PVP nanofibers has been developed by using hydrazine (with the structural formula given in Figure 10a.) as the reducing agent (Y. Wang et al., 2015). With this methodology, striking results were obtained, such as 75 S/cm with graphene-PAN and 25 S/cm with graphene-PVP (see Table 1).

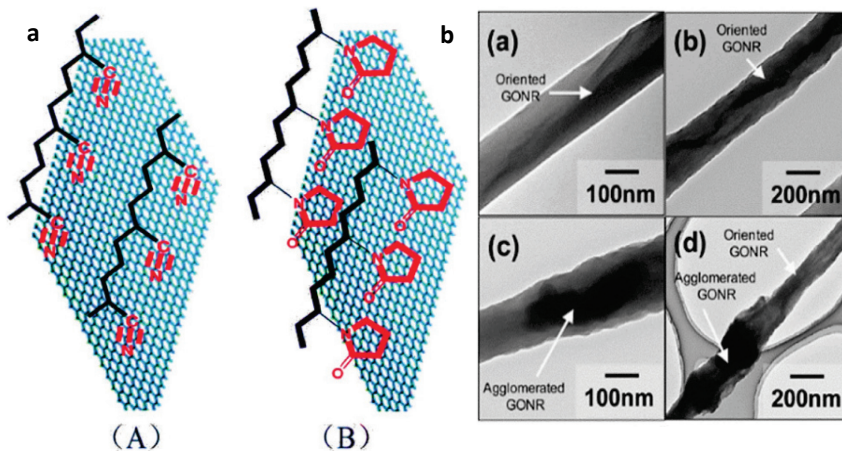


Figure 9. Proposed interactions of (a) graphene sheets with (A) PAN and (B) PVP, and (b) typical TEM images of the as-spun GONR/PAN composite nanofibers containing (a, b) 0.5 wt % and (c, d) 5 wt % GONR (the same as Figure 8).

Table 1 Summary of graphene based electrospun hybrids nanofibers.

Electrospinning hybrid materials	Reduction method	Resistivity/Conductivity	Reference
PAN and GONRs	Heated at 1000°C for 1 h	165.1± 4.3 S/cm	(Matsumoto et al., 2013)
GO, PAN and PVP	N ₂ H ₄ for 6h	Graphene–PAN 75 S/cm Graphene–PVP 25 S/cm	(Y. Wang et al., 2015)
PANi/G-PBASE and PMMA	Hydrazine monohydrate at 80°C 24 h	30 S/cm	(Moayeri & Ajji, 2016)
PVC/PLGA nanofibers	HI solution (55%) at 100°C for 1 h	10.0 S/cm	(Jin, Wu, Kuddannaya, Zhang, & Wang, 2016)
RuO ₂ /ACNF and graphene	Heated at 800°C for 1 h	0.59 S/cm	(K. S. Yang & Kim, 2015)
GCNF anchoring of MoS ₂	Heated at 800°C for 2 h	0.56 S/cm	(Gu, Huang, Zuo, Fan, & Liu, 2016)
ACF ultrasonic spray (S-rGO/ACF)	Heated at 800°C for 1 h	0.42 S/cm	(G. Wang et al., 2016)
RGO/PAN	Heated at 800°C for 1 h	0.24 S/cm	(Q. Dong et al., 2014)
PAN/Fe ₂ O ₃ /G	Carbonized at 650°C for 1 h	0.21 S/cm	(B. Zhang, Xu, & Kim, 2014)
PAN/PMMA, SbCl ₃ and GO	Heated at 700°C for 2 h	4.20×10 ⁻² S/cm	(Tang et al., 2015)
PANi with HCSA and PEO filled G-PBASE	N ₂ H ₄ heated to 80°C 24 h	9.92×10 ⁻⁴ S/cm	(Moayeri & Ajji, 2015)
PI, GNR and CNT	HI-H ₂ O at 98°C for 10h	8.3×10 ⁻² S/cm Parallel 7.2×10 ⁻⁸ S/cm Perpendicular	(M. Liu et al., 2015)
CNF, Si and graphene-covered Ni	Carbonization at 650°C for 1 h	9.5 × 10 ⁻⁵ S/cm	(Xu, Zhang, Zhou, et al., 2014)
PVA/ODA-MMT-poly(MA-alt-1-octadecene)-g-GO	No reduction	5.91- 4.42×10 ⁻⁵ S/cm	(Rzayev et al., 2016)
GO-g-[P(HEMA-g-PCL)]/gelatin	Bio-reduction	1.83×10 ⁻⁵ S/cm	(Massoumi, Ghandomi, Abbasian, Eskandani, & Jaymand, 2016)
PANI and PAN with G and GO nanosheets	Ammonia solution at 180°C for 1 h	1.59×10 ⁻⁶ S/cm	(Matin et al., 2016)
GO polyamide 66 (PA66)	0.1 wt% N ₂ H ₄ and annealing at 350°C	8.6×10 ³ Ω/sq	(Yuan-Li et al., 2011)
GNSs and silver nanopArticles (AgNps)	NaBH ₄ at 100°C for 24 h	150 Ω/sq	(Y-L. Huang et al., 2012)

Fabricating graphene oxide is a vital process, as it has a large impact on the nanofibers' conductivity. Therefore scientists, have been exploring new methods and techniques for the surface functionalization of the nanofibers with GO, in order to enhance the conductivity of hybrid electrospun fibers.

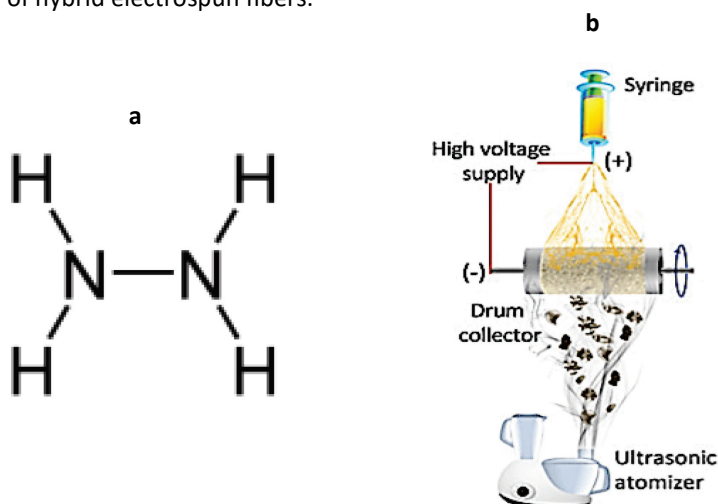


Figure 10. Chemical structure (a) of hydrazine as adapted from the ref. (Rabah, 2017) and schematic electrospinning with ultrasonic spraying of GO simultaneously (Ref. Figure 9b in Article III).

The most obvious method for utilizing GO in the industrial production of nanofibers is to use an ultrasonic atomizer to incorporate graphene through a mist of GO. With this method, it is relatively easy to fabricate sufficient amounts of graphene to the desired quality levels. An interesting strategy was employed by Gang Wang and Qiang Dong (G. Wang et al., 2016). They fabricated conductive nanofibers and doped GO by using electrospinning and ultra-sonication simultaneously, and by spraying graphene through an ultrasonic atomizer. This method was illustrated in Figure 10b, and it achieved conductivity up to 0.42 S/cm.

2.1.2 Electrospinning of cellulose acetate and GO

A number of synthetic polymers such as PVA, PAN, PANI, and PVP have been successfully hybridized with graphene sheets and carbon nanotubes to produce conductive nanofibers (Z-M. Huang et al., 2003; Wahab et al., 2016). However, very few contributions have been made to the electrospinning of biopolymers with carbon nanotubes or graphene. Of these contributions, carbon nanotubes (CNTs) are more popular and have been successfully electrospun with biopolymers such as chitosan, cellulose triacetate, and polylactide (Gouda & Abu-Abdeen, 2017; Mahdieh, Mottaghitalab, Piri, & Haghi, 2012; T. Yang, Wu, Lu, Zhou, & Zhang, 2011). Due to their high strength, flexibility, and high electrical and thermal conductivities, CNTs have attracted significant interest for a wide range of potential applications, but only two studies have been performed. Miyauchi studied the effect of CNTs on the electrospinning of cellulose, with a combination of 1-methyl-3-methylimidazolium acetate ([EMIM]Ac) as the IL. A core sheath of multi-walled CNT (MWNT) cellulose were prepared by co-axial electrospinning. Sheath removal was carried out by enzymatic reactions through a cellulase aqueous enzyme solution. At 45 wt% MWNT loading, maximum conductivity

(10.7 S/m) was achieved (Miyachi et al., 2010). The SEM images of these electrospun nanofibers are presented in Figure 11. In the second study, a composite electrode (Kuzmenko et al., 2017) for the development of a supercapacitor was prepared through the immersion method. Cellulose acetate was electrospun and the mats were immersed into the GO solution. To fabricate the conductive networks within the nanofibers, GO electrospun mats were treated under high temperatures to reduce GO into rGO. The maximum reported conductivity of this study was 49 S/cm. The schematic preparation of electrospun electrode from cellulose is presented in Figure 12.

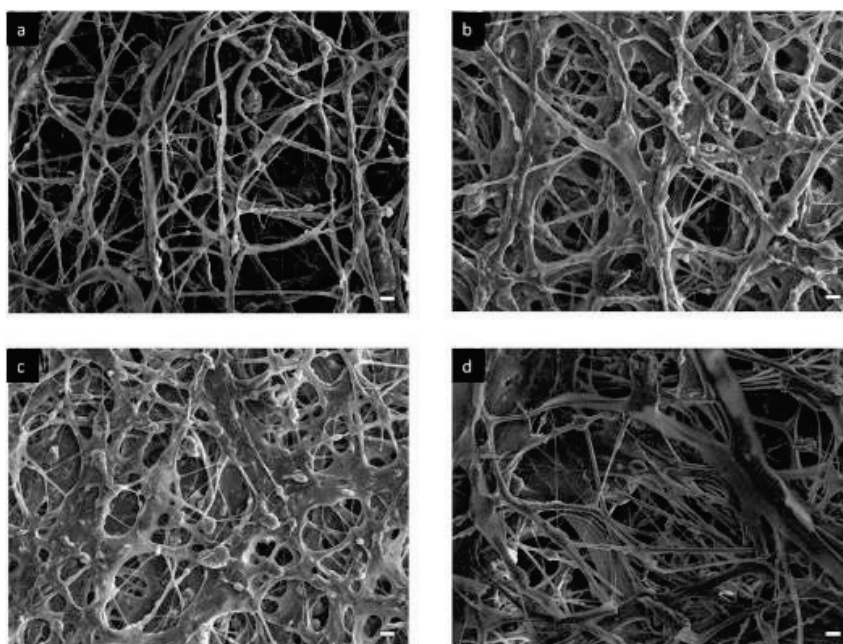


Figure 11. SEM images of core-sheath of MWNT-cellulose fibrous mats (Miyachi et al., 2010).

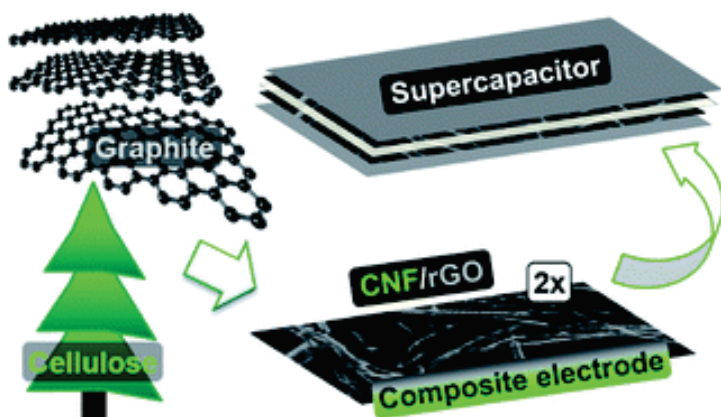


Figure 12. Schematic illustration of a cellulosic composite electrode using electrospinning (Kuzmenko et al., 2017).

2.2 The aim of the study

There is a distinct challenge to producing graphene/biopolymer nanofibers by electrospinning. This study's aim was to create conductive nanofibers by using graphene as a nanofiller. The main challenge was to blend the GO homogenously inside the nanofibers.

In comparison with synthetic polymers, bio-polymers are a new generation for composite materials that have emerged in the frontiers of materials science and nanotechnology. Cellulose acetate was chosen as a biopolymer, based on its compatibility with GO as it has (COCH₃) hydroxyl groups which have the tendency to form hydrogen bonds with adjacent spices.

To achieve the homogenous blending of GO into the biopolymer matrix, an IL was used as a dispersant for the GO. [BMIM]Cl was selected as the dispersant in this study. The choice was based on the affinity and chemical structure of [BMIM]Cl, in order to achieve better homogeneity in the spinning solution. It also disperses GO and breaks up the graphene sheets which have inherent insolubility, atomically smooth surfaces, and strong aggregation tendencies.

The additional aim was to reduce the GO within the nanofibers, which was also a critical step as the reduction of GO has the largest influence on the nanofibers' conductivity. Therefore, hydrazine was chosen as a reducing agent to impart conductivity within the nanofibers. This study's main objectives were as follows:

- Preparation of IL/CA/GO nanofibrous mats by electrospinning,
- Preparation of IL/CA/rGO mats by hydrazine vapors,
- Study of the nanofibers' conductive properties, and
- Analysis of the morphological and chemical properties of the nanofibers (e.g. SEM FTIR, Raman Spectroscopy XRD, and XPS).

3 Experimental

3.1 Materials

1-methylimidazolium (99%), ethyl acetate (99%) and 1-chlorobutane (99%) were purchased from Merck. CA powder ($M_n = 30,000$ Da, acetyl content 39.8 %), acetone, dimethylacetamide (DMAc) and hydrazine solution (35 wt% in H_2O), all from Sigma Aldrich, were used as received. Graphene oxide powder (15-20 sheets, 4-10% edge-oxidized) was purchased from Garmor Inc. U.S.A. 1-Butyl-3-methylimidazolium chloride [BMIM]Cl was synthesized by the method described elsewhere (Huddleston et al., 2001).

3.2 Methods

3.2.1 Preparation of CA, CA-[BMIM]Cl and [BMIM]Cl-GO blends

Cellulose acetate solution of 17 wt% was prepared by adding it to a mixture of acetone and dimethylacetamide with a volume ratio of 2:1 (v/v %), under constant stirring at room temperature, until a homogenous and transparent solution was formed. [BMIM]Cl was added to the prepared CA solution to obtain the desired concentrations of 0%-12% (v/v %) of [BMIM]Cl and stirred at room temperature again for another 2 h. This CA-[BMIM]Cl homogenous solution was then ready for electrospinning. The CA concentration was kept fixed at 17 wt% in all spinning solution preparations, while the IL concentration varied so as to investigate the influence of [BMIM]Cl on the electrospun CA fibers. A schematic preparation of CA-BMIM[Cl] solution is presented in Figure 13. [BMIM]Cl-GO solutions were prepared by adding GO (0.11-0.43% by weight of CA) to [BMIM]Cl (12% by weight of CA) under constant stirring at 60°C for 24 h. Finally, [BMIM]Cl-GO was added to the CA solution and stirred at room temperature for a further 2 h (experimental details provided in the supporting information). This solution, denoted as CA-[BMIM]Cl-GO throughout this thesis, was then ready for electrospinning.

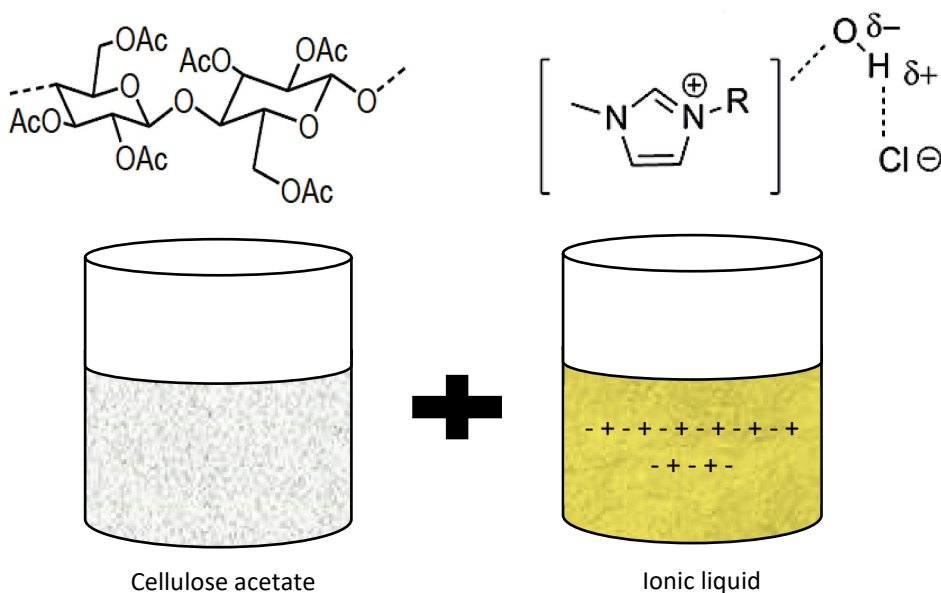


Figure 13. The schematic CA-[BMIM]Cl solution preparation (reproduced from Article II).

3.2.2 Preparation of CA-[BMIM]Cl and CA-[BMIM]Cl-rGO nanofibers

Electrospun solutions of CA with IL and GO were electrospun at room temperature by the horizontal electrospinning setup. Each polymer solution was placed into a 1ml syringe with a needle diameter of 0.6mm. The solution was electrospun at a voltage of 20-25 kV with a power supply (Gamma High Voltage Research, ES 40R-20W/), and the distance between the needle and the collector was adjusted to 8–10 cm. The feeding rate was maintained at 1.5ml/h by a syringe pump (NE-1010 New Era Pump Systems, Inc).

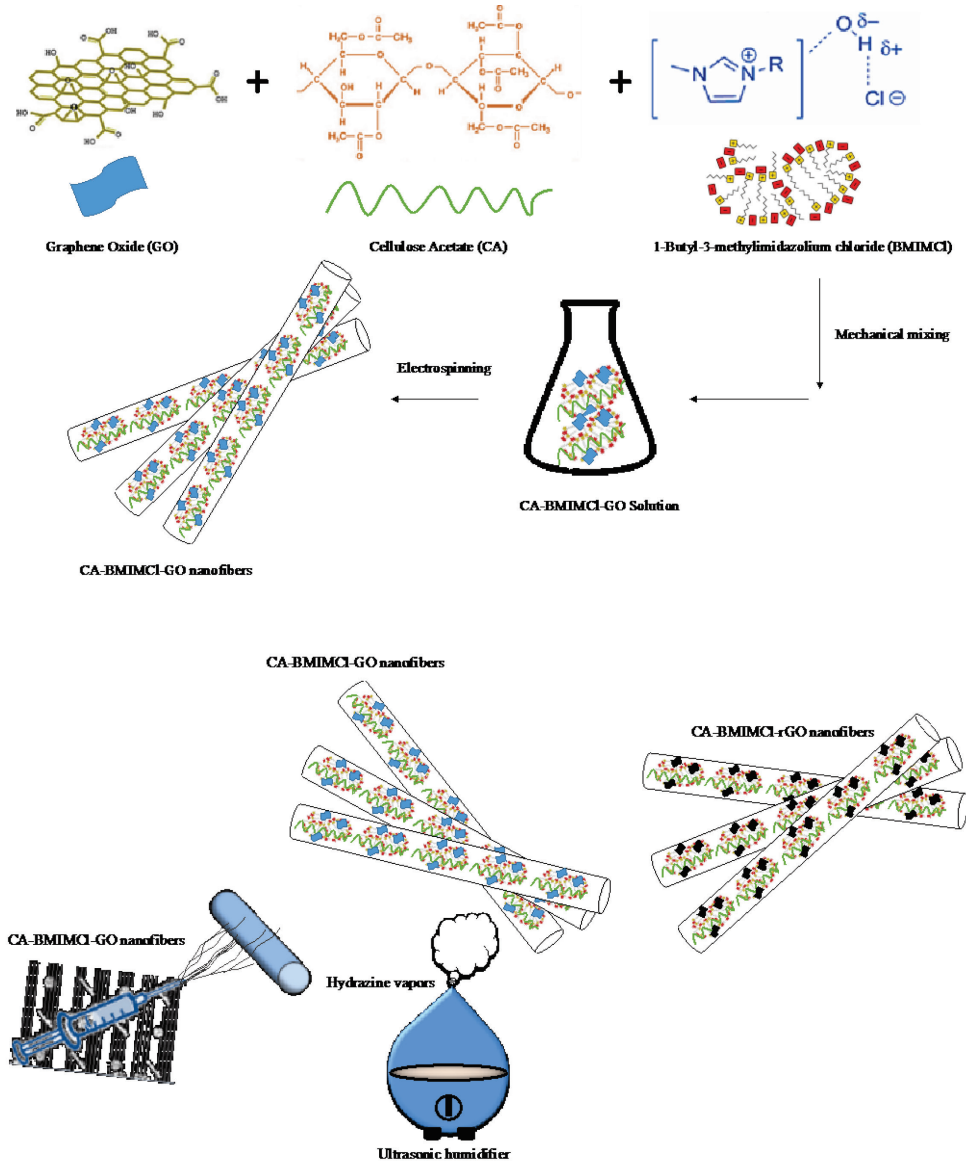


Figure 14. Preparation of [BMIM]Cl-GO blends, electrospinning of CA-[BMIM]Cl-GO nanofibers and reduction of nanofiber by hydrazine mist (reproduced from Article I).

The electrospun nanofibers were collected on a cylindrical rotatory drum, which was covered with aluminum foil. Cellulose acetates, CA-[BMIM]Cl and CA-[BMIM]Cl-GO membranes were detached from the foil and dried at room temperature for 2 h. To reduce the oxygen content of the GO for the creation of electrically conductive nanofibers, CA-[BMIM]Cl-GO nanofibrous mats were reduced by a hydrazine solution mist (Z. Wang et al., 2012; Youn et al., 2011). In other words, the hydrazine solution was placed in an ultrasound humidifier (BONECO Ultrasonic U7146, Switzerland). The fibrous mats were then clamped in a universal extension retort clamp and placed in the front of the humidifier at maximum humidity for 15-30 minutes (see supplementary video in the supporting Information), until the mats changed into the typical black graphitic color. Following reduction, the mats were allowed to dry at room temperature for 2 h to give CA-[BMIM]Cl-rGO the nanofibers. The whole process is illustrated in Figure 14.

3.2.3 Characterizations of the nanofibers

The surface morphologies of the nanofibers were analyzed by scanning electron microscopy (SEM, Zeiss FEG-SEM Ultra-55). The intermolecular interactions within the nanofibrous mats were analyzed by fourier-transform infrared spectroscopy (FTIR, Interspec 200-X).

The thickness of the mats was measured by a Mitutoyo Mischecker M519-402 micrometer and the approximate porosity of the final electrospun nanofibrous mats was calculated by image analysis, as described in Appendix B.

Chemical states and surface composition were characterized by X-ray photoelectron spectroscopy (XPS, Kratos AXIS Ultra DLD X-ray Photoelectron Spectrometer).

The transmittance FT-IR spectra was recorded on an Interspec 200-X FTIR spectrometer, with 16 scans averaged at the resolution of 1 cm^{-1} .

Raman spectroscopy (Renishaw inVia Raman spectrometer) was used to probe the surface composition. The X-ray diffraction (XRD) patterns were recorded by a Rigaku Ultima IV diffractometer with Cu K α radiation ($\lambda = 1.5406\text{ \AA}$, 40 kV at 40 mA), using a silicon strip detector D/teX Ultra with the scan range of $2\theta = 5.0 - 30.0^\circ$, scan step 0.02° , scan speed $5^\circ/\text{min}$.

The electrical conductivities of the electrospinning solutions were analyzed with a conductivity meter (SevenCompactS230 Mettler Toledo, Switzerland) at room temperature, while the conductivity of the nanofiber mats was measured with a two-probe method using an AlphaLab, Inc. multimeter, by placing the mats between two gold electrodes at a distance of 1 cm.

The thermal stability of CA, CA-[BMIM]Cl, CA-[BMIM]Cl-GO and CA-[BMIM]Cl-rGO nanofibers was analyzed with thermogravimetric analysis (TGA, Setaram LabsysEvo 1600 thermo analyzer) under argon between 25°C to 700°C at a heating rate of $10^\circ\text{C}/\text{min}$.

4 Results and discussion

4.1 Influence of [BMIM]Cl on the CA electrospun nanofibers

4.1.1 Influence of [BMIM]Cl on the CA solution's viscosity and conductivity

The impact of IL on the viscosity of the CA solutions can be seen in Figure 15. Without [BMIM]Cl, the viscosity was the lowest at 471cP. However, this increased sharply from 2% to 6% of [BMIM]Cl to a maximum of 650cP. Unexpectedly, when the solution exceeded 6%, the viscosity gradually decreased to 600cP at 12% of IL. This increase and decrease in viscosity can be attributed to the large BMIM⁺ and small Cl⁻ ions, which can interfere in the hydrogen bonding between cellulose acetate chains (Z. Liu et al., 2011; Xia, Yao, Gong, Wang, & Zhang, 2014). Therefore, initially low concentrations from 2% to 6% may not have been enough to break the extensive hydrogen bonding within CA, but at higher concentrations (8%-12% of IL) there was a breakdown of the hydrogen bonds between cellulosic chains, which reduced the viscosity of the CA solution.

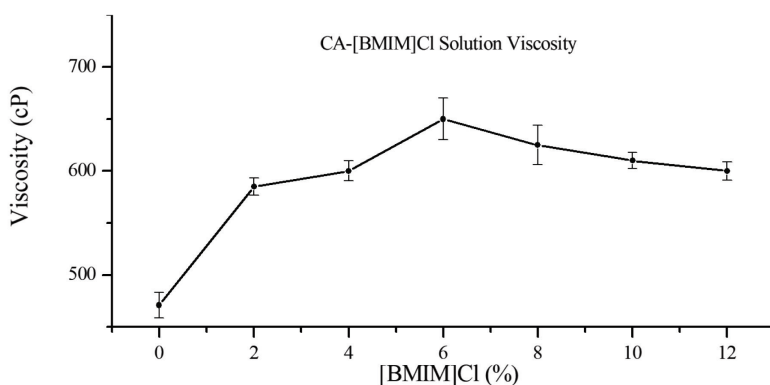


Figure 15. Influence of [BMIM]Cl on the viscosity (Same as Figure 2a in Article II).

From Figure 16 it can be seen that the higher the amount of IL, the higher the conductivity of the CA solution (0.01 mS/cm up to 2.6 mS/cm). This was caused by a gradual increase of BMIM⁺ and Cl⁻ ions which dissociated in the solution. The conductivity measurements are illustrated in Table 2 and membranes from 0%-4% displayed no conductivity because of the lesser number of free ions. However, as the volume ratio of IL increased, there was a significant rise in conductivity. This was due to the increased production of charge carriers by the IL. When membranes with 10% of IL were increased to 1.70×10^{-7} S/cm, CA nanofibers with 12% of IL had the highest conductivity at 2.71×10^{-7} S/cm.

4.1.2 Influence of [BMIM]Cl on the morphology of CA nanofibers

Scanning electron microscopy images of the pure CA electrospun nanofibers and CA-[BMIM]Cl electrospun nanofibers are displayed in Figure 17, along with their characteristics as illustrated in Table 2. The pure CA electrospun nanofibers were smooth with no droplets formed. However, as the concentration of [BMIM]Cl increased from 2 to 4%, the formations of the fibers changed significantly and there were minimal droplets with the fibers (Figure 17b and 17c).

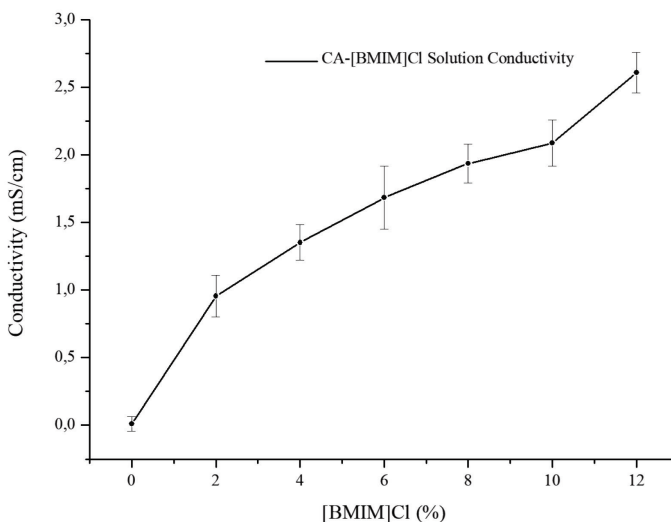


Figure 16. Influence of [BMIM]Cl on the conductivity of CA solutions (Figure 2b in Article II).

Generally, in the electrospinning process, fibers will be developed due to the surface tension of the droplets of polymer solution, which gather at the tip of a needle when an external electric field is applied. Therefore, the surface tension at low concentrations of IL was low enough to allow the polymer chains to stretch and form fibers under an applied electric field. In this study, the free IL ions promoted high charge density (conductivity) of the spinning solution for the jet formation and fiber stretching (Zavgorodnya, Shamshina, Bonner, & Rogers, 2017). Therefore, where there was reduced movement of free IL ions, the solution had low conductivity, leading to jet instability and the creation of droplets with fibers. On the other hand, higher amounts of IL enhanced the solution's conductivity, which increased jet stability and produced uniform nanofibers without droplets as shown in Figure 17d-g.

Table 2 Influence of [BMIM]Cl on the conductivity and morphology of the nanofibers (Same as Table 1 in Article II).

[BMIM]Cl Concentrations (v/v %)	Conductivity (S/cm)	Avg. Fibers Diameter (nm)	Fibrous membrane
0%	N/A	125	Uniform fibers
2%	N/A	150	Fibers with droplets
4%	N/A	204	Fibers with droplets
6%	1.93×10^{-9}	525	Uniform fibers
8%	6.80×10^{-9}	348	Uniform fibers
10%	1.70×10^{-7}	300	Uniform fibers
12%	2.71×10^{-7}	180	Uniform fibers

The concentration of IL not only affected the morphology, but also affected the diameter of the nanofibers, as illustrated in Table 2. The average diameter of the pure CA electrospun nanofibers was 125nm, which increased to 525nm with the addition of

6% of IL. This change was due to the reduced viscoelastic forces which were created by low concentrations of IL. Jet splitting is difficult when the viscoelastic force is too large, hence the diameters of the fibers were larger. Increasing the viscoelasticity of the electrospinning solution or increasing the concentration of dissolved salt (i.e IL) in the spinning solution tended to stabilize the jet against the formation of droplets (Reneker & Yarin, 2008). Therefore, with higher amounts of IL, 8 to 12% more nanosized fibers were observed, up to 180 nm.

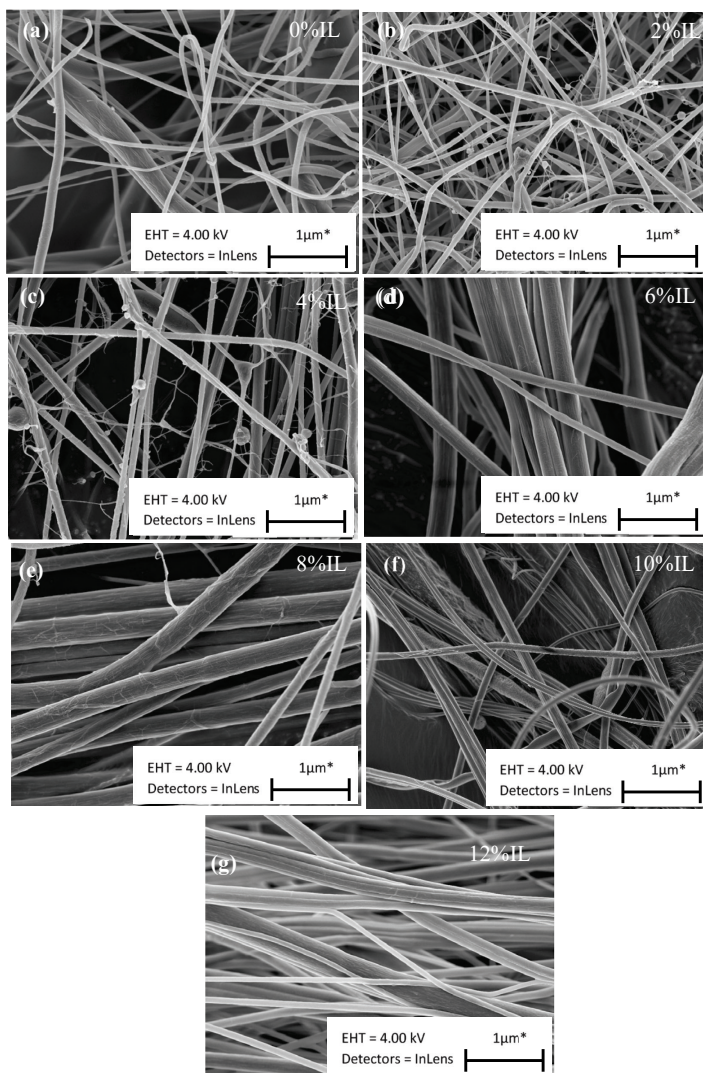


Figure 17. SEM of pure CA fibers (a) and CA with 2% IL (b) CA-4%IL, CA-6%IL (c, d) CA-8%IL, CA-10%IL and CA-12%IL (e, f, g) as adapted from Article II.

4.2 Influence of GO on the electrospun nanofibers

4.2.1 Influence of GO on the morphology and conductivity of the hybrid nanofibers

The conductivity of the CA-[BMIM]Cl solution (prior to the incorporation of GO) was measured at 6.23 mS/cm, and it remained almost constant as the amount of GO increased from 0.11 to 0.43 wt%. This was due to the presence of oxygenated groups on the surface of GO, which disrupts the sp^2 hybridization in graphene. The nanofibers produced, with controlled amounts of GO in the range of 0 - 0.43 wt%, are illustrated in Table 3. Pure CA, CA-[BMIM]Cl, CA-[BMIM]Cl-GO, and CA-[BMIM]Cl-rGO nanofibers were then examined by SEM. The surface morphologies of CA, CA-[BMIM]Cl, and CA-[BMIM]Cl-GO (see Figure 18a-d) were smooth and bead-free, while CA-[BMIM]Cl-rGO nanofibers had rough regions where GO appeared to have aggregated (as shown in Figure 18d). Higher concentrations of GO hindered the jet flow because the excess GO, which was not fully dispersed in the solution, clogged the needle. Therefore, electrospinning was unsuccessful. During chemical reduction, the CA-[BMIM]Cl-GO nanofibers became more fused (Figure 18d) and formed a CA-[BMIM]Cl-rGO nanofibrous mat. The conductivity of CA-[BMIM]Cl nanofibers was measured at 2.71×10^{-7} S/cm, which was significantly lower than the conductivity of pure [BMIM]Cl at 4.60×10^{-4} S/cm (Dharaskar, Varma, Shende, Yoo, & Wasewar, 2013). The incorporation of GO resulted in an increase in the conductivity of the nanofibers, both before and after the reduction. For non-reduced nanofibers, the presence of GO (0.11 wt%) increased the conductivity to 4.33×10^{-5} S/cm. At 0.43% GO, the conductivity reached an approximate plateau at 1.41×10^{-4} S/cm. The conductivity of the nanofibers is presented in Table 3 and Figure 19.

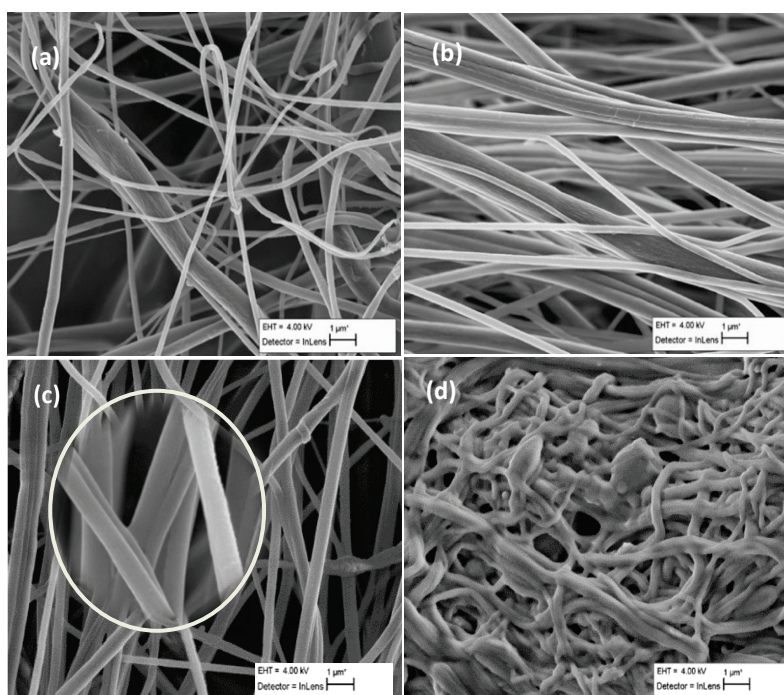


Figure 18. SEM images of (a) pure CA; (b) CA-[BMIM]Cl; (c) CA-[BMIM]Cl-GO; and (d) CA-[BMIM]Cl-rGO (GO conc. 0.43 wt%) nanofibers (Same as Figure 2 in Article I).

Compared to GO/CA nanocomposites reported in the literature, (Tripathi, Rao, Mathur, & Jasra, 2017) 0.43 wt% GO is a relatively low amount for such a significant conductivity increase.

Table 3 Conductivity of hybrid CA-[BMIM]Cl-rGO nanofibers (reproduced from Article I).

GO Content wt%	Conductivity (S/cm)	
	Before reduction	After reduction
0	2.71×10^{-7}	2.71×10^{-7}
0.11	4.33×10^{-5}	1.82×10^{-4}
0.21	1.11×10^{-4}	3.65×10^{-4}
0.32	1.29×10^{-4}	5.10×10^{-3}
0.43	1.41×10^{-4}	5.30×10^{-3}

Interestingly, reducing the hybrid nanofibers with hydrazine boosted the conductivity significantly, with the conductivity of pure [BMIM]Cl surpassed when the GO loading reached 0.32 wt% (4.60×10^{-4} S/cm). The highest conductivity attained was 5.30×10^{-3} S/cm with 0.43 wt% GO, which is $\sim 20,000$ times higher than that of the nanofibers without GO and over an order of magnitude higher than that of pure [BMIM]Cl.

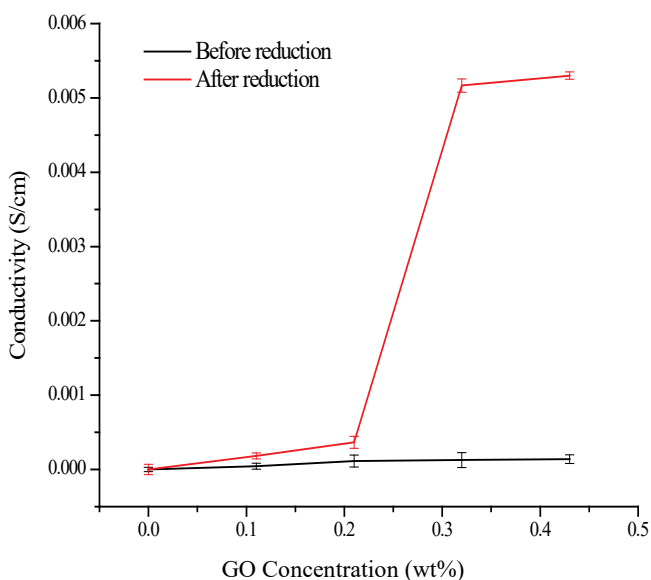


Figure 19. The effect of GO concentration in the hybrid CA-[BMIM]Cl-GO nanofibers on conductivity (Same as Figure 3a in Article I).

4.3 Structure of GO in the nanofibers before and after reduction

X-ray diffraction (XRD) was used to examine the crystal structure of CA and GO following the electrospinning and reduction processes. The XRD patterns of the CA, CA-[BMIM]Cl, CA-[BMIM]Cl-GO, and CA-[BMIM]Cl-rGO nanofibers are presented in Figure 20. Pure CA nanofibers exhibited three broad diffraction peaks at 9.0° , 17.9° , and 21.8° (Zhao, Zhang, Chen, & Lu, 2010).

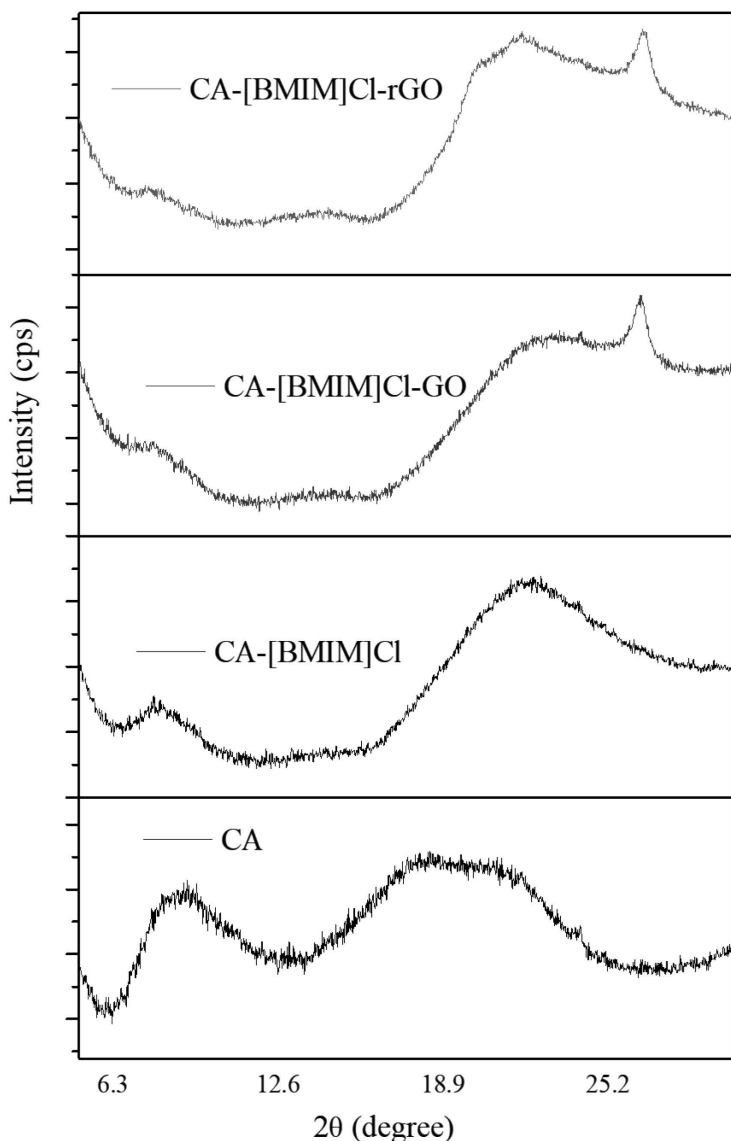


Figure 20. (a) XRD patterns of CA and hybrid CA-[BMIM]Cl nanofibers, (b) CA-[BMIM]Cl-GO and CA-[BMIM]Cl-rGO nanofibers (GO conc. 0.43 wt% for the latter two samples). Same as Figure 4a in Article I.

The peak at 21.8° is attributed to short-range spacing between neighboring cellulosic repeat units within the individual macromolecules. The peak at 9.0° indicates the longer-range interactions between CA chains (C. Bao, 2015). More specifically, the distance between adjacent cellulosic chains is normally characterized by a d-spacing of $\sim 9 - 10 \text{ \AA}$, and the neighboring anhydroglucose units in the cellulose chains have a d-spacing of $\sim 4 - 5.5 \text{ \AA}$. The peak at 17.9° could have arisen from the diffraction of the (021) plane. After the addition of [BMIM]Cl, the peak at 9.0° became significantly weaker and shifted

to 8.0° . This peak weakening and shifting to a lower angle reflected the decrease in CA concentration in the nanofibers from 100% to 53.4%, and the disruption of the cellulose packing by [BMIM]Cl. The presence of [BMIM]Cl broke up the H-bonding between the cellulosic chains and enlarged their d-spacing from 9.8 \AA to 11.0 \AA . A small shift of the 21.8° peak is also observed, illustrating that the addition of [BMIM]Cl did not significantly alter the anhydroglucose units in the CA chain. The peak at 17.9° almost completely disappeared from the nanofiber samples that were electrospun in the presence of [BMIM]Cl, indicating less short-range order in the amorphous CA. The addition of 0.11 wt% GO resulted in the appearance of a sharper peak at $\sim 26.5^\circ$, which is the (002) peak of graphite. The (002) peak shows that the interlayer spacing of the graphite sheets was approximately 0.33 nm (3.3 \AA).

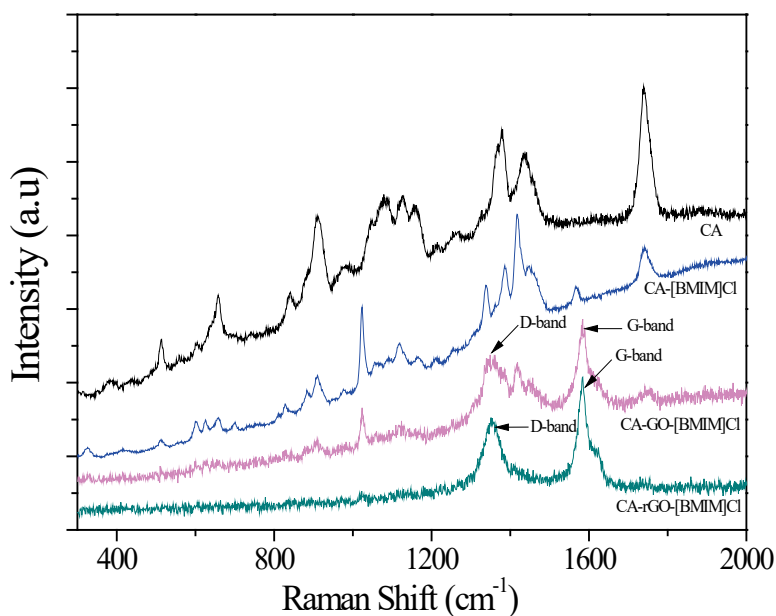


Figure 21. Raman spectra of CA and hybrid CA-[BMIM]Cl nanofibers, CA-[BMIM]Cl-GO and CA-[BMIM]Cl-rGO nanofibers (GO conc. 0.43 wt% for the latter two samples). Same as Figure 4b in Article I.

This result suggests that the graphene sheets were not fully exfoliated and remained in a graphitic-like state (Yuan, 2004). The oxygen-containing functional groups on the GO were mainly on the external surface of the nanoparticles. This result was in line with the specification of the GO nanoparticles purchased, that had 15-20 sheets and 4-10% edge-oxidized. After chemical reduction, this peak remained in the CA-[BMIM]Cl-rGO nanofibers, as expected.

To examine the influence of chemical reduction on the chemical structure of GO in more detail, the samples were studied by Raman spectroscopy, as illustrated in Figure 21. The Raman spectra of CA-[BMIM]Cl-GO and CA-[BMIM]Cl-rGO both displayed two bands at 1350 cm^{-1} and 1585 cm^{-1} . These can be assigned to the D and G bands of the carbon materials, respectively (Claramunt et al., 2015; Jorio et al., 2010). The G band represents

sp^2 -hybridized C-C bonds in a 2D hexagonal lattice, while the D band corresponds to the defects and disorders on the two-dimensional amorphization of the carbon network (Kudin et al., 2008; Malard, Pimenta, Dresselhaus, & Dresselhaus, 2009). These two peaks revealed that the graphene sheets of the GO have a significant proportion of carbon disordered away from a perfect 2D hexagonal lattice. More specifically, comparison of the CA-[BMIM]Cl-GO and CA-[BMIM]Cl-rGO spectra demonstrated that the D and G bands of CA-[BMIM]Cl-rGO nanofibers are more pronounced after chemical reduction, where the spectrum shows less signals from surface functional groups. The relative intensity of the G and D bands did not change significantly, supporting the evidence provided by XRD that the graphene sheets in the GO particles were not fully exfoliated. The graphene sheets contained sp^2 -hybridized C-C bonds in a 2D hexagonal lattice and had sheet spacing close to the 0.33 nm of graphite. Significantly, the chemical reduction did not significantly alter the stacking of the graphene sheets, but modified the surface functional groups through deoxygenation (Park et al., 2009; Shilpa, Basavaraja, Majumder, & Sharma, 2015; Stankovich et al., 2007; Yao, Li, Zhou, & Yan, 2015).

4.3.1 Chemical bonds and interactions within the nanofibers

The FTIR and XPS spectra are presented in Figure 22 and Figure 23, respectively. The Raman spectra of CA and CA-[BMIM]Cl demonstrated the asymmetric stretching vibration of the C-O-C glycosidic bond at 1121 cm^{-1} and the pyranose ring at 1080 cm^{-1} , with the presence of C-OH at 1265 cm^{-1} . The bands at 1736 , 1435 , and 1382 cm^{-1} are attributed to the carbonyl group (C=O) and the symmetric and asymmetric vibrations of C-H respectively in the acetyl group (Duverger et al., 1999; J. A. Sánchez-Márquez, 2015; Scherer et al., 1985). More interestingly, the [BMIM]Cl cation was observed in the CA-[BMIM]Cl sample with bands at 601 and 627 cm^{-1} . The intensities indicated the co-existence of gauche and trans conformations of the IL (Mizuno, Imafuji, Ochi, Ohta, & Maeda, 2000; Satoshi, Ryosuke, & Hiro-o, 2003). It is worth noting that the inclusion of GO resulted in the disappearance of most of the vibrational bands from the Raman spectra of the corresponding hybrid nanofibers.

The FTIR spectra of pure CA, CA-[BMIM]Cl, and CA-[BMIM]Cl-rGO nanofibers (Figure 22) demonstrated that pure CA nanofibers exhibited characteristic bands at 1735 cm^{-1} and 1367 cm^{-1} , respectively corresponding to C=O and C-H stretching from $-\text{OCOCH}_3$. The bands at 1220 cm^{-1} and 1030 cm^{-1} revealed the C-C and C-O stretching vibrations in the pyranoid ring and C-O-C (ether linkage) from the glycosidic units. In the CA-[BMIM]Cl spectrum, characteristic bands at 1746 cm^{-1} (C=C stretching), 1214 cm^{-1} (C=N stretching), and 1041 cm^{-1} (C-O stretching) indicated that the BMIM⁺ and Cl⁻ ions of [BMIM]Cl formed hydrogen bonds with CA, as expected. The FTIR spectrum of CA-[BMIM]Cl-GO was similar to that of CA-[BMIM]Cl while the spectrum of [BMIM]Cl-rGO displayed two new bands at 1659 cm^{-1} and 3229 cm^{-1} , suggesting strong interactions (hydrogen bonding) between the carboxylic ($-\text{COOH}$) groups of graphene and carbonyl (C=O) groups of CA. XPS was used to further examine the differences in chemical functionality in the hybrid nanofibers (Figure 23). The survey spectrum of pure CA nanofibers exhibited only two distinct peaks: C 1s at $\sim 285\text{ eV}$ and O 1s at $\sim 532\text{ eV}$ (Figure 23), while Cl 2p and N 1s peaks were present in all other spectra, confirming the presence of [BMIM]Cl. High resolution C 1s spectra were analyzed by a monochromatic Al K α X-ray source ($h\nu = 1486.6\text{ eV}$). Each spectrum was deconvoluted into five distinct peaks, as illustrated in Figure 24a-d for the nanofibers of pure CA, CA-[BMIM]Cl, CA-[BMIM]Cl-GO, and CA-[BMIM]Cl-rGO.

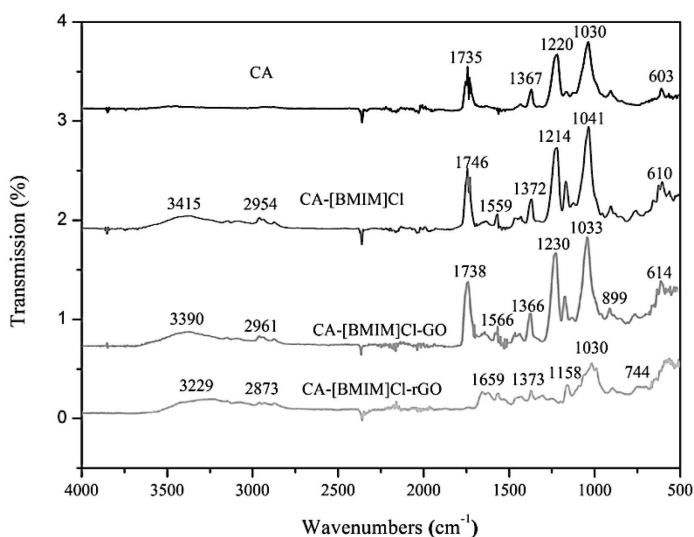


Figure 22. FTIR spectra patterns of CA and hybrid CA-[BMIM]Cl nanofibers, CA-[BMIM]Cl-GO and CA-[BMIM]Cl-rGO nanofibers (GO conc. 0.43 wt% for the latter two samples). Same as Figure 4c in Article I.

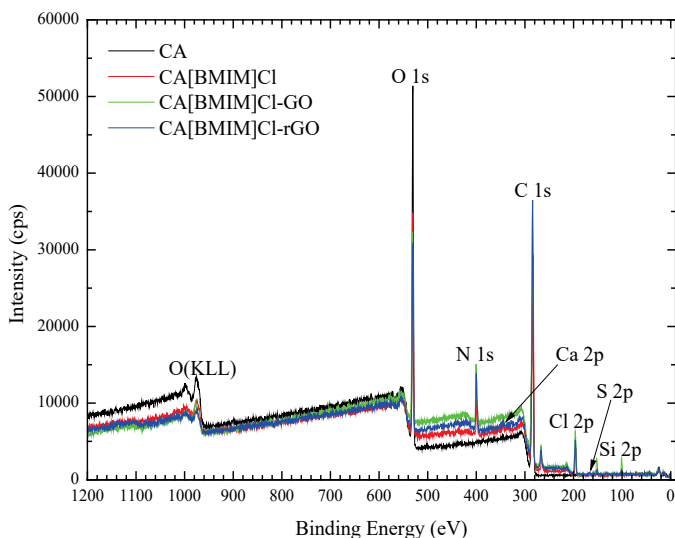


Figure 23. XPS survey spectra of CA (black), CA-[BMIM]Cl (red), CA-[BMIM]Cl-GO (green), CA-[BMIM]Cl-rGO (GO conc. 0.43 wt%, blue) same as Figure 5 in (Article I).

The sharp peak centered at 284.6 eV corresponded to C-C bonding and the relatively broad peak around 286.1 eV was attributed to three different functional groups: hydroxyl (C-OH); carbonyl (C=O), and imine (C=N). More specifically, the peaks in this region at 285.5, 285.7, 286.6 and 287.8 eV were attributed to carbon atoms in C-N, C=N, C-O, C=O, respectively.

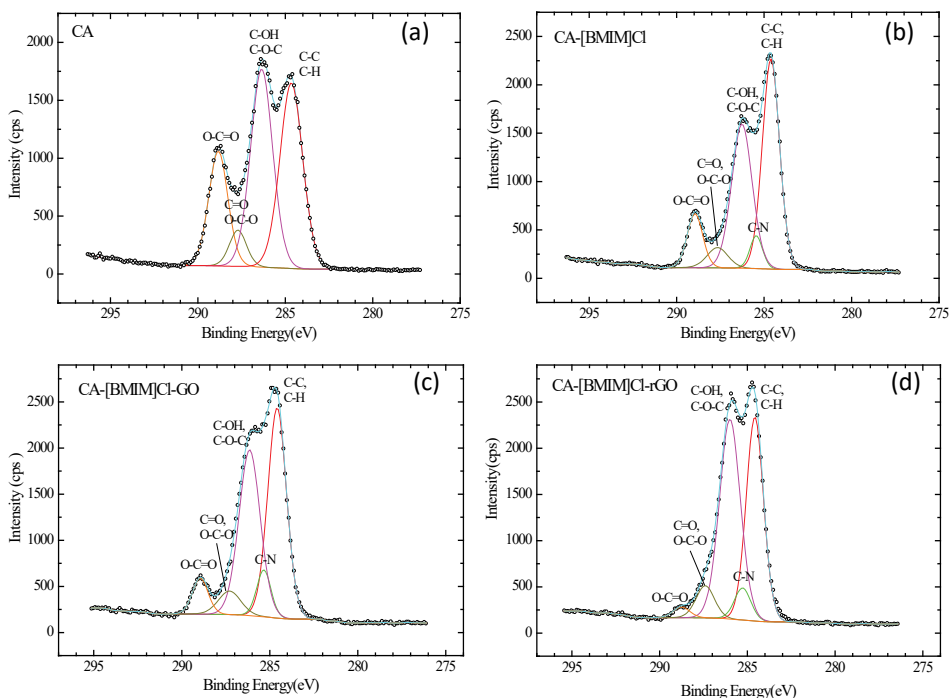


Figure 24. The C1s XPS spectra of (a) pristine CA nanofibers, (b) CA-[BMIM]Cl, (c) CA-[BMIM]Cl-GO, and (d) CA-[BMIM]Cl-rGO (GO conc. 0.43 wt%) same as Figure 6 in (Article I).

In the CA-[BMIM]Cl-rGO nanofibers, the peak centered at 288.9 eV came from the carboxyl group C(O)OH. Comparing the C 1s XPS spectra (Figure 24a and b), it can be seen that the addition of [BMIM]Cl significantly lowered the relative peak intensity of the oxygen-containing functional groups from CA, and introduced a new peak attributed to C-N from [BMIM]Cl. The introduction of GO resulted in some small changes in the relative peak intensities (comparing Figure 24b and c).

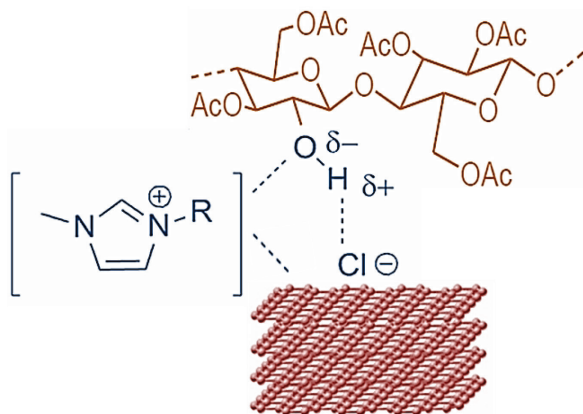


Figure 25. Schematic illustration of the suggested interaction of graphene with CA and [BMIM]Cl (Same as Figure 7 in Article I).

After the reduction of the CA-[BMIM]Cl-GO nanofibers, the C 1s spectrum of the CA-[BMIM]Cl-rGO (Figure 24d) demonstrated a dramatic decrease from the carboxyl peak. These changes suggest that the hydrazine vapor step indeed reduced the carboxyl groups in GO, but could also have partially reduced CA, while the peak intensity of the other oxygen-containing functional groups slightly increased. It is noteworthy that it has been demonstrated elsewhere that it is currently not possible to reduce GO completely by chemical reduction (Stankovich et al., 2007).

The proposed interactions of stacked graphene sheets with CA and [BMIM]Cl are schematically illustrated in Figure 25. The removal of carboxyl groups and formation of more hydroxyl groups may in turn promote the formation of hydrogen-bonds with dissociated BMIM⁺ and Cl⁻ ions, through unsubstituted hydroxyl functional groups in both GO and CA (Gross, Bell, & Chu, 2011; Isik, Sardon, & Mecerreyes, 2014). The π -electrons in the imidazole ring of BMIM⁺ may interact with the rich π -electron clouds of the graphene rings, resulting in some delocalization and enhanced electrical conductivity.

4.4 Thermal analysis of the hybrid nanofibers

Thermogravimetric analysis was carried out under argon to further examine the thermal stability and chemical bonding differences in CA, CA-[BMIM]Cl, CA-[BMIM]Cl-GO, and CA-[BMIM]Cl-rGO nanofibers. These weight loss profiles (Figure 26) demonstrated that pure CA was more stable than the composites. Pure CA decomposed in the range of 330 - 375°C with a corresponding weight loss of approximately 82 wt%. In contrast, the addition of [BMIM]Cl lowered the decomposition temperature range to 240 - 290°C with a corresponding weight loss of 85%. The addition of 0.43% GO did not cause significant change in the decomposition temperature but reduced the weight loss to ~75%.

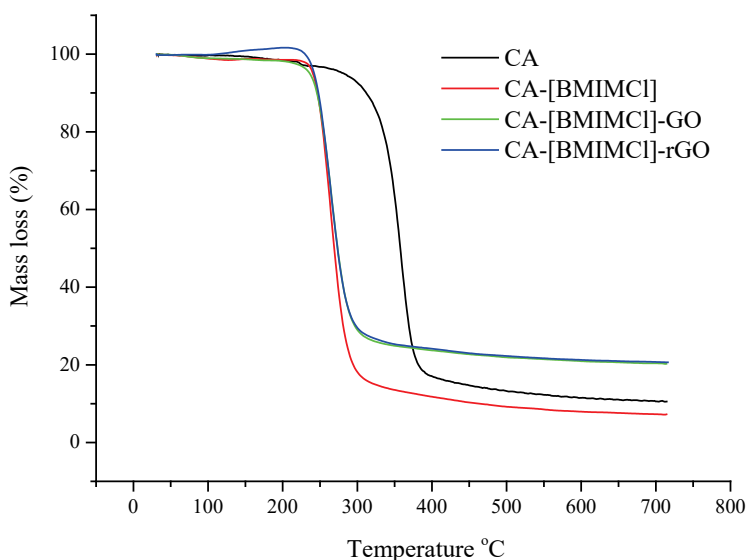


Figure 26. TGA profiles of pure CA (black), CA-[BMIM]Cl nanofibers (red), CA-[BMIM]Cl-GO nanofibers (green) and CA-[BMIM]Cl-rGO nanofibers (blue) (Same as the Figure 8 in Article I).

Reduction using hydrazine did not cause any identifiable changes in thermal decomposition or char formation. The addition of 0.43% GO did not affect the thermal

stability of the CA but introduced an effective mass transfer barrier and char formation nucleus, resulting in an increased amount of char formed. Such an enhancement could suggest that the graphene pallets were well aligned during the spinning process. The morphology, crystal structure, chemical bonding, and thermal analysis of the CA-[BMIM]Cl-GO nanofibers indicated that the graphene stacks had successfully incorporated into CA nanofibers by the dispersion of GO in a [BMIM]Cl IL. Polar functional groups, such as -C=O , -COOH and -OH on GO, not only assisted the GO's dispersion in the IL, but also facilitated strong and uniform interactions with CA in the hybrid nanofibers. The well-dispersed and strongly bonded system allowed the graphene stacks to form a continuous conductive network, achieving a drastic enhancement in electrical conductivity after reduction using hydrazine, similar to the polystyrene-GO system reported by Wu *et al.* (Wu et al., 2012). These insights indicate that this new graphene-based hybrid nanocomposite is a promising candidate for smart, flexible electronic and bio-electronic applications.

Conclusions

In summary, a new method of utilizing a [BMIM]Cl IL for the fabrication of graphene-based, bio-inspired (CA) conductive nanofibers through electrospinning has been introduced. The solution viscosity, conductivity, and the characteristics of the electrospun nanofibers were investigated. Based on the study the following conclusions can be made:

1. Adding [BMIM]Cl IL to CA spinning solution has demonstrated a substantial effect on the overall properties of the CA nanofibers such as morphology, diameter, and conductivity.
2. Nanofibers with higher concentrations of [BMIM]Cl were more uniform, and the average diameter of the fibers decreased as the concentration of IL increased.
3. 12% of [BMIM]Cl in the solution provided a uniform electrospinning process and imparted conductivity in the nanofibers produced.
4. The conductivity of the membranes changed significantly upto 2.71×10^{-7} S/cm.
5. 12% of IL produced uniform and smooth nanofibers with a diameter of 180nm.

The second part of the dissertation was based on the fabrication of conductive hybrid nanofibers by the combination of IL and GO, with CA, and the reduction of the GO nanofibers to rGO nanofibers. The conclusions from this section were as follows:

1. By mixing [BMIM]Cl, a homogeneous dispersion of GO was achieved.
2. The conductive paths were constructed by the chemical reduction of CA-[BMIM]Cl-GO nanofibers through a humidification process of hydrazine vapors, which created CA-[BMIM]Cl-rGO nanofibrous mats.
3. The incorporation of graphene oxide (from 0.11%-0.43%) into the combining matrix of CA and [BMIM]Cl greatly enhanced the nanofibers' conductivity (after the reduction process) up to 5.30×10^{-3} S/cm, at a GO content of 0.43%.
4. Furthermore, the Raman spectroscopy, XRD and FT-IR and SEM studies proved that the GO and IL was successfully incorporated inside the hybrid nanofibers.
5. The results of this current study can open new routes to further studies. A well-dispersed form of GO inside a polymeric matrix, accountable for uniform distribution of graphene sheets inside nanofibers, is a complicated process. GO stability on the solution-phase manipulation is a critical point in controlling the morphologies of the nanofibers. In this context, the solubility of GO with an appropriate loading, sonication, or mechanical mixing needs to be redesigned by exploring different types of ILs.
6. The reduction of GO-based nanofibers is definitely a key process and reducing GO-based nanofibers with high quality still remains a challenge. Several scientific experiments have been proposed; each of them has advantages and limitations. Different chemical reduction strategies have been attempted, which seek to transform the effect of the nanofibers' final performance. However, it is difficult to achieve flawless rGO through chemical reduction. Further research efforts are required, and they should be continuously carried out, in order to discover new methods for the reduction of GO-based biopolymeric nanofibers.

References

- Almecija, D., Blond, D., Sader, J. E., Coleman, J. N., & Boland, J. J. (2009). Mechanical properties of individual electrospun polymer-nanotube composite nanofibers. *Carbon*, 47(9), 2253-2258.
- An, X., Ma, H., Liu, B., & Wang, J. (2013). Graphene Oxide Reinforced Polylactic Acid/Polyurethane Antibacterial Composites. *Journal of Nanomaterials*, 7, 1-7.
- Ardeshirzadeh, B., Anaraki, N. A., Irani, M., Rad, L. R., & Shamshiri, S. (2015). Controlled release of doxorubicin from electrospun PEO/chitosan/graphene oxide nanocomposite nanofibrous scaffolds. *Materials Science and Engineering: C*, 48, 384-390.
- Arends, I. W. C. E., Gamez, P., & Sheldon, R. A. (2006). Green oxidation of alcohols using biomimetic Cu complexes and Cu enzymes as catalysts. In R. Van Eldik & J. Reedijk (Eds.), *Advances in Inorganic Chemistry* (Vol. 58, pp. 235-279). Cambridge, MA: Academic Press.
- Bao, C. (2015). Cellulose acetate / plasticizer systems: Structure, morphology and dynamics (Doctoral dissertation, Université Claude Bernard - Lyon I).
- Bao, Q., Zhang, H., Yang, J-X., Wang, S., Tang, D. Y., Jose, R., ... & Loh, K. P. (2010). Graphene-Polymer Nanofiber Membrane for Ultrafast Photonics. *Advanced Functional Materials*, 20(5), 782-791.
- Bhardwaj, N., & Kundu, S. C. (2010). Electrospinning: A fascinating fiber fabrication technique. *Biotechnology Advances*, 28(3), 325-347.
- Bridge, J. C., Aylott, J. W., Brightling, C. E., Ghaemmaghami, A. M., Knox, A. J., Lewis, M. P., ... & Morris, G. E. (2015). Adapting the electrospinning process to provide three unique environments for a tri-layered in vitro model of the airway wall. *Journal of Visualized Experiments*, 101, 1-11.
- Brodie, B. C. (1859). XIII. On the atomic weight of graphite. *Royal Society* 149, 249-259.
- Brown, R. M. (1996). The Biosynthesis of Cellulose. *Journal of Macromolecular Science, Part A*, 33(10), 1345-1373.
- Claramunt, S., Varea, A., López-Díaz, D., Velázquez, M. M., Cornet, A., & Cirera, A. (2015). The Importance of Interbands on the Interpretation of the Raman Spectrum of Graphene Oxide. *The Journal of Physical Chemistry C*, 119(18), 10123-10129.
- Cooley, J. F. (1902). *US Patent No.US692631A*. Alexandria, USA: U.S. Patent and Trademark Office.
- Deka, M., & Kumar, A. (2010). *Nanofiber Reinforced Composite Polymer Electrolyte Membranes* (Ch. 02). London, United Kingdom: InTech.
- Dharaskar, S. A., Varma, M. N., Shende, D. Z., Yoo, C. K., & Wasewar, K. L. (2013). Synthesis, Characterization and Application of 1-Butyl-3 Methylimidazolium Chloride as Green Material for Extractive Desulfurization of Liquid Fuel. *The Scientific World Journal*, 12, 1-9.
- Ding, R., Luo, Z., Ma, X., Fan, X., Xue, L., Lin, X., & Chen, S. (2015). High Sensitive Sensor Fabricated by Reduced Graphene Oxide/Polyvinyl Butyral Nanofibers for Detecting Cu (II) in Water. *International Journal of Analytical Chemistry*, 16, 1-7.
- Dong, H. S., & Qi, S. J. (2015). Realising the potential of graphene-based materials for biosurfaces – A future perspective. *Biosurface and Biotribology*, 1(4), 229-248.

- Dong, Q., Wang, G., Qian, B., Hu, C., Wang, Y., & Qiu, J. (2014). Electrospun Composites Made of Reduced Graphene Oxide and Activated Carbon Nanofibers for Capacitive Deionization. *Electrochimica Acta*, *137*, 388-394.
- Duverger, C., Nedelec, J. M., Benatsou, M., Bouazaoui, M., Capoen, B., Ferrari, M., & Turrell, S. (1999). Waveguide Raman spectroscopy: A non-destructive tool for the characterization of amorphous thin films. *Journal of Molecular Structure*, *480-481*, 169-178.
- Feldman, D. (2015). Cellulose Nanocomposites. *Journal of Macromolecular Science, Part A*, *52*(4), 322-329.
- Geim, A. K. (2009). Graphene: Status and Prospects. *Science*, *324*(5934), 1530-1534.
- Geim, A. K., & Novoselov, K. S. (2007). The rise of graphene. *Nat Mater*, *6*(3), 183-191.
- Gouda, M., & Abu-Abdeen, M. (2017). Highly conductive cellulosic nanofibers for efficient water desalination. *Fibers and Polymers*, *18*(11), 2111-2117.
- Gross, A. S., Bell, A. T., & Chu, J-W. (2011). Thermodynamics of Cellulose Solvation in Water and the Ionic Liquid 1-Butyl-3-Methylimidazolium Chloride. *The Journal of Physical Chemistry B*, *115*(46), 13433-13440.
- Gu, H., Huang, Y., Zuo, L., Fan, W., & Liu, T. (2016). Graphene sheets wrapped carbon nanofibers as a highly conductive three-dimensional framework for perpendicularly anchoring of MoS₂: Advanced electrocatalysts for hydrogen evolution reaction. *Electrochimica Acta*, *219*, 604-613.
- Gudkova, V., Krumme, A., Märtson, T., Rikko, M., Tarasova, E., Savest, N., & Viirsalu, M. (2015). 1-butyl-3-methylimidazolium chloride assisted electrospinning of SAN/MWCNTs conductive reinforced composite membranes. *Journal of Electrostatics*, *78*, 11-16.
- Hu, K., Kulkarni, D. D., Choi, I., & Tsukruk, V. V. (2014). Graphene-polymer nanocomposites for structural and functional applications. *Progress in Polymer Science*, *39*(11), 1934-1972.
- Huang, Y-L., Baji, A., Tien, H-W., Yang, Y-K., Yang, S-Y., Wu, S-Y., ... & Wang, N-H. (2012). Self-assembly of silver-graphene hybrid on electrospun polyurethane nanofibers as flexible transparent conductive thin films. *Carbon*, *50*(10), 3473-3481.
- Huang, Z-M., Zhang, Y. Z., Kotaki, M., & Ramakrishna, S. (2003). A review on polymer nanofibers by electrospinning and their applications in nanocomposites. *Composites Science and Technology*, *63*(15), 2223-2253.
- Huddleston, J. G., Visser, A. E., Reichert, W. M., Willauer, H. D., Broker, G. A., & Rogers, R. D. (2001). Characterization and comparison of hydrophilic and hydrophobic room temperature ionic liquids incorporating the imidazolium cation. *Green Chemistry*, *3*(4), 156-164.
- Hummers, W. S., & Offeman, R. E. (1958). Preparation of Graphitic Oxide. *Journal of the American Chemical Society*, *80*(6), 1339-1339.
- Isik, M., Sardon, H., & Mecerreyes, D. (2014). Ionic Liquids and Cellulose: Dissolution, Chemical Modification and Preparation of New Cellulosic Materials. *International Journal of Molecular Sciences*, *15*(7), 11922-11940.
- Jeong, J. S., Moon, J. S., Jeon, S. Y., Park, J. H., Alegaonkar, P. S., & Yoo, J. B. (2007). Mechanical properties of electrospun PVA/MWNTs composite nanofibers. *Thin Solid Films*, *515*(12), 5136-5141.

- Jin, L., Wu, D., Kuddannaya, S., Zhang, Y., & Wang, Z. (2016). Fabrication, Characterization, and Biocompatibility of Polymer Cored Reduced Graphene Oxide Nanofibers. *ACS Applied Materials & Interfaces*, 8(8), 5170-5177.
- Jorio, A., Ferreira, E. H. M., Moutinho, M. V. O., Stavale, F., Achete, C. A., & Capaz, R. B. (2010). Measuring disorder in graphene with the G and D bands. *physica status solidi (b)*, 247(11-12), 2980-2982.
- Kaplan, D. L. (Ed.) (1998). *Biopolymers from Renewable Resources*. Berlin, Germany: Springer.
- Kaszyńska, J., Rachocki, A., Bielejewski, M., & Tritt-Goc, J. J. C. (2017). Influence of cellulose gel matrix on BMIMCl ionic liquid dynamics and conductivity. *24(4)*, 1641-1655.
- Kudin, K. N., Ozbas, B., Schniepp, H. C., Prud'homme, R. K., Aksay, I. A., & Car, R. (2008). Raman Spectra of Graphite Oxide and Functionalized Graphene Sheets. *Nano Letters*, 8(1), 36-41.
- Kuzmenko, V., Wang, N., Haque, M., Naboka, O., Flygare, M., Svensson, K., ... & Enoksson, P. (2017). Cellulose-derived carbon nanofibers/graphene composite electrodes for powerful compact supercapacitors. *RSC Advances*, 7(73), 45968-45977.
- Lavanya, T., Satheesh, K., Dutta, M., Victor Jaya, N., & Fukata, N. (2014). Superior photocatalytic performance of reduced graphene oxide wrapped electrospun anatase mesoporous TiO₂ nanofibers. *Journal of Alloys and Compounds*, 615, 643-650.
- Leach, M. K., Feng, Z-Q., Tuck, S. J., & Corey, J. M. (2011). Electrospinning Fundamentals: Optimizing Solution and Apparatus Parameters. *Journal of Visualized Experiments*, 6(47), 1-4.
- Lee, H., Nishino, M., Sohn, D., Lee, J. S., & Kim, I. S. J. C. (2018). Control of the morphology of cellulose acetate nanofibers via electrospinning. *Cellulose* 25(5), 2829-2837.
- Liu, M., Du, Y., Miao, Y-E., Ding, Q., He, S., Tjiu, W. W., ... & Liu, T. (2015). Anisotropic conductive films based on highly aligned polyimide fibers containing hybrid materials of graphene nanoribbons and carbon nanotubes. *Nanoscale*, 7(3), 1037-1046.
- Liu, Z., Wang, H., Li, Z., Lu, X., Zhang, X., Zhang, S., & Zhou, K. (2011). Characterization of the regenerated cellulose films in ionic liquids and rheological properties of the solutions. *Materials Chemistry and Physics*, 128(1-2), 220-227.
- Mahdiah, Z. M., Mottaghitalab, V., Piri, N., & Haghi, A. K. (2012). Conductive chitosan/multi walled carbon nanotubes electrospun nanofiber feasibility. *Korean Journal of Chemical Engineering*, 29(1), 111-119.
- Malard, L. M., Pimenta, M. A., Dresselhaus, G., & Dresselhaus, M. S. (2009). Raman spectroscopy in graphene. *Physics Reports*, 473(5-6), 51-87.
- Marsh, K. N., Boxall, J. A., & Lichtenthaler, R. (2004). Room temperature ionic liquids and their mixtures—a review. *Fluid Phase Equilibria*, 219(1), 93-98.
- Massoumi, B., Ghandomi, F., Abbasian, M., Eskandani, M., & Jaymand, M. (2016). Surface functionalization of graphene oxide with poly(2-hydroxyethyl methacrylate)-graft-poly(ϵ -caprolactone) and its electrospun nanofibers with gelatin. *Applied Physics A*, 122(12), 1000.
- Matin, M., Masoud, S., Shadie, H., Soheila, Z., Parviz, R., Manouchehr, V., & Simzar, H. (2016). The different fate of satellite cells on conductive composite electrospun nanofibers with graphene and graphene oxide nanosheets. *Biomedical Materials*, 11(2), 1-12.

- Matsumoto, H., Imaizumi, S., Konosu, Y., Ashizawa, M., Minagawa, M., Tanioka, A., ... & Tour, J. M. (2013). Electrospun Composite Nanofiber Yarns Containing Oriented Graphene Nanoribbons. *ACS Applied Materials & Interfaces*, 5(13), 6225-6231.
- Miyauchi, M., Miao, J., Simmons, T. J., Lee, J-W., Doherty, T. V., Dordick, J. S., & Linhardt, R. J. (2010). Conductive Cable Fibers with Insulating Surface Prepared by Coaxial Electrospinning of Multiwalled Nanotubes and Cellulose. *Biomacromolecules*, 11(9), 2440-2445.
- Mizuno, K., Imafuji, S., Ochi, T., Ohta, T., & Maeda, S. (2000). Hydration of the CH Groups in Dimethyl Sulfoxide Probed by NMR and IR. *The Journal of Physical Chemistry B*, 104(47), 11001-11005.
- Moayeri, A., & Ajji, A. (2015). Fabrication of polyaniline/poly(ethylene oxide)/non-covalently functionalized graphene nanofibers via electrospinning. *Synthetic Metals*, 200, 7-15.
- Moayeri, A., & Ajji, A. (2016). Core-Shell Structured Graphene Filled Polyaniline/Poly (methyl methacrylate) Nanofibers by Coaxial Electrospinning. *Nanoscience and Nanotechnology Letters*, 8(2), 129-134.
- Mohanty, A. K., Misra, M., & Drzal, L. T. (2002). Sustainable Bio-Composites from Renewable Resources: Opportunities and Challenges in the Green Materials World. *Journal of Polymers and the Environment*, 10(1), 19-26.
- Nain, A. S., Wong, J. C., Amon, C., & Sitti, M. (2006). Drawing suspended polymer micro-/nanofibers using glass micropipettes. *Applied Physics Letters*, 89(18), 183105.
- Novoselov, K. S., Falko, V. I., Colombo, L., Gellert, P. R., Schwab, M. G., & Kim, K. (2012). A roadmap for graphene. *Nature*, 490(7419), 192-200.
- Novoselov, K. S., Geim, A. K., Morozov, S. V., Jiang, D., Zhang, Y., Dubonos, S. V., ... & Firsov, A. A. (2004). Electric Field Effect in Atomically Thin Carbon Films. *Science*, 306(5696), 666-669.
- Pant, H. R., Park, C. H., Tijing, L. D., Amarjargal, A., Lee, D-H., & Kim, C. S. (2012). Bimodal fiber diameter distributed graphene oxide/nylon-6 composite nanofibrous mats via electrospinning. *Colloids and Surfaces A: Physicochemical and Engineering Aspects*, 407, 121-125.
- Pant, H. R., Pokharel, P., Joshi, M. K., Adhikari, S., Kim, H. J., Park, C. H., & Kim, C. S. (2015). Processing and characterization of electrospun graphene oxide/polyurethane composite nanofibers for stent coating. *Chemical Engineering Journal*, 270, 336-342.
- Park, S., An, J., Jung, I., Piner, R. D., An, S. J., Li, X., ... & Ruoff, R. S. (2009). Colloidal suspensions of highly reduced graphene oxide in a wide variety of organic solvents. *Nano Letters*, 9(4), 1593-1597.
- Peng, H., Meng, L., Niu, L., & Lu, Q. (2012). Simultaneous Reduction and Surface Functionalization of Graphene Oxide by Natural Cellulose with the Assistance of the Ionic Liquid. *The Journal of Physical Chemistry C*, 116(30), 16294-16299.
- Peng, R., Wang, Y., Tang, W., Yang, Y., & Xie, X. (2013). Progress in Imidazolium Ionic Liquids Assisted Fabrication of Carbon Nanotube and Graphene Polymer Composites. *Polymers*, 5(2), 847-872.
- Priyadarsini, S., Mohanty, S., Mukherjee, S., Basu, S., & Mishra, M. J. J. o. N. i. C. (2018). Graphene and graphene oxide as nanomaterials for medicine and biology application. *Journal of Nanostructure in Chemistry*, 8(2), 123-137.

- Puerto, E. d., Cuesta, A., Sanchez-Cortes, S., Garcia-Ramos, J. V., & Domingo, C. (2013). Electrochemical SERS study on a copper electrode of the insoluble organic pigment quinacridone quinone using ionic liquids (BMIMCl and TBAN) as dispersing agents. *Analyst*, *138*(16), 4670-4676.
- Puls, J., Wilson, S. A., Höltzer, D. (2011). Degradation of Cellulose Acetate-Based Materials: A Review. *Journal of Polymers and the Environment*, *19*(1), 152-165.
- Qi, Y. Y., Tai, Z. X., Sun, D. F., Chen, J. T., Ma, H. B., Yan, X. B., ... & Xue, Q. J. (2013). Fabrication and characterization of poly(vinyl alcohol)/graphene oxide nanofibrous biocomposite scaffolds. *Journal of Applied Polymer Science*, *127*(3), 1885-1894.
- Rabah, M. A. (2017). Lead, zinc and copper fine powder with controlled size and shape. *AIMS Materials Science*, *4*(6), 1358-1371.
- Ramakrishna, S. (2005). *An Introduction to Electrospinning and Nanofibers* (pp. 1-21). Singapore, Singapore: World Scientific.
- Ramazani, S., & Karimi, M. (2016). Electrospinning of poly(ϵ -caprolactone) solutions containing graphene oxide: Effects of graphene oxide content and oxidation level. *Polymer Composites*, *37*(1), 131-140.
- Reneker, D. H., & Yarin, A. L. (2008). Electrospinning jets and polymer nanofibers. *Polymer*, *49*(10), 2387-2425.
- Rezaei, A., Nasirpour, A., & Fathi, M. (2015). Application of Cellulosic Nanofibers in Food Science Using Electrospinning and Its Potential Risk. *Comprehensive Reviews in Food Science and Food Safety*, *14*(3), 269-284.
- Rzayev, Z. M. O., Salimi, K., Bunyatova, U., Acar, S., Salamov, B., & Turk, M. (2016). Fabrication and characterization of PVA/ODA-MMT-poly(MA-alt-1-octadecene)-g-graphene oxide e-spun nanofiber electrolytes and their response to bone cancer cells. *Materials Science and Engineering: C*, *61*, 257-268.
- Sánchez-Márquez, J. A., Fuentes-Ramírez, R., Cano-Rodríguez, I., Gamiño-Arroyo, Z., Rubio-Rosas, E., Kenny, J. M., & Rescignano, N. (2015). Membrane Made of Cellulose Acetate with Polyacrylic Acid Reinforced with Carbon Nanotubes and Its Applicability for Chromium Removal. *International Journal of Polymer Science*, *2015*, 1-12.
- Satoshi, H., Ryosuke, O., & Hiro-o, H. (2003). Raman Spectra, Crystal Polymorphism, and Structure of a Prototype Ionic-liquid [bmim]Cl. *Chemistry Letters*, *32*(6), 498-499.
- Scherer, J. R., Bailey, G. F., Kint, S., Young, R., Malladi, D. P., & Bolton, B. (1985). Water in polymer membranes. 4. Raman scattering from cellulose acetate films. *The Journal of Physical Chemistry*, *89*(2), 312-319.
- Schiffman, J. D., & Schauer, C. L. (2008). A Review: Electrospinning of Biopolymer Nanofibers and their Applications. *Polymer Reviews*, *48*(2), 317-352.
- Seifert, M., Hesse, S., Kabrelian, V., & Klemm, D. (2004). Controlling the water content of never dried and reswollen bacterial cellulose by the addition of water-soluble polymers to the culture medium. *Journal of Polymer Science Part A: Polymer Chemistry*, *42*(3), 463-470.
- Shilpa, Basavaraja, B. M., Majumder, S. B., & Sharma, A. (2015). Electrospun hollow glassy carbon-reduced graphene oxide nanofibers with encapsulated ZnO nanoparticles: A free standing anode for Li-ion batteries. *Journal of Materials Chemistry A*, *3*(10), 5344-5351.

- Shin, Y. C., Lee, J. H., Jin, L., Kim, M. J., Kim, Y-J., Hyun, J. K., ... & Han, D-W. (2015). Stimulated myoblast differentiation on graphene oxide-impregnated PLGA-collagen hybrid fibre matrices. *Journal of Nanobiotechnology*, 13(1), 1-11.
- Soldano, C., Mahmood, A., & Dujardin, E. (2010). Production, properties and potential of graphene. *Carbon*, 48(8), 2127-2150.
- Song, J., Gao, H., Zhu, G., Cao, X., Shi, X., & Wang, Y. (2015). The preparation and characterization of polycaprolactone/graphene oxide biocomposite nanofiber scaffolds and their application for directing cell behaviors. *Carbon*, 95, 1039-1050.
- Stankovich, S., Dikin, D. A., Piner, R. D., Kohlhaas, K. A., Kleinhammes, A., Jia, Y., ... & Ruoff, R. S. (2007). Synthesis of graphene-based nanosheets via chemical reduction of exfoliated graphite oxide. *Carbon*, 45(7), 1558-1565.
- Subbiah, T., Bhat, G. S., Tock, R. W., Parameswaran, S., & Ramkumar, S. S. (2005). Electrospinning of nanofibers. *Journal of Applied Polymer Science*, 96(2), 557-569.
- Suwantong, O., & Supaphol, P. (2015). Applications of Cellulose Acetate Nanofiber Mats. In J. K. Pandey, H. Takagi, A. N. Nakagaito, & H-J. Kim (Eds.), *Handbook of Polymer Nanocomposites. Processing, Performance and Application* (pp. 355-368). Berlin, Germany Springer.
- Swatloski, R. P., Spear, S. K., Holbrey, J. D., & Rogers, R. D. (2002). Dissolution of Cellulose with Ionic Liquids. *Journal of the American Chemical Society*, 124(18), 4974-4975.
- Tan, L., Gan, L., Hu, J., Zhu, Y., & Han, J. (2015). Functional shape memory composite nanofibers with graphene oxide filler. *Composites Part A: Applied Science and Manufacturing*, 76, 115-123.
- Tang, X., Yan, F., Wei, Y., Zhang, M., Wang, T., & Zhang, T. (2015). Encapsulating SnxSb Nanoparticles in Multichannel Graphene-Carbon Fibers As Flexible Anodes to Store Lithium Ions with High Capacities. *ACS Applied Materials & Interfaces*, 7(39), 21890-21897.
- Torres-Giner, S., Pérez-Masiá, R., & Lagaron, J. M. (2016). A review on electrospun polymer nanostructures as advanced bioactive platforms. *Polymer Engineering & Science*, 56(5), 500-527.
- Tripathi, S. N., Rao, G. S. S., Mathur, A. B., & Jasra, R. (2017). Polyolefin/graphene nanocomposites: A review. *RSC Advances*, 7(38), 23615-23632.
- Tungprapa, S., Puangparn, T., Weerasombut, M., Jangchud, I., Fakum, P., Semongkhon, S., ... & Supaphol, P. J. C. (2007). Electrospun cellulose acetate fibers: Effect of solvent system on morphology and fiber diameter. *Cellulose*, 14(6), 563-575.
- Van de Ven, T. G. M. (Ed.) (2013). *Cellulose: Medical, Pharmaceutical and Electronic Applications* (Ch. 08). London, United Kingdom: InTech.
- Wahab, I. F., Razak, S. I. A., Azmi, N. S., Dahli, F. N., Yusof, A. H. M., & Nayan, N. H. M. (2016). Electrospun Graphene Oxide-Based Nanofibres. In A. M. T. Silva & S. A. C. Carabineiro (Eds.), *Advances in Carbon Nanostructures* (Ch. 05). London, United Kingdom: InTech.
- Wang, C., Li, Y., Ding, G., Xie, X., & Jiang, M. (2013). Preparation and characterization of graphene oxide/poly(vinyl alcohol) composite nanofibers via electrospinning. *Journal of Applied Polymer Science*, 127(4), 3026-3032.

- Wang, G., Dong, Q., Wu, T., Zhan, F., Zhou, M., & Qiu, J. (2016). Ultrasound-assisted preparation of electrospun carbon fiber/graphene electrodes for capacitive deionization: Importance and unique role of electrical conductivity. *Carbon*, *103*, 311-317.
- Wang, Y., Tang, J., Xie, S., Liu, J., Xin, Z., Liu, X., & Belfiore, L. A. (2015). Leveling graphene sheets through electrospinning and their conductivity. *RSC Advances*, *5*(52), 42174-42177.
- Wang, Z., Wu, S., Zhang, J., Chen, P., Yang, G., Zhou, X., ... Zhang, H. (2012). Comparative studies on single-layer reduced graphene oxide films obtained by electrochemical reduction and hydrazine vapor reduction. *Nanoscale Research Letters*, *7*(1), 1-7.
- Wu, N., She, X., Yang, D., Wu, X., Su, F., & Chen, Y. (2012). Synthesis of network reduced graphene oxide in polystyrene matrix by a two-step reduction method for superior conductivity of the composite. *Journal of Materials Chemistry*, *22*(33), 17254-17261.
- Xia, X., Yao, Y., Gong, M., Wang, H., & Zhang, Y. (2014). Rheological behaviors of cellulose/[BMIM]Cl solutions varied with the dissolving process. *Journal of Polymer Research*, *21*(7), 1-7.
- Xu, Z-L., Zhang, B., & Kim, J-K. (2014). Electrospun carbon nanofiber anodes containing monodispersed Si nanoparticles and graphene oxide with exceptional high rate capacities. *Nano Energy*, *6*, 27-35.
- Xu, Z-L., Zhang, B., Zhou, Z-Q., Abouali, S., Akbari Garakani, M., Huang, J., ... & Kim, J-K. (2014). Carbon nanofibers containing Si nanoparticles and graphene-covered Ni for high performance anodes in Li ion batteries. *RSC Advances*, *4*(43), 22359-22366.
- Yang, K. S., & Kim, B-H. (2015). Highly conductive, porous RuO₂/activated carbon nanofiber composites containing graphene for electrochemical capacitor electrodes. *Electrochimica Acta*, *186*, 337-344.
- Yang, T., Wu, D., Lu, L., Zhou, W., & Zhang, M. (2011). Electrospinning of polylactide and its composites with carbon nanotubes. *Polymer Composites*, *32*(8), 1280-1288.
- Yao, S., Li, Y., Zhou, Z., & Yan, H. (2015). Graphene oxide-assisted preparation of poly(vinyl alcohol)/carbon nanotube/reduced graphene oxide nanofibers with high carbon content by electrospinning technology. *RSC Advances*, *5*(111), 91878-91887.
- Yoon, O. J., Jung, C. Y., Sohn, I. Y., Kim, H. J., Hong, B., Jhon, M. S., & Lee, N-E. (2011). Nanocomposite nanofibers of poly(D, L-lactic-co-glycolic acid) and graphene oxide nanosheets. *Composites Part A: Applied Science and Manufacturing*, *42*(12), 1978-1984.
- Youn, S. C., Geng, J., Son, B. S., Yang, S. B., Kim, D. W., Cho, H. M., & Jung, H-T. (2011). Effect of the Exposure Time of Hydrazine Vapor on the Reduction of Graphene Oxide Films. *Journal of Nanoscience and Nanotechnology*, *11*(7), 5959-5964.
- Yuan, Q. (2004). Intumescent Mechanisms of Fire-retarding polyurethane systems and development of graphite/polymer nano-composites (Doctoral dissertation, Nottingham Trent University, Nottingham, United Kingdom).
- Yuan-Li, H., Avinash, B., Hsi-Wen, T., Ying-Kui, Y., Shin-Yi, Y., Chen-Chi, M. M., ... & Nian-Hau, W. (2011). Self-assembly of graphene onto electrospun polyamide 66 nanofibers as transparent conductive thin films. *Nanotechnology*, *22*(47), 1-7.
- Zavgorodnya, O., Shamshina, J. L., Bonner, J. R., & Rogers, R. D. (2017). Electrospinning Biopolymers from Ionic Liquids Requires Control of Different Solution Properties than Volatile Organic Solvents. *ACS Sustainable Chemistry & Engineering*, *5*(6), 5512-5519.

Zhang, B., Xu, Z-L., & Kim, J-K. (2014). In situ grown graphitic carbon/Fe₂O₃/carbon nanofiber composites for high performance freestanding anodes in Li-ion batteries. *RSC Advances*, 4(24), 12298-12301.

Zhang, C., Wang, L., Zhai, T., Wang, X., Dan, Y., & Turng, L-S. (2016). The surface grafting of graphene oxide with poly(ethylene glycol) as a reinforcement for poly(lactic acid) nanocomposite scaffolds for potential tissue engineering applications. *Journal of the Mechanical Behavior of Biomedical Materials*, 53, 403-413.

Zhao, X., Zhang, Q., Chen, D., & Lu, P. (2010). Enhanced Mechanical Properties of Graphene-Based Poly(vinyl alcohol) Composites. *Macromolecules*, 43(5), 2357-2363.

Acknowledgements

All tribute and gratitude are for Almighty "ALLAH" (عزوجل) The Glorious and Forgiving and His messenger Muhammad (صلى الله عليه واله وسلم) who is persistently a source of leadership and facts for mankind. I feel honored to express my bottomless sense of gratitude towards my supervisor Professor Andres Krumme whose supervision, assistance, and valued suggestions have assisted me in my achievement of this goal. In spite of his busy routine, he has stayed with me in every difficult situation.

I am also grateful towards Malle Krunks, the director of Department of Material and Environmental Technology, and all the staff members of the Department of Material and Environmental Technology, TalTech for their support with all my problems in my PhD course. I express my gratefulness to Prof. Paul D. Topham and Dr. Qingchun Yuan, who gave me an opportunity to work at the Aston Institute of Materials Research (AIMR), Aston University, Birmingham, UK. I am also grateful to Dr. Tiia Plamus, Dr. Viktoria Vassiljeva, Dr. Elvira Tarasova, and Dr. Natalja Savest for their laboratory support. I am grateful to Dr. Illia Krasnou for his generous backing in research activities.

I acknowledge Prof. Arvo Mere, Prof. Valdek Mikli, Dr. Mati Danilson, Prof. Tiit Kaljuvee, and Dr. Sven Lange for their help in characterizations of nanofibers. It was my privilege to have good friends and colleagues here at TalTech, especially the laboratory engineer Dr. Mihkel Viirsalu. I express my happiness for the friendly cooperation and inspiration of my friend Tea-mall Krumme, whom I often call my Estonia mother.

I am also very thankful to all the members of our group. They are the source of courage for me to accomplish my tasks. Last but not least, I want to express my obligation to my loving wife, mother and father, sisters and others who consistently stood beside me in critical situations. Their optimistic love enhanced my conscientious to achieve my goal. Estonian state scholarship and the Archimedes Foundation has always played a leading role in developing research work in Estonia. I acknowledge their financial support during my PhD studies.

Abstract

Electrospinning of Nanofibrous Composites of Cellulose Acetate with Ionic Liquids and Graphene Oxide

Using synthetic polymers, graphene-based conductive nanofibers have been widely prepared through electrospinning, whereas electrospun graphene-biopolymer nanofibers have been rarely reported, due to the poor compatibility of graphene with biopolymers. Most biopolymers from renewable resources, such cellulose, have been considered to be excellent matrices for nanocomposites. Biopolymers have properties such as bio-compatibility, biodegradability, and multiple functional groups. They are also one of the most abundant polymers on earth. All these factors make them superior to synthetic polymers.

Owing to its high electrical conductivity, graphene has been incorporated into polymeric nanofibers for the creation of advanced materials for flexible electronics and sensors. In this PhD, a new method was devised for the preparation of graphene-biopolymer nanofibers using the judicious combination of an ionic liquid and graphene, followed by the versatile technique called electrospinning. Ionic liquids improve both the dispersion of the carbonous constituent in the biopolymer matrix and conductivity of the fibres.

To fabricate conductive composite nanofibers (CA-[BMIM]Cl-GO), cellulose acetate was used as the biopolymer, GO nanoparticles was the source of graphene, while 1-butyl-3-methylimidazolium chloride ([BMIM]Cl) was used as the ionic liquid. Two solvents, acetone (AC) and dimethylacetamide (DMAc) with the volume ratio of 2:1 AC: DMAc were used as a versatile solvent mixture for electrospinning. A fixed weight ratio of 17% of cellulose acetate with different ratios of [BMIM]Cl (0-12%) and GO (wt%, 0.25%, 0.50%, 0.75%, 1%) were used in the electrospinning solutions. Moreover, a new route was developed for the conversion of CA-[BMIM]Cl-GO nanofibers to reduced GO nanofibers, using hydrazine vapour under ambient conditions to enhance the electrical conductivity of the composite nanofibers. During the characterization of the composite nanofibers, graphene sheets were demonstrated to have been uniformly incorporated into the matrix. 0.43 wt% of GO (after reduction) was enough to increase the electrical conductivity of CA-[BMIM]Cl nanofibers by more than four orders of magnitude (from 2.71×10^{-7} S/cm to 5.30×10^{-3} S/cm). This ultra-high enhancement opens up a new route for the conductive enhancement of biopolymer nanofibers, to be used in smart (bio) electronic devices.

Lühikokkuvõte

Tselluloosatsetaadi, ionsete vedelike ja grafeenoksiidi nanokiuliste komposiitide elektroketrus

Süntetilistel polümeeridel ja grafeenil põhinevaid nanokiude on elektroketruse teel laialdaselt valmistatud. Grafeenil ja biopolümeeridel põhinevate nanokiudude kohta on samas informatsiooni vähe kuna grafeenil ja biopolümeeridel on halb kokkusobivus. Enamikkü taastuvatel loodusvaradel põhinevaid biopolümeere, nagu näiteks tselluloos, on siiski käsitletud suurepärase nanokomposiitide maatriksina. Biopolümeeride omadused, nagu bioloogiline kokkusobivus, bioloogiline lagunevus ja paljude funktsionaalsete rühmade esinemine ning laialdane levik, muudavad need sünteetiliste polümeeridega võrreldes eelistatuks.

Kõrge elektrijuhtivuse tõttu lisatakse grafeeni polümeeridesse nanokiududesse, millest valmistatakse painduvaid elektroonikaseadmeid ja sensoreid. Käesolevas doktoritöös töötati välja grafeenil ja biopolümeeridel põhinevate nanokiudude valmistamise meetod kasutades ionsete vedelike (IL) ja grafeeni hoolikalt planeeritud kombineerimist elektroketrusprotsessis. IL parandab süsinikupõhise lisandi dispergeerimist biopolümeeri maatriksis ja suurendab kiudude juhtivust. Juhtivate nanokiuliste komposiitide (CA-[BMIM]Cl-GO) valmistamiseks kasutati biopolümeerina tselluloosatsetaati (CA), grafeenoksiidi (GO) nanoosakeste allikana ja 1-butüül-3-metüülimidasoolkloriidi ([BMIM]Cl) ioonse vedelikuna.

Elektroketruslahuste valmistamiseks kasutati kahte lahustit, atsetooni (AC) ja dimetüülatsetaamiidi (DMAc) mahusuhtes 2:1 AC:DMAc. Elektroketruslahustes kasutati fikseeritud CA kogust 17 massi-%, [BMIM]Cl muutuvat kogust 0-12 massi-% ja GO muutuvat kogust 0,25, 0,50, 0,75 või 1,00 massiprotsenti.

CA-[BMIM]Cl-GO nanokiuliste komposiitide elektrijuhtivuse parandamiseks töötati välja uus meetod GO redutseerimiseks normaaltingimustes hüdrasiini aurudega, et muuta GO põhine komposiit redutseeritud GO põhiseks komposiidiks. Nanokiuliste komposiitide analüüs näitas, et grafeeni lehed on maatriksis ühtlaselt jaotunud ja ainult 0,43 massi-% GO lisamine suurendab CA-[BMIM]Cl nanokiudude elektrijuhtivust (peale redutseerimist) enam kui nelja suurusjärgu võrra (esialgselt väärtuselt 2.71×10^{-7} S/cm väärtuseni 5.30×10^{-3} S/cm). Selline suur juhtivuse kasv loob uued võimalused biopolümeeridel põhinevate nanokiudude juhtivuse suurendamiseks ja nende kasutamiseks nutikates (bio)elektroonilistes seadmetes.

Appendix A

A. I. Publications

Publication I

Javed, K.; Krumme, A.; Viirsalu, M.; Krasnou, I.; Plamus, T.; Vassiljeva, V.; Tarasova, E.; Savest, N.; Mere, A.; Mikli, V.; Danilson, M.; Kaljuvee, T.; Lange, S.; Yuan, Q.; Topham, P. D.; Chen, C.-M. (2018). A method for producing conductive graphene biopolymer nanofibrous fabrics by exploitation of an ionic liquid dispersant in electrospinning. *Carbon*, 140, 148–156.



ELSEVIER

Contents lists available at ScienceDirect

Carbon

journal homepage: www.elsevier.com/locate/carbon

A method for producing conductive graphene biopolymer nanofibrous fabrics by exploitation of an ionic liquid dispersant in electrospinning

Kashif Javed ^{a, b, *}, Andres Krumme ^a, Mihkel Viirsalu ^a, Illia Krasnou ^a, Tiia Plamus ^a, Viktoria Vassiljeva ^a, Elvira Tarasova ^a, Natalja Savest ^a, Arvo Mere ^a, Valdek Mikli ^a, Mati Danilson ^a, Tiit Kaljuvee ^a, Sven Lange ^c, Qingchun Yuan ^b, Paul D. Topham ^b, Cheng-Meng Chen ^d

^a Department of Materials and Environmental Technology, Tallinn University of Technology, Tallinn, Ehitajate tee 5, 19086, Estonia

^b Aston Institute of Materials Research, Aston University, Birmingham, B4 7ET, UK

^c Institute of Physics, University of Tartu, Ülikooli 18, 50090, Tartu, Estonia

^d Key Laboratory of Carbon Materials Institute of Coal Chemistry, Chinese Academy of Sciences, Taiyuan, 030001, PR China

ARTICLE INFO

Article history:

Received 30 May 2018

Received in revised form

7 August 2018

Accepted 17 August 2018

Available online 22 August 2018

ABSTRACT

Owing to its high conductivity, graphene has been incorporated into polymeric nanofibers to create advanced materials for flexible electronics, sensors and tissue engineering. Typically, these graphene-based nanofibers are prepared by electrospinning synthetic polymers, whereas electrospun graphene-biopolymer nanofibers have been rarely reported due to poor compatibility of graphene with biopolymers. Herein, we report a new method for the preparation of graphene-biopolymer nanofibers using the judicious combination of an ionic liquid and electrospinning. Cellulose acetate (CA) has been used as the biopolymer, graphene oxide (GO) nanoparticles as the source of graphene and 1-butyl-3-methylimidazolium chloride ([BMIM]Cl) as the ionic liquid (IL) to create CA-[BMIM]Cl-GO nanofibers by electrospinning for the first time. Moreover, we developed a new route to convert CA-[BMIM]Cl-GO nanofibers to reduced GO nanofibers using hydrazine vapor under ambient conditions to enhance the conductivity of the hybrid nanofibers. The graphene sheets were shown to be uniformly incorporated in the hybrid nanofibers and only 0.43 wt% of GO increase the conductivity of CA-[BMIM]Cl nanofibers by more than four orders of magnitude (from 2.71×10^{-7} S/cm to 5.30×10^{-3} S/cm). This ultra-high enhancement opens up a new route for conductive enhancement of biopolymer nanofibers to be used in smart (bio) electronic devices.

© 2018 Elsevier Ltd. All rights reserved.

1. Introduction

Enormous volumes of synthetic polymers accumulating in the natural environment has become a major threat to the planet due to their poor degradability and high CO₂ footprint. In response to this growing concern, the past decade has seen a considerable interest in the replacement of synthetic polymers with biopolymers owing to their abundance in nature and excellent biocompatibility and biodegradability [1]. In parallel, biopolymeric nanofibrous fabrics can deliver superior performance in terms of functionality and degradability due to their high surface area-to-volume ratio.

Electrospinning has been shown to be a versatile method for fabricating nanofibers from a wide range of polymers, allowing the facile incorporation of additives, such as drugs, nanoparticles or nanofillers to produce hybrid nanofibrous materials for a wide range of applications (e.g. as therapeutic, protective, electrical or sensing materials) [2–7]. Developing functionalized polymer materials such as conductive nanofibers from abundant and biodegradable biopolymers is more challenging and has attracted an increasing amount of attention for the benefit of energy utilization and the environment [1]. A number of synthetic polymers, such as poly(vinyl alcohol) (PVA), polyacrylonitrile (PAN), polyaniline

* Corresponding author. Department of Materials and Environmental Technology, Tallinn University of Technology, Tallinn, Ehitajate tee 5, 19086, Estonia.
E-mail address: kashif.javed@ttu.ee (K. Javed).

(PANI) and poly(vinyl pyrrolidone) (PVP), have been successfully combined with graphene sheets and carbon nanotubes to produce conductive nanofibers [8,9]. However, very few contributions have been made to the electrospinning of biopolymers with carbon nanotubes or graphene. Of these contributions, carbon nanotubes are more popular and have been successfully electrospun with biopolymers such as chitosan, cellulose triacetate and biodegradable polylactide [10–12]. Graphene (layered sp^2 -hybridized honeycomb lattice carbon sheets) has gained particular interest owing to its multifunctional properties such as high specific surface area, electrical and thermal conductivity and superior mechanical strength [13]. Most pertinently, the excellent electrical properties of graphene renders it a promising nanomaterial for novel practical applications such as smart fabrics, nanosensors and flexible electrode materials [14,15].

Producing graphene/biopolymer nanofibers by electrospinning has three distinct challenges: 1) disrupting the extensive hydrogen bonding within the biopolymer; 2) breaking the aggregation of the graphene sheets into nanoparticles to prepare a uniform mixture for electrospinning; and 3) establishing appropriate interactions in the hybrid material to facilitate electron transport. A dispersing agent is required to break-up the graphene sheets due to its inherent insolubility, atomically smooth surfaces and strong aggregation tendency. Choosing an appropriate dispersing agent therefore becomes the key to formulating spinnable mixtures to fabricate hybrid biopolymer nanofibers. Ionic liquids (ILs) present an interesting class of reagents that can be used as dispersing agents because of their novel dissolution ability and have the potential to play more functional roles such as stabilizers, compatibilizers, modifiers and additives in the fabrication of polymer composites containing carbon nanotubes or graphene sheets [16]. ILs are organic salts which exist in the liquid state below 100 °C, preferably at room temperature, and offer chemical and thermal stability, non-flammability and immeasurably low vapor pressure [17,18].

Imidazolium chloride-based ILs show outstanding dissolving capacity of many biopolymers such as cellulose, cellulose acetate, chitin, wool and chitosan. The high chloride concentration of the IL breaks the extensive hydrogen-bonding network of these biopolymers to enable successful electrospinning [18–25]. In such ILs, graphene oxide sheets can be effectively exfoliated, stabilized and reduced by chemical and thermal treatment methods [26,27]. Peng and colleagues fabricated graphene-cellulose nanocomposite films successfully by casting, through the exploitation of imidazolium chloride-based ILs [28]. These cast films showed conductivities up to 3.2×10^{-2} S/cm, thus demonstrating an approach for ionic liquid-biopolymer conductive nanocomposites with graphene. Further, the use of IL, 1-butyl-3-methylimidazolium chloride ([BMIM]Cl, 20%), in the production of electrospun hybrid carbon nanotube nanofibers with styrene-acrylonitrile resin showed a significant increase in the conductivity from 1.08×10^{-6} S/cm to 5.9×10^{-6} S/cm for samples containing 3 wt% carbon nanotubes [29]. However, the fabrication of electrospun graphene-biopolymer conductive nanofibers remains a significant challenge.

In the first report of its kind, we present an electrospinning study of cellulose acetate (biopolymer), graphene oxide (source of graphene) and [BMIM]Cl (ionic liquid) to create hybrid nanofibers. A chemical reduction method using hydrazine in an ultrasound humidifier has been developed to reduce graphene oxide to enhance the electrical conductivity of the biopolymer nanofibers. Scanning Electron Microscopy (SEM), X-ray Diffraction (XRD) and Raman, Fourier Transform Infrared (FTIR) and X-ray Photoelectron (XPS) spectroscopies have been used extensively to probe the interactions within our novel hybrid nanofibers.

2. Experimental

2.1. Materials

1-Methylimidazolium (99%), ethyl acetate (99%) and 1-chlorobutane (99%) were purchased from Merck. CA powder ($M_n = 30,000$ Da, acetyl content 39.8%), acetone, dimethylacetamide (DMAc) and hydrazine solution (35 wt% in H_2O), all from Sigma Aldrich, were used as received. Graphene oxide powder (15–20 sheets, 4–10% edge-oxidized) was purchased from Garmor Inc. U.S.A. 1-Butyl-3-methylimidazolium chloride [BMIM]Cl was synthesized by the method described elsewhere [30].

2.2. Preparation CA and [BMIM]Cl-GO blends

First, a 17 wt% CA solution was prepared in 2:1 (w/w) acetone/DMAc at room temperature under constant stirring until a homogenous, transparent solution was obtained. [BMIM]Cl-GO solutions were prepared by adding a given amount of GO (0.11–0.43% by weight of CA) to [BMIM]Cl (12% by weight of CA) under constant stirring at 60 °C for 24 h. Finally, [BMIM]Cl-GO was added to the CA solution and stirred at room temperature for a further 2 h (experimental details given in the Supporting Information). This solution, denoted as CA-[BMIM]Cl-GO throughout this work, was then ready for electrospinning.

2.3. Electrospinning of CA-[BMIM]Cl-GO nanofibers

Solutions for electrospinning were loaded into a 1 mL syringe with a stainless-steel needle (0.6 mm inner diameter). Electrospinning was performed at room temperature in a horizontal geometry with an applied voltage of 20–25 kV (Gamma High Voltage Research power supply, ES 40R-20W/DM/M1127 Ormond Beach FL). The flow rate of the solution was fixed at 1.5 mL/h using a syringe pump (NE-1010 Programmable Single Syringe Pump, New Era Pump Systems, Inc). The distance between the needle tip and the collector was maintained at 8–10 cm. CA-[BMIM]Cl-GO nanofibers were continuously deposited onto an electrically grounded rotatory collector covered with aluminum foil. The CA-[BMIM]Cl-GO hybrid nanofibers were then carefully removed from the aluminum foil and dried at room temperature for 24 h.

2.4. Preparation of CA-[BMIM]Cl-rGO nanofibers

To reduce the oxygen content of the GO to create electrically conductive nanofibers, CA-[BMIM]Cl-GO nanofibrous mats were reduced by a hydrazine solution mist [31,32]. In short, the hydrazine solution was placed in an ultrasound humidifier (BONECO Ultrasonic U7146, Switzerland). The fibrous mats were clamped in a universal extension retort clamp in the front of the humidifier at maximum humidity (see supplementary video in the Supporting Information) for 15–30 min until the mats changed into the typical black graphitic color. Following reduction, the mats were allowed to dry at room temperature for 2 h to give CA-[BMIM]Cl-rGO nanofibers.

Supplementary video related to this article can be found at <https://doi.org/10.1016/j.carbon.2018.08.034>.

2.5. Characterization

The surface morphologies of the nanofibers were analyzed by scanning electron microscopy (SEM, Zeiss FEG-SEM Ultra-55) and intermolecular interactions within the nanofibrous mats were analyzed by FTIR (Interspec 200-X) spectroscopy. The thickness of

the mats was measured by a Mitutoyo Mucchecker M519–402 micrometer and the approximate porosity of the final electrospun nanofibrous mats was calculated by image analysis, as described in the Supporting Information. Chemical states and surface composition were characterized by X-ray photoelectron spectroscopy (XPS, Kratos AXIS Ultra DLD X-ray Photoelectron Spectrometer). Raman spectroscopy (Renishaw inVia Raman spectrometer) was used to probe the surface composition and X-ray diffraction (XRD) patterns were recorded by a Rigaku Ultima IV diffractometer with Cu K α radiation ($\lambda = 1.5406 \text{ \AA}$, 40 kV at 40 mA) using a silicon strip detector D/teX Ultra with the scan range of $2\theta = 5.0\text{--}30.0^\circ$, scan step 0.02° , scan speed $5^\circ/\text{min}$. The electrical conductivities of the solutions were analyzed using a conductivity meter (SevenCompact S230 Mettler Toledo, Switzerland) at room temperature while the conductivity of the nanofiber mats was measured using a two-probe method with an AlphaLab, Inc. multimeter by placing the mats between two gold electrodes at a separation of 1 cm. The thermal stability of CA, CA-[BMIM]Cl, CA-[BMIM]Cl-GO and CA-[BMIM]Cl-rGO nanofibers was analyzed using Thermogravimetric Analysis (TGA, Setaram LabsysEvo 1600 thermo analyzer) under argon between 25°C and 700°C at a heating rate of $10^\circ\text{C}/\text{min}$.

3. Results and discussion

3.1. The morphology and the conductivity of the hybrid nanofibers

A schematic of the preparation method of CA-[BMIM]Cl-rGO nanofibers is presented in Fig. 1a, where GO was first dispersed in [BMIM]Cl and then mechanically mixed in a solution of CA. Dispersing GO into [BMIM]Cl was carried out by magnetic stirring at approximately 60°C to ensure that the ionic liquid had fully melted. As the melt has a viscosity larger than $150 \text{ mPa}\cdot\text{s}$ [33], mixing was performed for 24 h to ensure dispersion of the GO nanoparticles in [BMIM]Cl, which is a critical step for successful electrospinning. The CA-[BMIM]Cl-GO solution was electrospun prior to reduction by hydrazine mist using an ultrasound humidifier. Compared to other chemical reduction methods [31,32], our ultrasound reduction method by hydrazine mist significantly reduces GO at a lower temperature (room temperature) than previously reported in the literature [31,32,34]. This provides a new method to easily control the reduction process for highly conductive graphene-based nanofibers. The conductivity of the CA-[BMIM]Cl solution (prior to the incorporation of GO) was measured at $6.23 \text{ mS}/\text{cm}$ and remained almost constant (Fig. 1b) as the amount of GO increased from 0.11 to 0.43 wt%. This is due to the presence of oxygenated groups on the surface of GO which disrupts the sp^2 hybridization in graphene. Produced nanofibers with controlled amounts of GO in the range of 0–0.43 wt% are shown in Table 1. Pure CA, CA-[BMIM]Cl, CA-[BMIM]Cl-GO and CA-[BMIM]Cl-rGO nanofibers were then examined by SEM. Surface morphologies of CA, CA-[BMIM]Cl and CA-[BMIM]Cl-GO (see Fig. 2a and b) were smooth and bead-free, while CA-[BMIM]Cl-rGO nanofibers have rough regions where GO appears to have aggregated (as shown in Fig. 2d). Higher concentrations of GO hindered the jet flow due to excess GO, which was not fully dispersed in the solution, clogging the needle and therefore electrospinning was unsuccessful. During chemical reduction, the CA-[BMIM]Cl-GO nanofibers became more fused (Fig. 2d) to form a CA-[BMIM]Cl-rGO nanofibrous mat. The conductivity of CA-[BMIM]Cl nanofibers was measured at $2.71 \times 10^{-7} \text{ S}/\text{cm}$, which was significantly lower than the conductivity of pure [BMIM]Cl *i.e.* $4.60 \times 10^{-4} \text{ S}/\text{cm}$ [35].

Incorporation of GO resulted in an increase in the conductivity of the nanofibers, before and after the reduction. For non-reduced nanofibers, the presence of GO (0.11 wt%) increased the conductivity (to $4.33 \times 10^{-5} \text{ S}/\text{cm}$) and reaching an approximate plateau at

$1.41 \times 10^{-4} \text{ S}/\text{cm}$ at 0.43% GO. The conductivity of the nanofibers is presented in Table 1 and Fig. 3. Comparing to GO/CA nanocomposites reported in the literature [34], 0.43 wt% GO is a relatively low loading for such a significant conductivity enhancement.

Interestingly, reduction of the hybrid nanofibers using hydrazine boosted the conductivity significantly, surpassing the conductivity of pure [BMIM]Cl when GO loading reached 0.32 wt% ($4.60 \times 10^{-4} \text{ S}/\text{cm}$). The highest conductivity attained was $5.30 \times 10^{-3} \text{ S}/\text{cm}$ with 0.43 wt% GO, which is $\sim 20,000$ times higher than that of the nanofibers without GO and over an order of magnitude higher than that of pure [BMIM]Cl.

3.2. Structure of graphene oxide in the nanofibers

X-ray diffraction (XRD) was used to examine the crystal structure of CA and GO following the electrospinning and reduction processes. The XRD patterns of the CA, CA-[BMIM]Cl, CA-[BMIM]Cl-GO and CA-[BMIM]Cl-rGO nanofibers are shown in Fig. 4a. Pure CA nanofibers exhibited three broad diffraction peaks at 9.0° , 17.9° and 21.8° [36]. The peak at 21.8° is attributed to short-range spacing between neighboring cellulosic repeat units within the individual macromolecules and the peak at 9.0° shows the longer range interactions between cellulose acetate chains [37]. More specifically, the distance between the adjacent cellulosic chains is normally characterized by a d-spacing of $\sim 9\text{--}10 \text{ \AA}$, and the neighboring anhydroglucose units in the cellulose chains have a d-spacing of $\sim 4\text{--}5.5 \text{ \AA}$. The peak at 17.9° could arise from the diffraction of the (021) plane. After addition of [BMIM]Cl, the peak at 9.0° became significantly weaker and shifted to 8.0° . This peak weakening and shifting to a lower angle reflects the decrease in CA concentration in the nanofibers from 100% to 53.4% and the cellulose packing disrupted by [BMIM]Cl. The presence of [BMIM]Cl breaks up the H-bonding between the cellulosic chains and enlarges their d-spacing from 9.8 \AA to 11.0 \AA . A small shift of the 21.8° peak is also observed, illustrating that the addition of [BMIM]Cl did not significantly alter the anhydroglucose units in the cellulose acetate chain. The peak at 17.9° almost completely disappeared from the nanofiber samples electrospun in the presence of [BMIM]Cl, showing less short range order in the amorphous cellulose acetate. The addition of 0.11 wt% GO resulted in the appearance of a sharper peak at $\sim 26.5^\circ$, which is the (002) peak of graphite. The (002) peak shows that the interlayer spacing of the graphite sheets was approximately 0.33 nm (3.3 \AA).

This suggests that the graphene sheets are not fully exfoliated and remained in a graphitic-like state [38]. The oxygen-containing functional groups on the GO are mainly on the external surface of the nanoparticles. This result is in line with the specification of GO nanoparticles purchased that have 15–20 sheets and 4–10% edge-oxidized. After chemical reduction, this peak remained in the CA-[BMIM]Cl-rGO nanofibers, as expected.

To examine the influence of chemical reduction on the chemical structure of GO in more detail, the samples were studied by Raman spectroscopy, as shown in Fig. 4b. The Raman spectra of CA-[BMIM]Cl-GO and CA-[BMIM]Cl-rGO both showed two bands at 1350 cm^{-1} and 1585 cm^{-1} . These can be assigned to the D and G bands of the carbon materials, respectively [39,40]. The G band represents sp^2 -hybridized C–C bonds in a 2D hexagonal lattice, while the D band corresponds to the defects and disorder on the two-dimensional amorphization of the carbon network [41,42]. These two peaks reveal that the graphene sheets of the GO have a significant proportion of carbon disordered away from a perfect 2D hexagonal lattice. More specifically, comparison of the CA-[BMIM]Cl-GO and CA-[BMIM]Cl-rGO spectra shows that the D and G bands of CA-[BMIM]Cl-rGO nanofibers are more pronounced after chemical reduction, where the spectrum shows less signals from surface functional groups. The relative intensity of the G and D bands does

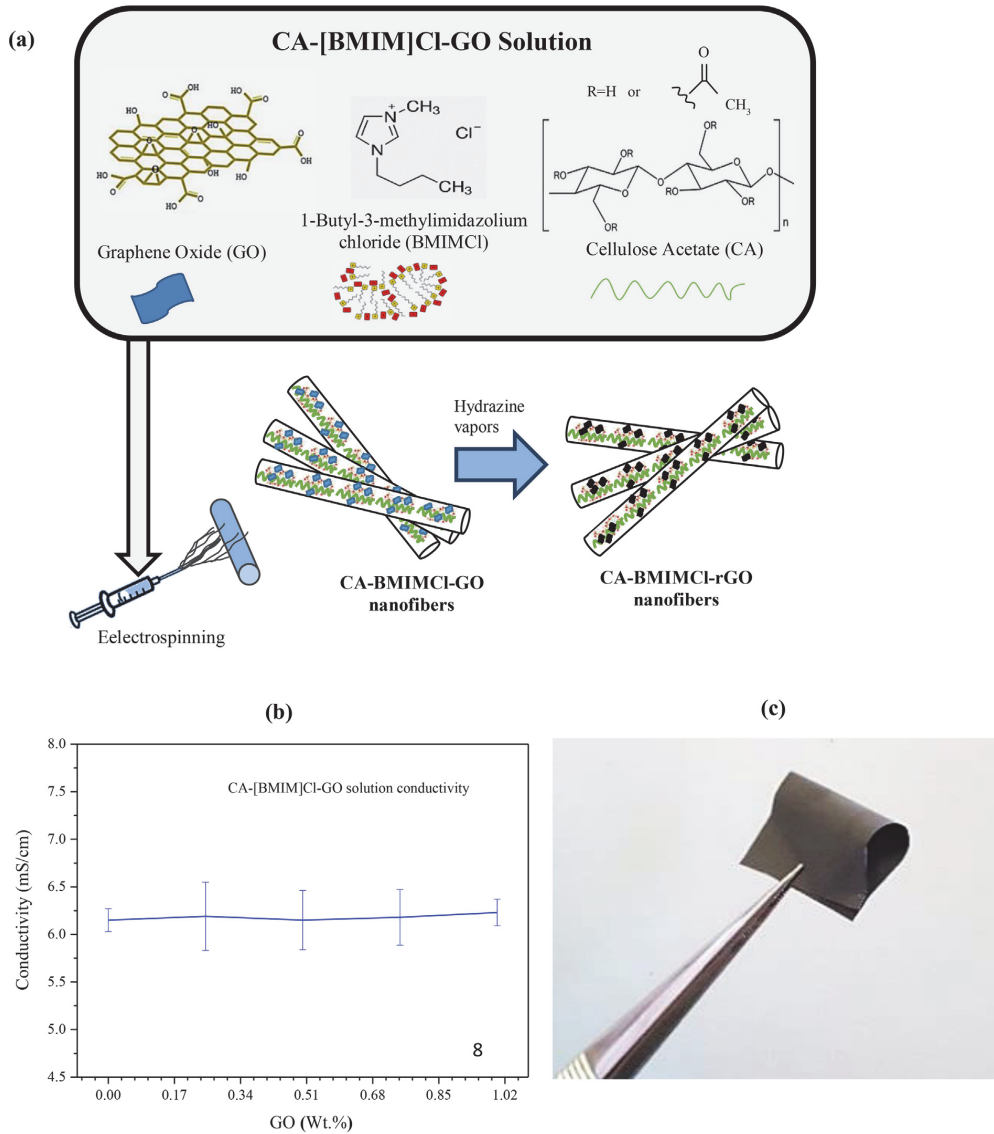


Fig. 1. (a) Schematic of the preparation of CA-[BMIM]Cl-rGO nanofibers, (b) Influence of GO concentration on the conductivity of the CA-[BMIM]Cl solution and (c) a photographic image to demonstrate the flexibility and durability of the final hybrid nanofibrous material. (A colour version of this figure can be viewed online.)

Table 1
Conductivity of the hybrid CA-[BMIM]Cl-rGO nanofibers.

Content, wt%			Conductivity (S/cm)	
GO	[BMIM]Cl	CA	before reduction	after reduction
0.00	46.60	53.40	2.71×10^{-7}	2.71×10^{-7}
0.11	46.50	53.39	4.33×10^{-5}	1.82×10^{-4}
0.21	46.41	53.38	1.11×10^{-4}	3.65×10^{-4}
0.32	46.31	53.37	1.29×10^{-4}	5.10×10^{-3}
0.43	46.21	53.36	1.41×10^{-4}	5.30×10^{-3}

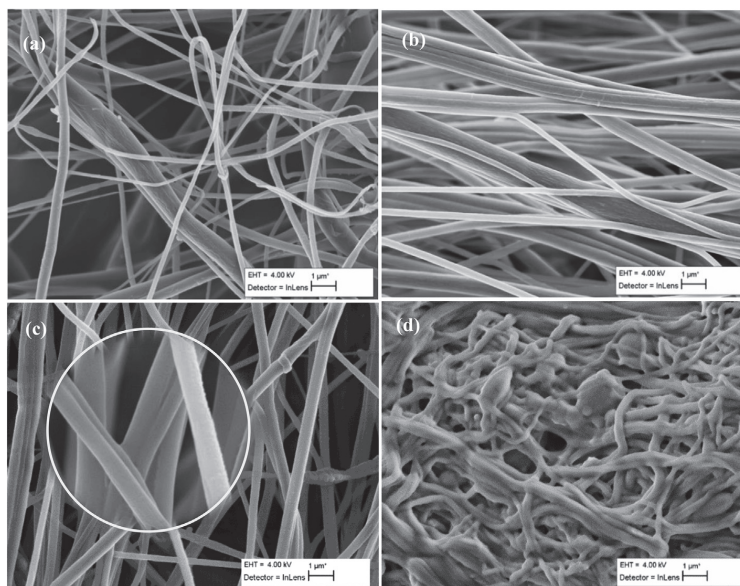


Fig. 2. SEM images of (a) pure CA; (b) CA-[BMIM]Cl; (c) CA-[BMIM]Cl-GO and (d) CA-[BMIM]Cl-rGO(GO conc. 0.43 wt%) nanofibers.

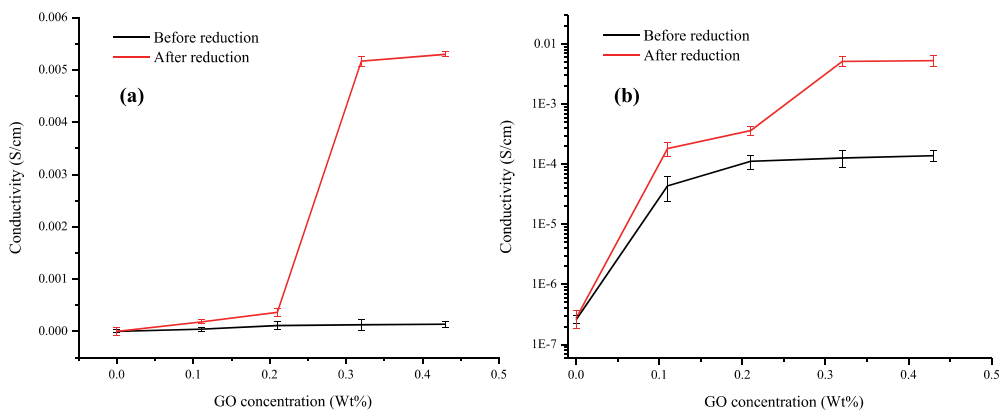


Fig. 3. The effect of GO concentration in the hybrid CA-[BMIM]Cl-GO nanofibers on conductivity [(a) linear and (b) log scales] before and after reduction. (A colour version of this figure can be viewed online.)

not change significantly, supporting the evidence provided by XRD that graphene sheets in the GO particles were not fully exfoliated showing sp^2 -hybridized C–C bonds in a 2D hexagonal lattice and having sheet spacing close to the 0.33 nm of graphite. Importantly, the chemical reduction did not significantly alter the stacking of the graphene sheets, but modified the surface functional groups through deoxygenation [43–46].

3.3. Chemical bonds and their interactions within the hybrid nanofibers

The structure and interactions of each component in the hybrid nanofibers were revealed by Raman, FTIR and XPS giving insights

into the reason for the enhancement in conductivity. As aforementioned, the Raman spectra of CA, CA-[BMIM]Cl, CA-[BMIM]Cl-GO and CA-[BMIM]Cl-rGO are shown in Fig. 4b, whereas the FTIR and XPS spectra are presented in Figs. 4c and 5, respectively. The Raman spectra of CA and CA-[BMIM]Cl showed the asymmetric stretching vibration of the C–O–C glycosidic bond at 1121 cm^{-1} and the pyranose ring at 1080 cm^{-1} with the presence of C–OH at 1265 cm^{-1} . The bands at 1736 , 1435 , and 1382 cm^{-1} are attributed to the carbonyl group (C=O) and symmetric and asymmetric vibrations of C–H, respectively, in the acetyl group [47–49]. More interestingly, the [BMIM]Cl cation is observed in the CA-[BMIM]Cl sample with bands at 601 and 627 cm^{-1} . The intensities show the co-existence of gauche and trans conformations of the IL [50,51]. It

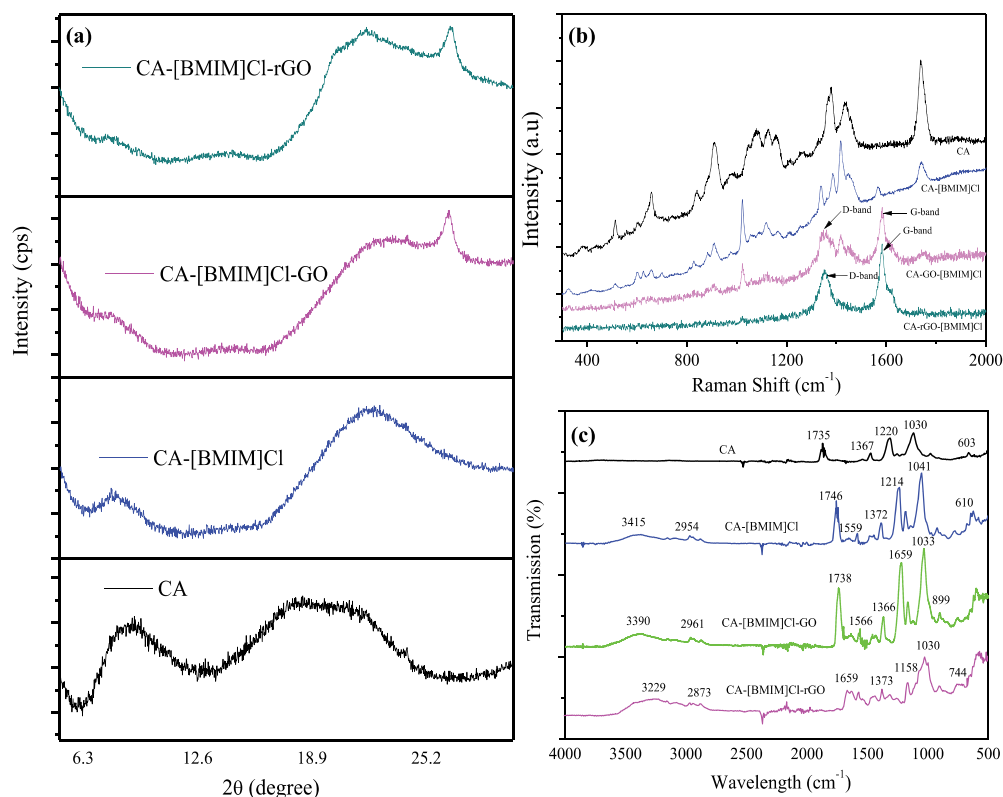


Fig. 4. (a) XRD patterns; (b) Raman spectra and (c) FTIR spectra of CA nanofibers, hybrid CA-[BMIM]Cl, CA-[BMIM]Cl-GO and CA-[BMIM]Cl-rGO nanofibers (GO conc. 0.43 wt% for the latter two samples). (A colour version of this figure can be viewed online.)

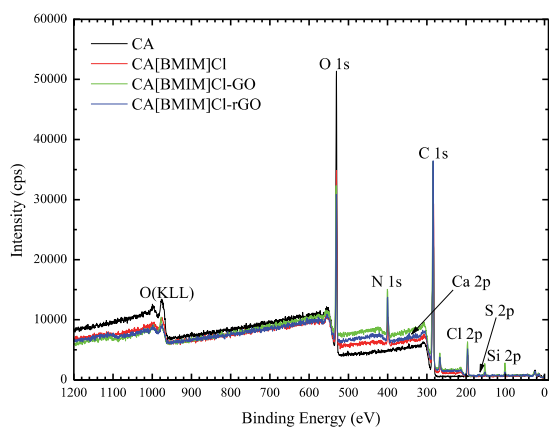


Fig. 5. XPS survey spectra of CA (black), CA-[BMIM]Cl (red), CA-[BMIM]Cl-GO (green), CA-[BMIM]Cl-rGO (GO conc. 0.43 wt%, blue). (A colour version of this figure can be viewed online.)

is worth noting that the inclusion of GO has resulted in the disappearance of most of the vibrational bands from the Raman spectra of the corresponding hybrid nanofibers.

The FTIR spectra of pure CA, CA-[BMIM]Cl and CA-[BMIM]Cl-rGO nanofibers in Fig. 4c show that pure CA nanofibers exhibited characteristic bands at 1735 cm⁻¹ and 1367 cm⁻¹ corresponding to C=O and C-H stretching from -OCOCH₃, respectively. Bands at 1220 cm⁻¹ and 1030 cm⁻¹ reveal the C-C and C-O stretching vibrations in the pyranoid ring and C-O-C (ether linkage) from the glycosidic units. In the CA-[BMIM]Cl spectrum, characteristic bands at 1746 cm⁻¹ (C=C stretching), 1214 cm⁻¹ (C=N stretching) and 1041 cm⁻¹ (C-O stretching) indicate that the BMIM⁺ and Cl⁻ ions of [BMIM]Cl formed hydrogen bonds with CA, as expected. The FTIR spectrum of CA-[BMIM]Cl-GO is similar to that of CA-[BMIM]Cl while the spectrum of [BMIM]Cl-rGO shows two new bands at 1659 cm⁻¹ and 3229 cm⁻¹ suggesting strong interactions (hydrogen bonding) between the carboxylic (-COOH) groups of graphene and carbonyl (C=O) groups of CA.

XPS was used to further examine the differences in chemical functionality in the hybrid nanofibers (Fig. 5). The survey spectrum of pure CA nanofibers exhibits only two distinct peaks: C 1s at ~285 eV and O 1s at ~532 eV (Fig. 5), while Cl 2p and N 1s peaks are present in all other spectra, confirming the presence of [BMIM]Cl. High resolution C 1s spectra were analyzed by monochromatic Al K α X-ray source (h ν = 1486.6 eV). Each spectrum has been deconvoluted into five distinct peaks, as shown in Fig. 6a–d for the

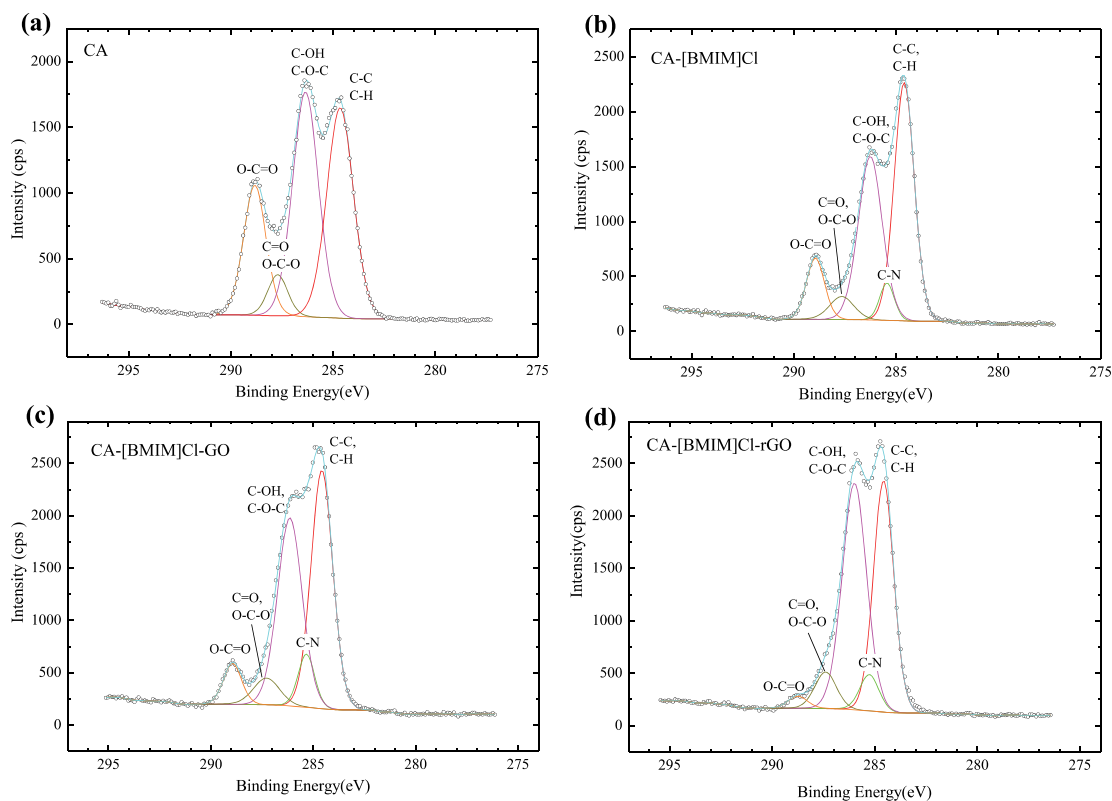


Fig. 6. The C1s XPS spectra of (a) pristine CA nanofibers, (b) CA-[BMIM]Cl, (c) CA-[BMIM]Cl-GO, and (d) CA-[BMIM]Cl-rGO (GO conc. 0.43 wt%), (A colour version of this figure can be viewed online.)

nanofibers of pure CA, CA-[BMIM]Cl, CA-[BMIM]Cl-GO and CA-[BMIM]Cl-rGO, respectively. The sharp peak centered at 284.6 eV corresponds to C–C bonding and the relatively broad peak around 286.1 eV is attributed to three different functional groups: hydroxyl (C–O); carbonyl (C=O) and imine (C–N). More specifically, the peaks in this region at 285.5, 285.7, 286.6 and 287.8 eV are attributed to carbon atoms in C–N, C=N, C–O, C=O, respectively. In the CA-[BMIM]Cl-rGO nanofibers, the peak centered at 288.9 eV comes from the carboxyl group [C(O)O]. Comparing the C 1s XPS spectra (Fig. 6a and b), it can be seen that the addition of [BMIM]Cl significantly lowers the relative peak intensity of the oxygen-containing functional groups from CA, and introduces a new peak attributed to C–N from [BMIM]Cl. The introduction of GO results in some small changes in the relative peak intensities (comparing Fig. 6b and c). After the reduction of the CA-[BMIM]Cl-GO nanofibers, the C 1s spectrum of the CA-[BMIM]Cl-rGO (Fig. 6d) shows a dramatic decrease of the carboxyl peak. These changes suggest that the hydrazine vapor step has indeed reduced the carboxyl groups in GO, but may have also partially reduced CA, while the peak intensity of the other oxygen-containing functional groups slightly increased. It is noteworthy to state that it has been shown elsewhere that it is not yet possible to reduce GO completely by chemical reduction [44].

The proposed interactions of stacked graphene sheets with CA and [BMIM]Cl are schematically shown in Fig. 7. Removal of

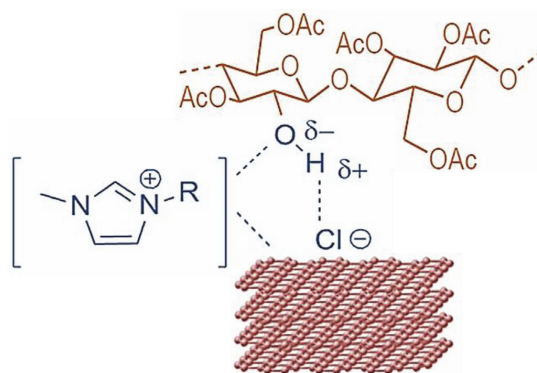


Fig. 7. Schematic illustration of the suggested interaction of graphene with CA and [BMIM]Cl. (A colour version of this figure can be viewed online.)

carboxyl groups and formation of more hydroxyl groups may promote the formation of hydrogen-bonds with dissociated BMIM⁺ and Cl[−] ions through unsubstituted hydroxyl functional groups in both GO and CA [52,53]. The π -electrons in the imidazole ring of

BMIM⁺ may interact with the rich π -electron clouds of the graphene rings resulting in some delocalization and enhanced electrical conductivity.

3.4. Thermal analysis of the hybrid nanofibers

TGA has been carried out under argon to further examine the thermal stability and chemical bonding differences in CA, CA-[BMIM]Cl, CA-[BMIM]Cl-GO and CA-[BMIM]Cl-rGO nanofibers. These weight loss profiles (Fig. 8) show that pure CA is more stable than the composites. Pure CA decomposes in the range of 330–375 °C with a corresponding weight loss of approximately 82 wt%. In contrast, the addition of [BMIM]Cl lowers the decomposition temperature range to 240–290 °C with a corresponding weight loss of 85%.

The addition of 0.43% GO did not cause significant change in the decomposition temperature but does decrease the weight loss to ~75%. Reduction using hydrazine does not cause any identifiable changes in thermal decomposition nor char formation. These findings confirm that the ionic liquid has fully separated CA molecular chains with no CA H-bonding following mechanical mixing. This separation lowers the thermal stability of the CA by approximately 90 °C. The addition of 0.43% GO does not affect the thermal stability of the CA, but introduced an effective mass transfer barrier and char formation nucleus, resulting in an increased amount of char formed. Such an enhancement could suggest that the graphene pallets were well aligned during extrusion and spinning. The morphology, crystal structure, chemical bonding and thermal analysis of the CA-[BMIM]Cl-GO nanofibers show that graphene stacks have been successfully incorporated into CA nanofibers by dispersing GO in a [BMIM]Cl ionic liquid. Polar functional groups, such as $-C=O$, $-COOH$ and $-OH$ on GO have not only assisted its dispersion in the ionic liquid, but also facilitate strong and uniform interactions with CA in the hybrid nanofibers. The well-dispersed and strongly bonded system allowed the graphene stacks to form a continuous conductive network, achieving a drastic enhancement in electrical conductivity after reduction using hydrazine, similar to the polystyrene-GO system reported by Wu et al. [54]. These insights demonstrate that this new graphene-based hybrid nanocomposite is a promising candidate for smart and flexible electronic and bio-electronic applications, particularly in those systems which require high electrical conductivity.

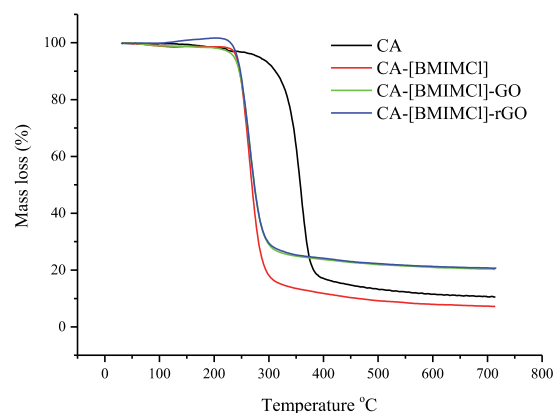


Fig. 8. TGA profiles of pure CA (black), CA-[BMIM]Cl nanofibers (red), CA-[BMIM]Cl-GO nanofibers (green) and CA-[BMIM]Cl-rGO nanofibers (blue). (A colour version of this figure can be viewed online.)

4. Conclusions

In summary, a new method of exploiting a [BMIM]Cl ionic liquid for the fabrication of graphene-based, bio-inspired (cellulose acetate) conductive CA-[BMIM]Cl-GO nanofibers through electrospinning has been introduced. Combining the advantages of both GO and [BMIM]Cl materials allowed a homogeneous dispersion of GO and better solubility of CA to be achieved. The modest incorporation of 0.43% graphene oxide into the hybrid material greatly enhanced the conductivity of the nanofiber mats by more than four orders of magnitude to 5.30×10^{-3} S/cm. The uniform nanostructure of graphite oxide and BMIM in CA nanofibers forms the conductive paths, which has been enhanced by chemical reduction of hydrazine via an ultrasonic process. Such a facile strategy for the fabrication of bio-based, ultrathin, lightweight, flexible nanofibers could open a new avenue towards sustainable material development in the quest for high-performance next-generation smart electronic devices.

Acknowledgements

This work was supported by Estonian Academy of Science, Estonian Research Council (IUT19-4) and by the European Regional Development Fund project TK141 “Advanced materials and high-technology devices for energy recuperation systems.” The authors acknowledge the Estonian Ministry of Education under institutional research financing IUT 19–28 and the European Union through the European Regional Development Fund. The authors are also grateful for the financial support from the Estonian PhD allowance and Estonian Ministry of Education and Research to support for this research at Tallinn University of Technology Tallinn Estonia. Finally, KJ and PDT thank Christian Burton at Aston University for assistance with physical characterization of the nanofibrous mats.

Appendix A. Supplementary data

Supplementary data related to this article can be found at <https://doi.org/10.1016/j.carbon.2018.08.034>.

References

- [1] J.D. Schiffman, C.L. Schauer, A review: electrospinning of biopolymer nanofibers and their applications, *Polym. Rev.* 48 (2) (2008) 317–352.
- [2] T. Subbiah, G.S. Bhat, R.W. Tock, S. Parameswaran, S.S. Ramkumar, Electrospinning of nanofibers, *J. Appl. Polym. Sci.* 96 (2) (2005) 557–569.
- [3] S. Ramakrishna, K. Fujihira, W.-E. Teo, T. Yong, Z. Ma, R. Ramaseshan, Electrospun nanofibers: solving global issues, *Mater. Today* 9 (3) (2006) 40–50.
- [4] A. Baji, Y.-W. Mai, S.-C. Wong, M. Abtahi, P. Chen, Electrospinning of polymer nanofibers: effects on oriented morphology, structures and tensile properties, *Compos. Sci. Technol.* 70 (5) (2010) 703–718.
- [5] I.S. Chronakis, S. Grapenson, A. Jakob, Conductive polypyrrole nanofibers via electrospinning: electrical and morphological properties, *Polymer* 47 (5) (2006) 1597–1603.
- [6] A. Isakova, O. Efremova, N. Pullan, L. Luer, P.D. Topham, Design, synthesis and RAFT polymerisation of a quinoline-based monomer for use in metal-binding composite microfibers, *RSC Adv.* 6 (8) (2016) 6598–6606.
- [7] L. Wang, M. Wang, P.D. Topham, Y. Huang, Fabrication of magnetic drug-loaded polymeric composite nanofibers and their drug release characteristics, *RSC Adv.* 2 (6) (2012) 2433–2438.
- [8] Z.-M. Huang, Y.Z. Zhang, M. Kotaki, S. Ramakrishna, A review on polymer nanofibers by electrospinning and their applications in nanocomposites, *Compos. Sci. Technol.* 63 (15) (2003) 2223–2253.
- [9] I.F. Wahab, S.I.A. Razak, N.S. Azmi, F.N. Dahli, A.H.M. Yusof, N.H.M. Nayan, Electrospun graphene oxide-based nanofibers, in: A.M.T. Silva, S.A.C. Carabineiro (Eds.), *Advances in Carbon Nanostructures*, InTech, Rijeka, 2016. Ch. 05.
- [10] Z.M. Mahdieh, V. Mottaghtalab, N. Piri, A.K. Haghi, Conductive chitosan/multi walled carbon nanotubes electrospun nanofiber feasibility, *Kor. J. Chem. Eng.* 29 (1) (2012) 111–119.
- [11] M. Gouda, M. Abu-Abdeen, Highly conductive cellulosic nanofibers for efficient water desalination, *Fibers Polym.* 18 (11) (2017) 2111–2117.

- [12] T. Yang, D. Wu, L. Lu, W. Zhou, M. Zhang, Electrospinning of polylactide and its composites with carbon nanotubes, *Polym. Compos.* 32 (8) (2011) 1280–1288.
- [13] K. Hu, D.D. Kulkarni, I. Choi, V.V. Tsukruk, Graphene-polymer nanocomposites for structural and functional applications, *Prog. Polym. Sci.* 39 (11) (2014) 1934–1972.
- [14] W.K. Chee, H.N. Lim, Z. Zainal, N.M. Huang, I. Harrison, Y. Andou, Flexible graphene-based supercapacitors: a review, *J. Phys. Chem. C* 120 (8) (2016) 4153–4172.
- [15] F. Meng, W. Lu, Q. Li, J.-H. Byun, Y. Oh, T.-W. Chou, Graphene-based fibers: a review, *Adv. Mater.* 27 (35) (2015) 5113–5131.
- [16] R. Peng, Y. Wang, W. Tang, Y. Yang, X. Xie, Progress in imidazolium ionic liquids assisted fabrication of carbon nanotube and graphene polymer composites, *Polymers* 5 (2) (2013) 847.
- [17] K.N. Marsh, J.A. Boxall, R. Lichtenhaler, Room temperature ionic liquids and their mixtures—a review, *Fluid Phase Equil.* 219 (1) (2004) 93–98.
- [18] R.P. Swatloski, S.K. Spear, J.D. Holbrey, R.D. Rogers, Dissolution of cellulose with ionic liquids, *J. Am. Chem. Soc.* 124 (18) (2002) 4974–4975.
- [19] L. Meli, J. Miao, J.S. Dordick, R.J. Linhardt, Electrospinning from room temperature ionic liquids for biopolymer fiber formation, *Green Chem.* 12 (11) (2010) 1883–1892.
- [20] G. Viswanathan, S. Murugesan, V. Pushparaj, O. Nalamasu, P.M. Ajayan, R.J. Linhardt, Preparation of biopolymer fibers by electrospinning from room temperature ionic liquids, *Biomacromolecules* 7 (2) (2006) 415–418.
- [21] H. Xie, S. Zhang, S. Li, Chitin and chitosan dissolved in ionic liquids as reversible sorbents of CO₂, *Green Chem.* 8 (7) (2006) 630–633.
- [22] K. Javed, A. Krumme, I. Krasnou, V. Mikli, M. Viirsalu, T. Plamus, et al., Impact of 1-butyl-3-methylimidazolium chloride on the electrospinning of cellulose acetate nanofibers, *J. Macromol. Sci., Part A* (2017) 1–6.
- [23] O. Zavgorodnya, J.L. Shamshina, J.R. Bonner, R.D. Rogers, Electrospinning biopolymers from ionic liquids requires control of different solution properties than volatile organic solvents, *ACS Sustain. Chem. Eng.* 5 (6) (2017) 5512–5519.
- [24] G. Zhang, M. Sun, Y. Liu, H. Liu, J. Qu, J. Li, Ionic liquid assisted electrospun cellulose acetate fibers for aqueous removal of triclosan, *Langmuir* 31 (5) (2015) 1820–1827.
- [25] M.G. Freire, A.R.R. Teles, R.A.S. Ferreira, L.D. Carlos, J.A. Lopes-da-Silva, J.A.P. Coutinho, Electrospun nanosized cellulose fibers using ionic liquids at room temperature, *Green Chem.* 13 (11) (2011) 3173–3180.
- [26] C. He, S. Sun, H. Peng, C.P. Tsui, D. Shi, X. Xie, et al., Poly(ionic liquid)-assisted reduction of graphene oxide to achieve high-performance composite electrodes, *Compos. B Eng.* 106 (2016) 81–87.
- [27] Q. Lyu, H. Yan, L. Li, Z. Chen, H. Yao, Y. Nie, Imidazolium ionic liquid modified graphene oxide: as a reinforcing filler and catalyst in epoxy resin, *Polymers* 9 (9) (2017) 447.
- [28] H. Peng, L. Meng, L. Niu, Q. Lu, Simultaneous reduction and surface functionalization of graphene oxide by natural cellulose with the assistance of the ionic liquid, *J. Phys. Chem. C* 116 (30) (2012) 16294–16299.
- [29] V. Gudkova, A. Krumme, T. Mårtson, M. Rikko, E. Tarasova, N. Savest, et al., 1-butyl-3-methylimidazolium chloride assisted electrospinning of SAN/MWCNTs conductive reinforced composite membranes, *J. Electroanal. Chem.* 78 (2015) 11–16.
- [30] J.G. Huddleston, A.E. Visser, W.M. Reichert, H.D. Willauer, G.A. Broker, R.D. Rogers, Characterization and comparison of hydrophilic and hydrophobic room temperature ionic liquids incorporating the imidazolium cation, *Green Chem.* 3 (4) (2001) 156–164.
- [31] Z. Wang, S. Wu, J. Zhang, P. Chen, G. Yang, X. Zhou, et al., Comparative studies on single-layer reduced graphene oxide films obtained by electrochemical reduction and hydrazine vapor reduction, *Nanoscale Res. Lett.* 7 (1) (2012) 161.
- [32] S.C. Youn, J. Geng, B.S. Son, S.B. Yang, D.W. Kim, H.M. Cho, et al., Effect of the exposure time of hydrazine vapor on the reduction of graphene oxide films, *J. Nanosci. Nanotechnol.* 11 (7) (2011) 5959–5964.
- [33] S. Fendt, S. Padmanabhan, H.W. Blanch, J.M. Prausnitz, Viscosities of acetate or chloride-based ionic liquids and some of their mixtures with water or other common solvents, *J. Chem. Eng. Data* 56 (1) (2011) 31–34.
- [34] S.N. Tripathi, G.S.S. Rao, A.B. Mathur, R. Jasra, Polyolefin/graphene nanocomposites: a review, *RSC Adv.* 7 (38) (2017) 23615–23632.
- [35] S.A. Dharaskar, M.N. Varma, D.Z. Shende, C.K. Yoo, K.L. Wasewar, Synthesis, characterization and application of 1-butyl-3-methylimidazolium chloride as green material for extractive desulfurization of liquid fuel, *Sci. World J.* 2013 (2013) 9.
- [36] X. Zhao, Q. Zhang, D. Chen, P. Lu, Enhanced mechanical properties of graphene-based poly(vinyl alcohol) composites, *Macromolecules* 43 (5) (2010) 2357–2363.
- [37] C. Bao, Cellulose acetate/plasticizer systems: structure, morphology and dynamics, PhD thesis, Université Claude Bernard Lyon 1, 2015.
- [38] Q. Yuan, Intumescent Mechanisms of Fire-retarding Polyurethane Systems and Development of Graphite/polymer Nano-composites, 2004.
- [39] S. Claramunt, A. Varea, D. López-Díaz, M.M. Velázquez, A. Cornet, A. Cirera, The importance of interbands on the interpretation of the Raman spectrum of graphene oxide, *J. Phys. Chem. C* 119 (18) (2015) 10123–10129.
- [40] A. Jorio, E.H.M. Ferreira, M.V.O. Moutinho, F. Stavale, C.A. Achete, R.B. Capaz, Measuring disorder in graphene with the G and D bands, *Phys. Status Solidi* 247 (11–12) (2010) 2980–2982.
- [41] L.M. Malard, M.A. Pimenta, G. Dresselhaus, M.S. Dresselhaus, Raman spectroscopy in graphene, *Phys. Rep.* 473 (5–6) (2009) 51–87.
- [42] K.N. Kudin, B. Ozbas, H.C. Schniepp, R.K. Prud'homme, L.A. Aksay, R. Car, Raman spectra of graphite oxide and functionalized graphene sheets, *Nano Lett.* 8 (1) (2008) 36–41.
- [43] S. Park, J. An, I. Jung, R.D. Piner, S.J. An, X. Li, et al., Colloidal suspensions of highly reduced graphene oxide in a wide variety of organic solvents, *Nano Lett.* 9 (4) (2009) 1593–1597.
- [44] S. Stankovich, D.A. Dikin, R.D. Piner, K.A. Kohlhaas, A. Kleinhammes, Y. Jia, et al., Synthesis of graphene-based nanosheets via chemical reduction of exfoliated graphite oxide, *Carbon* 45 (7) (2007) 1558–1565.
- [45] Shilpa, B.M. Basavaraja, S.B. Majumder, A. Sharma, Electrospun hollow glassy carbon-reduced graphene oxide nanofibers with encapsulated ZnO nanoparticles: a free standing anode for Li-ion batteries, *J. Mater. Chem.* 3 (10) (2015) 5344–5351.
- [46] S. Yao, Y. Li, Z. Zhou, H. Yan, Graphene oxide-assisted preparation of poly(vinyl alcohol)/carbon nanotube/reduced graphene oxide nanofibers with high carbon content by electrospinning technology, *RSC Adv.* 5 (111) (2015) 91878–91887.
- [47] C. Duverger, J.M. Nedelec, M. Benatsou, M. Bouazaoui, B. Capoen, M. Ferrari, et al., Waveguide Raman spectroscopy: a non-destructive tool for the characterization of amorphous thin films, *J. Mol. Struct.* 480–481 (1999) 169–178.
- [48] J.A. Sánchez-Márquez RF-R, I. Cano-Rodríguez, Z. Gamiño-Arroyo, E. Rubio-Rosas, J.M. Kenny, N. Rescignano, Membrane made of cellulose acetate with polyacrylic acid reinforced with carbon nanotubes and its applicability for chromium removal, *Int. J. Polymer Sci.* 2015 (2015) 12.
- [49] J.R. Scherer, G.F. Bailey, S. Kint, R. Young, D.P. Malladi, B. Bolton, Water in polymer membranes Raman scattering from cellulose acetate films, *J. Phys. Chem.* 89 (2) (1985) 312–319.
- [50] H. Satoshi, O. Ryosuke, H. Hiro-o, Raman spectra, crystal polymorphism, and structure of a prototype ionic-liquid [bmim]Cl, *Chem. Lett.* 32 (6) (2003) 498–499.
- [51] K. Mizuno, S. Imafuji, T. Ochi, T. Ohta, S. Maeda, Hydration of the CH groups in dimethyl sulfoxide probed by NMR and IR, *J. Phys. Chem. B* 104 (47) (2000) 11001–11005.
- [52] M. Isik, H. Sardon, D. Mecerreyes, Ionic liquids and cellulose: dissolution, chemical modification and preparation of new cellulosic materials, *Int. J. Mol. Sci.* 15 (7) (2014) 11922–11940.
- [53] A.S. Gross, A.T. Bell, J.-W. Chu, Thermodynamics of cellulose solvation in water and the ionic liquid 1-butyl-3-methylimidazolium chloride, *J. Phys. Chem. B* 115 (46) (2011) 13433–13440.
- [54] N. Wu, X. She, D. Yang, X. Wu, F. Su, Y. Chen, Synthesis of network reduced graphene oxide in polystyrene matrix by a two-step reduction method for superior conductivity of the composite, *J. Mater. Chem.* 22 (33) (2012) 17254–17261.

Publication II

Javed, K.; Krumme, A.; Krasnou, I.; Mikli, V.; Viirsalu, M.; Plamus, T.; Vassiljeva, V.; Tarasova, E.; Savest, N.; Mendez, J. D. (2018). Impact of 1-butyl-3-methylimidazolium chloride on the electrospinning of cellulose acetate nanofibers. *Journal of Macromolecular Science, Part A*, 55 (2), 142–147.



Impact of 1-butyl-3-methylimidazolium chloride on the electrospinning of cellulose acetate nanofibers

Kashif Javed^a, Andres Krumme^a, Illia Krasnou^a, Valdek Mikli^a, Mihkel Viirsalu^a, Tiia Plamus^a, Viktoria Vassiljeva^a, Elvira Tarasova^a, Natalja Savest^a and James D. Mendez^b

^aDepartment of Materials and Environmental Technology, Tallinn University of Technology, Tallinn, Ehitajate tee 5, Estonia; ^bDivision of Science, Indiana University—Purdue University Columbus, 4601 Central Avenue, Columbus Indiana, United States

ABSTRACT

Additives like ionic liquids (ILs) have proven to be excellent materials useful in improving the electrospinnability and conductivity of both synthetic and biopolymers. The aim of this study is to investigate the effect of 1-butyl-3-methylimidazolium chloride [BMIM]Cl on the electrospinnability of cellulose acetate (CA). The results showed that [BMIM]Cl has the greater effect on viscosity and conductivity of the spinning solution while the morphology of the nanofibers significantly improved as the concentration of the IL increases from 0% to 12% (v/v) of [BMIM]Cl. To understand the interaction between CA and [BMIM]Cl, Fourier-transform infrared spectroscopy (FTIR) has been used. Observations by scanning electron microscopy (SEM) suggested that [BMIM]Cl significantly altered the morphology of the CA nanofibers and 12% (v/v) of [BMIM]Cl would be an ideal concentration producing uniform fibers with a mean diameter of 180nm. In addition, the membranes showed a significant increase in conductivity (from 0 to 2.21×10^{-7} S/cm) as the concentration of ionic liquid increases up to 12% (v/v) that indicates a successful loading of IL inside the nanofibers.

ARTICLE HISTORY

Received April 2017,
Revised and Accepted
October 2017

KEYWORDS

Ionic liquids; Cellulose acetate; Electrospinning; Nanofibers; 1-butyl-3-methylimidazolium chloride

1. Introduction

In the fabrication of micro- and nanofibers, electrospinning has been extensively used as a versatile and efficient method.^[1, 2] The two primary components necessary for electrospinning of nanofibers are a charged polymer solution electrostatically ejected through a needle tip to a stationary or rotatory grounded collector.^[3–5] Compared to conventional spun fibers, electrospun fibers can have a much smaller diameter on the nano scale, providing a high surface area with porous structure.^[6] These nanofibers with high surface area have shown a potential to be used in number of applications e.g. healthcare, biotechnology, environmental engineering and energy storage applications.^[1,7–15] Although electrospinning is developing fast in creating novel nanostructures, including core-sheath, tri-layer and Janus,^[16–19] many materials are currently incompatible with this technique.

Ionic liquids (IL) have received much attention in recent years. These organic salts have many promising applications such as the processing of polysaccharides to enhance unique chemical and physical properties. Ionic liquids can modify both synthetic and biopolymers, which can impart excellent chemical, electrical and physical properties for nano composites.^[20–26] At room temperature, ILs show good ionic conductivity and thermal stability owing outstanding dissolving properties for cellulose. It provides excellent inter molecular forces inside cellulosic materials.^[27,28] 1-butyl-3-methylimidazolium chloride a well-known ionic liquid for electrospinning of both synthetic and biopolymers and the results revealed

that it has a positive impact on solution properties i.e. conductivity viscosity together with the conductivity and morphology of the fibers.^[29–32]

Cellulose acetate, a derivative from cellulose^[33,34] has attracted considerable interest due to its biocompatibility, biodegradable, nontoxic, and low cost.^[35] The compatibility of cellulose acetate with [BMIM]Cl was investigated by the researchers and publicized that these porous composites are excellent for water purification from industrial waste water.^[36] M.B.I. Tsivintzelis et. al. showed that cellulose could be electrospun using [BMIM]Cl and [AMIM]Cl with obtained fibers showing a diameter ranging between 300 – 1000 nm.^[37]

But to the author's knowledge, there is no such study reported previously to investigate the influence of different concentrations of [BMIM]Cl on the electrospinning of cellulose acetate (CA) and study the effect on the spinning solution and on the fiber chemistry.

2. Experimental

2.1. Materials

CA powder ($M_n = 30,000$ Da, acetyl content 39.8%) was purchased from Sigma-Aldrich. 1-methylimidazolium, ethyl acetate and chlorobutane were purchased from Merk. Acetone (AC) and dimethylacetamide (DMAc) solvents were purchased from Sigma-Aldrich.

2.2. Preparation of [BMIM]Cl and CA-[BMIM]Cl solution

1-butyl-3-methylimidazolium chloride [BMIM]Cl was synthesized by the method described by Jairton Dupont.^[38] In short, chlorobutane (purity 99%, 260 g) and 1-methylimidazolium (purity 99%, 164 g) were placed into a round bottom flask fitted with condenser and refluxed at 75°C for 72 h under nitrogen until two phases formed. Then the viscous liquid was cooled and washed several times with ethyl acetate to remove unreacted starting material. Finally, the ionic liquid was dried for 3 h under vacuum to remove residual solvents.

In parallel, 17 wt.% of CA was prepared by adding to a mixture of acetone and dimethylacetamide with a volume ratio of 2:1 (v/v%) under constant stirring at room temperature until a homogenous and transparent solution was formed. [BMIM]Cl was added to previously made CA solution to get the desired concentrations of 0%–12% (v/v %) of [BMIM]Cl and stir again at room temperature for another 2 h. This CA-[BMIM]Cl homogenous solution was then ready for electrospinning. The CA concentration was kept fixed at 17 wt.% in all spinning solution preparations while ionic liquid concentration varies to investigate the influence of [BMIM]Cl on the electrospun CA fibers.

2.3. Electrospinning of CA-[BMIM]Cl nanofibers

CA solutions with and without IL were electrospun at room temperature by horizontal electrospinning setup. Each polymer solution was placed into 1 ml syringe with a needle diameter of 0.6 mm. The solution was electrospun at a voltage of 20–25 kV by a power supply (Gamma High Voltage Research, ES 40R-20W/DM/M1127 Ormond Beach FL) and the distance between the needle and the collector was adjusted to 8–10 cm. The feeding rate was maintained at 1.5 ml/h by a syringe pump (NE-1010 Programmable Single Syringe Pump, New Era Pump Systems, Inc). The electrospun nanofibers were collected on a cylindrical rotatory drum, which was covered with the aluminum foil. CA and CA-[BMIM]Cl membranes were detached from the foil and dried at room temperature for 24 h. A schematic diagram of mechanical mixing of CA and [BMIM]Cl presented in Figure 1 where IL entrapped inside the solution and then electrospinning was performed.

2.4. Characterizations

Scanning electron microscopy (SEM, Zeiss FEG-SEM Ultra-55) was utilized to determine the morphology and the average diameter of the nanofibers. Intermolecular interactions between CA and [BMIM]Cl were analyzed with FTIR (InterSpec 200-X). The viscosity of the solution was measured by concentric cylinder viscometer Brookfield RVDVII+ (Brookfield ENG LABS Inc., USA), using spindle #21 at 23.3°C. The temperature was maintained with a MGW Lauda C6 thermostat (Berner Osakeyhtio, Finland). The electrical conductivities of the solutions were measured with SevenCompact Conductivity S230 (Mettler Toledo, Switzerland) at a room temperature. X-ray diffraction (XRD)

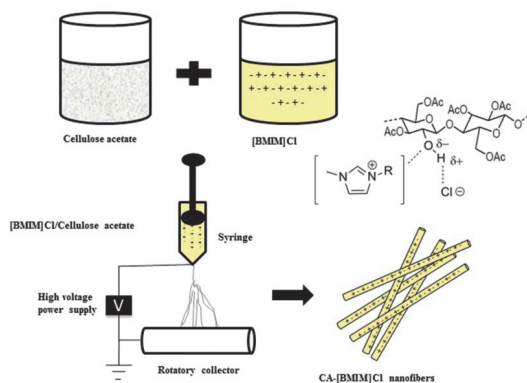


Figure 1. A schematic diagram of the electrospinning of CA-[BMIM]Cl nanofibers and a proposed interaction between [BMIM]Cl and CA.

patterns were recorded by a Rigaku Ultima IV diffractometer with Cu K α radiation ($\lambda = 1.5406 \text{ \AA}$, 40 kV at 40 mA) using a silicon strip detector D/teX Ultra with the scan range of $2\theta = 5.0\text{--}30.0^\circ$, scan step 0.02° , scan speed $5^\circ/\text{min}$. The conductivity of CA-[BMIM]Cl nanofibers was measured by two probe method, placing the membranes between two gold electrodes at a distance of 1 cm using an AlphaLab, Inc. multimeter.

3. Results and discussion

3.1. CA-[BMIM]Cl solution viscosity measurements

The impact of IL on the viscosity of CA solutions can be seen in Figure 2a. Without [BMIM]Cl the viscosity was lowest at 471 cP however, this increases sharply from 2% to 6% of [BMIM]Cl with a maximum of 650 cP. Unexpectedly, the solution behavior changes suddenly above 6% gradually decreases in viscosity to 600 cP at 12% of IL. This increase and decrease in viscosity can be attributed to the large BMIM^+ and small Cl^- ions which can interfere with hydrogen bonding between cellulose acetate chains.^[39,40] Therefore, initially low concentrations from 2% to 6% may not be enough to break the extensive hydrogen bonding but at higher concentrations, 8%–12% of IL, there is a breakdown of the hydrogen bonds between cellulosic chains, thus decrease the viscosity of the CA solution.

3.2. CA-[BMIM]Cl solutions and membranes conductivity measurements

From the Figure 2b it can be seen that the higher the amount of IL, the higher the conductivity of the CA solution (0.01 mS/cm up to 2.6 mS/cm). This is caused by a gradual increase of BMIM^+ and Cl^- ions which dissociated in the solution. The conductivity measurements have illustrated in the Table 1 and membranes from 0%–4 percentage showed no conductivity because of less free ions but as the volume ratio of IL increases, there was a significant rise in the conductivity. This is due to producing more charge carriers by IL therefore, membranes with 10% of ionic liquid

Table 1. Influence of [BMIM]Cl on the conductivity and on the formation of the nanofibers.

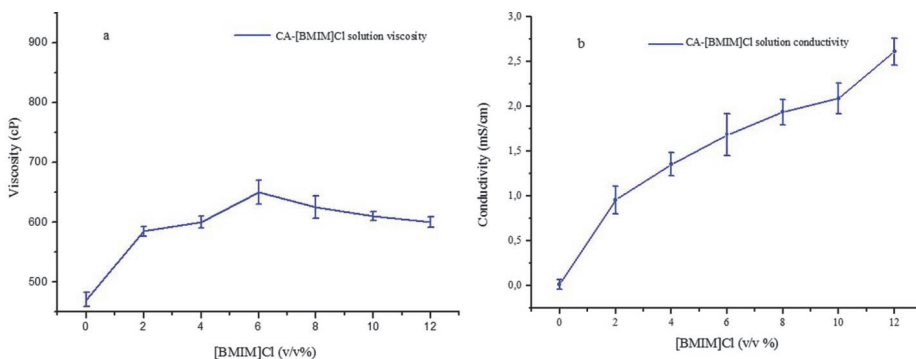
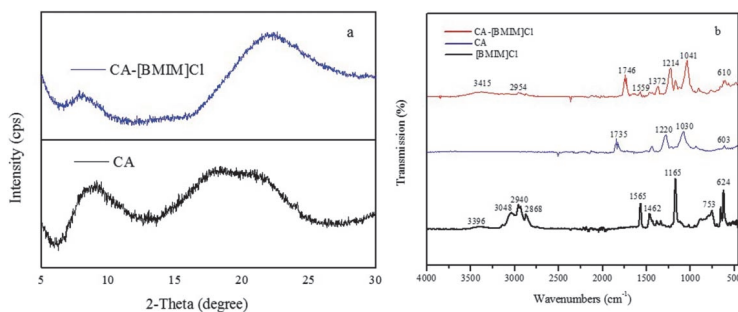
[BMIM]Cl Concentration (v/v %)	Conductivity (S/cm)	Avg. Fibers Diameter (nm)	Fibrous membrane
0%	0.00	125	Uniform fibers
2%	0.00	150	Fibers with beads
4%	0.00	204	Fibers with beads
6%	1.93×10^{-9}	525	Uniform fibers
8%	6.80×10^{-9}	348	Uniform fibers
10%	1.70×10^{-7}	300	Uniform fibers
12%	2.71×10^{-7}	180	Uniform fibers

was increased upto 1.70×10^{-7} S/cm and finally, the conductivity of CA nanofibers with 12% of IL showed the highest value of 2.71×10^{-7} S/cm.

3.3. XRD and FTIR analysis of CA-[BMIM]Cl nanofibers

To examine the changes in the crystal structure of CA and CA-[BMIM]Cl during electrospinning, X-ray diffraction (XRD) was used (Figure 3a). Pure CA nanofibers exhibited two typical wide bands at 8.9° and 17.9° . The peak intensity of CA nanofibers at 8.7° decreased incrementally with the addition of [BMIM]Cl, indicating a reduction in crystallinity due to [BMIM]Cl disrupting the molecular packing of the

CA. The [BMIM]Cl FTIR spectrum (Figure 3b) exhibit multiple peaks 3396 cm^{-1} for secondary amines, for O—H stretching at $2960\text{--}2140 \text{ cm}^{-1}$, 1643 cm^{-1} for C=N and C=C bonding and $1567\text{--}696 \text{ cm}^{-1}$ corresponds to stretching C—C, C—O, or C—N bonds. Respective wavelength (cm^{-1}) and transmittance (%T) confirm the chemical structure of [BMIM]Cl.^[41] Cellulose acetate can also accept and/or donate a proton due to the presence of carboxylic and unsubstituted hydroxyl functional groups. By comparing FTIR spectra of pure CA with FTIR spectra of CA-[BMIM]Cl nanofibers, sharper peaks of wavelengths 1746 cm^{-1} , 1214 cm^{-1} and 1041 cm^{-1} assigned to C—C, C—N or C—O bonding were observed as shown in the Figure 3b.^[42,43] The FTIR spectra of pure CA, CA-[BMIM]Cl shows that pure CA nanofibers exhibit characteristic bands at 1735 cm^{-1} , and 1372 cm^{-1} corresponding to C=O and C—H stretching from —OCOCH₃, respectively. Bands at 1220 cm^{-1} and 1030 cm^{-1} reveal the C—C and C—O stretching vibrations in the pyranoid ring and C—O—C (ether linkage) from the glycosidic units. In the CA-[BMIM]Cl spectrum, characteristic bands at 1746 cm^{-1} (C—C stretching), 1214 cm^{-1} (C—N stretching) and 1041 cm^{-1} (C—O stretching) indicate that the BMIM⁺ and Cl[−] ions of [BMIM]Cl formed hydrogen bonds with CA, as expected.^[42,44] A proposed interaction between CA and [BMIM]Cl is presented in Figure 1. However, further

**Figure 2.** Influence of [BMIM]Cl on the viscosity (a) and on the conductivity of CA solutions (b).**Figure 3.** XRD patterns of CA nanofibers, hybrid CA-[BMIM]Cl (a), FTIR spectrum of [BMIM]Cl, CA and CA-[BMIM]Cl (b).

investigation is needed to study the basic mechanism and interaction between CA and [BMIM]Cl in such solvent systems.

3.4. Morphology of CA-[BMIM]Cl electrospun nanofibres

SEM images of the pure CA electrospun nanofibers and CA-[BMIM]Cl electrospun nanofibers are shown in Figure 4 along with their respected characteristics illustrated in Table 1. The pure CA electrospun nanofibers show no beads but as the concentration of [BMIM]Cl increases from 2 to 4%, the formations of the fibers change significantly and show beads with fibers (Figure 4b and 4c). These are caused by low concentration of IL, which leads to the low conductivity of the

electrospun solution thus promoting jet instability and creating beads with fibers. Similarly, higher amounts of IL enhance the conductivity of the solution, which increases jet stability and produces no beads with fibers as shown in Figure 4. The concentration of IL not only affects the morphology, but also affects the diameter of the nanofibers as shown in Figure 5, the average diameter of the pure CA electrospun nanofibers was 125nm which escalated up to 525nm with an addition of 6% of IL. This change is due to less viscoelastic forces that were created by decreasing concentrations of IL during electrospinning process which decreases the stretching force, hence obtained fibers showed greater diameters. With higher amounts of IL, i.e. 8% to 12%, the solution electrical conductivity increases significantly which results an increase in

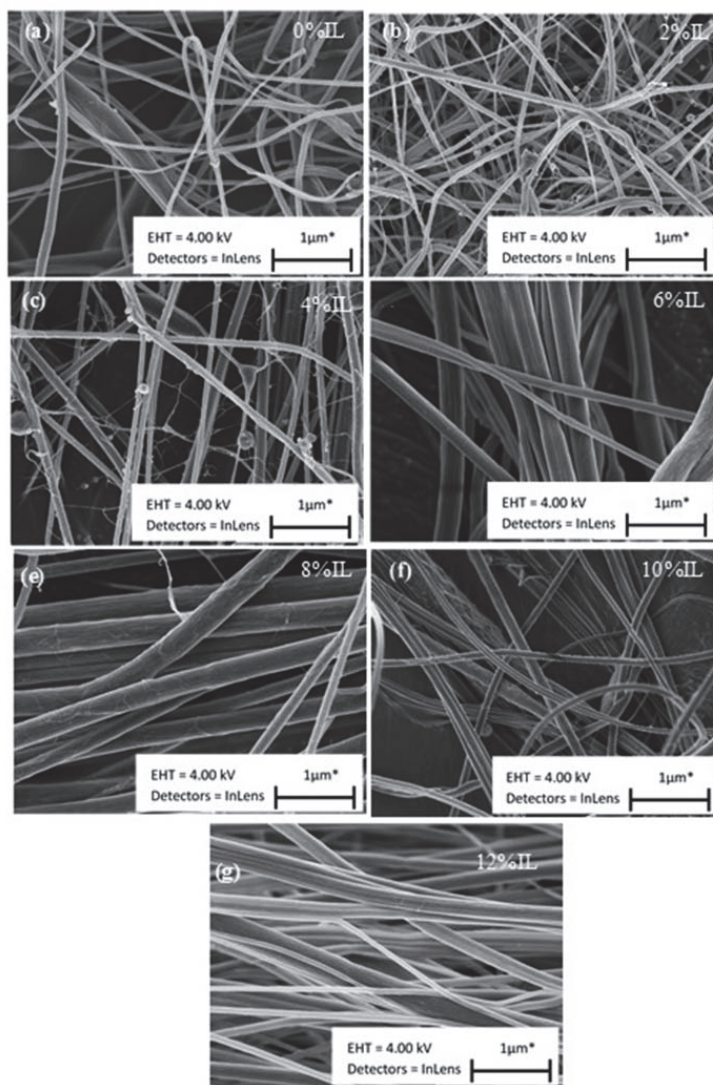


Figure 4. SEM images of pure CA nanofibers (a) and CA with 2%IL, 4%IL, 6%IL, 8%IL, 10%IL and 12%IL (b-g).

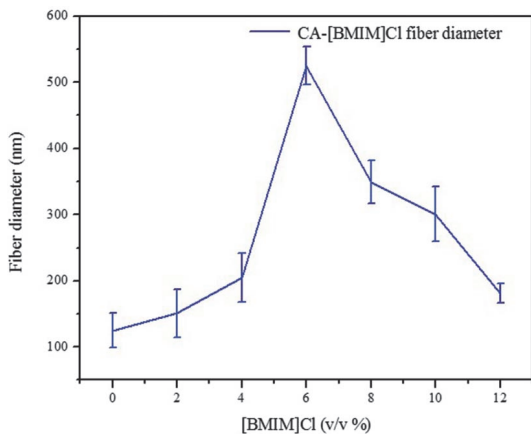


Figure 5. Effect of [BMIM]Cl on the average diameter of the CA nanofibers.

viscoelastic forces therefore more nanosized fibers were observed e.g. 180 nm.

4. Conclusion

CA-[BMIM]Cl nanofibrous membranes were prepared by electrospinning. The solution viscosity, conductivity and the characteristics of electrospun nanofibers were investigated. Scanning electron microscopy images revealed that the nanofibers with higher concentrations of [BMIM]Cl were created very fine fiber and the average diameter of the fibers decreased as the addition of IL increased in the polymeric solution i.e. 12% of ionic liquid produce a diameter of 180nm as of the nearly the same as pure CA electrospun nanofibers. It was also noted that 12% of [BMIM]Cl is enough for uniform fibers with enhanced conductivity of the fibers up to 2.21×10^{-7} S/cm. The study also concluded that [BMIM]Cl can dissolve cellulose acetate useful for electrospinning and create materials with high conductivity. This new class of cellulosic nanofibers has practical significance in the fabrication of bio based smart device applications.

References

- Agarwal, S.; Wendorff, J.-H.; Greiner, A. Use of electrospinning technique for biomedical applications. *Polymer*. **2008**, *49*(26), 5603–5621. <https://doi.org/10.1016/j.polymer.2008.09.014>.
- Wang, X.; Drew, C.; Lee, S.-H.; Senecal, K.-J.; Kumar, J.; Samuelson, L.-A. ELECTROSPINNING TECHNOLOGY: A NOVEL APPROACH TO SENSOR APPLICATION, *Journal of Macromolecular Science. Part A*. **2002**, *39*(10), 1251–1258.
- Huang, Z.-M.; Zhang, Y.-Z.; Kotaki, M.; Ramakrishna, S. A review on polymer nanofibers by electrospinning and their applications in nanocomposites. *Composites Science and Technology*. **2003**, *63*(15), 2223–2253. [https://doi.org/10.1016/S0266-3538\(03\)00178-7](https://doi.org/10.1016/S0266-3538(03)00178-7).
- Leach, M.-K.; Feng, Z.-Q.; Tuck, S.-J.; Corey, J.-M. Electrospinning Fundamentals: Optimizing Solution and Apparatus Parameters. *Journal of Visualized Experiments: JoVE*. **2011**, (47), 2494.
- Garg, K.; Bowlin, G.-L. Electrospinning jets and nanofibrous structures. *Biomicrofluidics*. **2011**, *5*(1), 013403. <https://doi.org/10.1063/1.3567097>.
- Zussman, E.; Theron, A.; Yarin, A.-L. Formation of nanofiber cross-bars in electrospinning. *Applied Physics Letters*. **2003**, *82*(6), 973–975. <https://doi.org/10.1063/1.1544060>.
- Ramakrishna, S.; Fujihara, K.; Teo, W.-E.; Yong, T.; Ma, Z.; Ramaseshan, R. Electrospun nanofibers: solving global issues. *Materials Today*. **2006**, *9*(3), 40–50. [https://doi.org/10.1016/S1369-7021\(06\)71389-X](https://doi.org/10.1016/S1369-7021(06)71389-X).
- Sill, T.-J.; von Recum, H.-A. Electrospinning: Applications in drug delivery and tissue engineering. *Biomaterials*. **2008**, *29*(13), 1989–2006. <https://doi.org/10.1016/j.biomaterials.2008.01.011>.
- Martins, A.; Reis, R.-L.; Neves, N.-M. Electrospinning: Processing technique for tissue engineering scaffolding. *International Materials Reviews*. **2008**, *53*(5), 257–274. <https://doi.org/10.1179/174328008X353547>.
- Murthy, N.; Campbell, J.; Fausto, N.; Hoffman, A.-S.; Stayton, P.-S. Design and synthesis of pH-responsive polymeric carriers that target uptake and enhance the intracellular delivery of oligonucleotides. *Journal of Controlled Release*. **2003**, *89*(3), 365–374. [https://doi.org/10.1016/S0168-3659\(03\)00099-3](https://doi.org/10.1016/S0168-3659(03)00099-3).
- Kattamuri, N.; Shin, J.-H.; Kang, B.; Lee, C.-G.; Lee, J.-K.; Sung, C. Development and surface characterization of positively charged filters. *Journal of Materials Science*. **2005**, *40*(17), 4531–4539. <https://doi.org/10.1007/s10853-005-2803-0>.
- Jia, H.; Zhu, G.; Vugrinovich, B.; Kataphinan, W.; Reneker, D.-H.; Wang, P. Enzyme-Carrying Polymeric Nanofibers Prepared via Electrospinning for Use as Unique Biocatalysts. *Biotechnology Progress*. **2002**, *18*(5), 1027–1032. <https://doi.org/10.1021/bp020042m>.
- Xie, J.; Li, X.; Xia, Y. Putting Electrospun Nanofibers to Work for Biomedical Research. *Macromolecular Rapid Communications*. **2008**, *29*(22), 1775–1792. <https://doi.org/10.1002/marc.200800381>.
- Kim, K.; Yu, M.; Zong, X.; Chiu, J.; Fang, D.; Seo, Y.-S.; Hsiao, B.-S.; Chu, B.; Hadjiargyrou, M. Control of degradation rate and hydrophilicity in electrospun non-woven poly(DL-lactide) nanofiber scaffolds for biomedical applications. *Biomaterials*. **2003**, *24*(27), 4977–4985. [https://doi.org/10.1016/S0142-9612\(03\)00407-1](https://doi.org/10.1016/S0142-9612(03)00407-1).
- Zhang, Y.-Z.; Venugopal, J.; Huang, Z.-M.; Lim, C.-T.; Ramakrishna, S. Crosslinking of the electrospun gelatin nanofibers. *Polymer*. **2006**, *47*(8), 2911–2917. <https://doi.org/10.1016/j.polymer.2006.02.046>.
- Yu, D.-G.; Li, J.-J.; Zhang, M.; Williams, G.-R. High-quality Janus nanofibers prepared using three-fluid electrospinning. *Chemical Communications*. **2017**, *53*(33), 4542–4545. <https://doi.org/10.1039/C7CC01661A>.
- Yang, G.-Z.; Li, J.-J.; Yu, D.-G.; He, M.-F.; Yang, J.-H.; Williams, G.-R. Nanosized sustained-release drug depots fabricated using modified tri-axial electrospinning. *Acta Biomaterialia*. **2017**, *53*, 233–241. <https://doi.org/10.1016/j.actbio.2017.01.069>.
- Yu, D.-G.; Li, X.-Y.; Wang, X.; Yang, J.-H.; Bligh, S.-W.-A.; Williams, G.-R. Nanofibers Fabricated Using Triaxial Electrospinning as Zero Order Drug Delivery Systems. *ACS Applied Materials & Interfaces*. **2015**, *7*(33), 18891–18897. <https://doi.org/10.1021/acsami.5b06007>.
- Wu, Y.-H.; Yu, D.-G.; Li, X.-Y.; Diao, A.-H.; Illangakoon, U.-E.; Williams, G.-R. Fast-dissolving sweet sedative nanofiber membranes. *Journal of Materials Science*. **2015**, *50*(10), 3604–3613. <https://doi.org/10.1007/s10853-015-8921-4>.
- Olivier-Bourbigou, H.; Magna, L.; Morvan, D. Ionic liquids and catalysis: Recent progress from knowledge to applications. *Applied Catalysis A: General*. **2010**, *373*(1-2), 1–56. <https://doi.org/10.1016/j.apcata.2009.10.008>.
- Kubisa, P. Ionic liquids as solvents for polymerization processes-Progress and challenges. *Progress in Polymer Science (Oxford)*. **2009**, *34*(12), 1333–1347. <https://doi.org/10.1016/j.progpolymsci.2009.09.001>.
- English, N.-J.; Mooney, D.-A.; O'Brien, S. Ionic liquids in external electric and electromagnetic fields: a molecular dynamics study. *Molecular Physics*. **2011**, *109*(4), 625–638. <https://doi.org/10.1080/00268976.2010.544263>.
- Datta, R.-S.; Said, S.-M.; Shahriar, S.-R.; Abdullah, N.; Sabri, M.-F.-M.; Balamurugan, S.; Miyazaki, Y.; Hayashi, K.; Hashim, N.-A.; Habiba, U.; Afifi, A.-M. Ionic liquid entrapment by an electrospun polymer nanofiber matrix as a high conductivity polymer electrolyte. *RSC Advances*. **2015**, *5*(60), 48217–48223. <https://doi.org/10.1039/C5RA03935E>.

- [24] Savest, N.; Plamus, T.; Tarasova, E.; Viirsalu, M.; Krasnou, I.; Gudkova, V.; Küppar, K.-A.; Krumme, A. The effect of ionic liquids on the conductivity of electrospun polyacrylonitrile membranes. *Journal of Electrostatics*. **2016**, *83*, 63–68. <https://doi.org/10.1016/j.elstat.2016.07.006>.
- [25] Xiong, Y.; Wang, H.; Wu, C.; Wang, R. Preparation and characterization of conductive chitosan–ionic liquid composite membranes. *Polymers for Advanced Technologies*. **2012**, *23*(11), 1429–1434. <https://doi.org/10.1002/pat.2061>.
- [26] Ou, R.; Xie, Y.; Shen, X.; Yuan, F.; Wang, H.; Wang, Q. Solid biopolymer electrolytes based on all-cellulose composites prepared by partially dissolving cellulose fibers in the ionic liquid 1-butyl-3-methylimidazolium chloride. *Journal of Materials Science*. **2012**, *47*(16), 5978–5986. <https://doi.org/10.1007/s10853-012-6502-3>.
- [27] Kosan, B.; Michels, C.; Meister, F. Dissolution and forming of cellulose with ionic liquids. *Cellulose*. **2008**, *15*(1), 59–66. <https://doi.org/10.1007/s10570-007-9160-x>.
- [28] Seddon, K.-R. Ionic Liquids for Clean Technology. *Journal of Chemical Technology & Biotechnology*. **1997**, *68*(4), 351–356. [https://doi.org/10.1002/\(SICI\)1097-4660\(199704\)68:4%3c351::AID-JCTB613%3e3.0.CO;2-4](https://doi.org/10.1002/(SICI)1097-4660(199704)68:4%3c351::AID-JCTB613%3e3.0.CO;2-4).
- [29] Xing, C.; Guan, J.; Li, Y.; Li, J. Effect of a Room-Temperature Ionic Liquid on the Structure and Properties of Electrospun Poly(vinylidene fluoride) Nanofibers. *ACS Applied Materials & Interfaces*. **2014**, *6*(6), 4447–4457. <https://doi.org/10.1021/am500061v>.
- [30] Viswanathan, G.; Murugesan, S.; Pushparaj, V.; Nalamasu, O.; Ajayan, P.-M.; Linhardt, R.-J. Preparation of Biopolymer Fibers by Electrospinning from Room Temperature Ionic Liquids. *Biomacromolecules*. **2006**, *7*(2), 415–418. <https://doi.org/10.1021/bm050837s>.
- [31] Meli, L.; Miao, J.; Dordick, J.-S.; Linhardt, R.-J. Electrospinning from room temperature ionic liquids for biopolymer fiber formation. *Green Chemistry*. **2010**, *12*(11), 1883–1892. <https://doi.org/10.1039/c0gc00283f>.
- [32] Gudkova, V.; Krumme, A.; Märtson, T.; Rikko, M.; Tarassova, E.; Viirsalu, M. The impact of 1-butyl-3-methylimidazolium chloride on electrospinning process of SAN polymer solutions and electrospun fiber morphology. *Journal of Electrostatics*. **2014**, *72*(6), 433–436. <https://doi.org/10.1016/j.elstat.2014.08.003>.
- [33] Brown, R.-M. The Biosynthesis of Cellulose. *Journal of Macromolecular Science. Part A*. **1996**, *33*(10), 1345–1373.
- [34] Feldman, D. Cellulose Nanocomposites. *Journal of Macromolecular Science. Part A*. **2015**, *52*(4), 322–329.
- [35] Seifert, M.; Hesse, S.; Kabrelian, V.; Klemm, D. Controlling the water content of never dried and reswollen bacterial cellulose by the addition of water-soluble polymers to the culture medium. *Journal of Polymer Science Part A: Polymer Chemistry*. **2004**, *42*(3), 463–470. <https://doi.org/10.1002/pola.10862>.
- [36] Liu, X.; Chang, P.-R.; Zheng, P.; Anderson, D.-P.; Ma, X. Porous cellulose facilitated by ionic liquid [BMMIM]Cl: fabrication, characterization, and modification. *Cellulose*. **2015**, *22*(1), 709–715. <https://doi.org/10.1007/s10570-014-0467-0>.
- [37] Tsivintzelis, M.-B.-I.; Philippou, J.-L.; Panayiotou, C. *Electrospinning of Cellulose and Cellulose Acetate Nanofibers*. Proceedings of the 4th Workshop on Nanosciences and Nanotechnologies, Thessaloniki, Greece, **2007**, p. 103.
- [38] Dupont, J.; Consorti, C.-S.; Suarez, P.-A.-Z.; de Souza, R.-F. *Preparation of 1-Butyl-3-Methyl Imidazolium-Based Room Temperature Ionic Liquids, Organic Syntheses*, John Wiley & Sons, Inc. **2003**. <https://doi.org/10.1002/0471264180.os079.28>.
- [39] Liu, Z.; Wang, H.; Li, Z.; Lu, X.; Zhang, X.; Zhang, S.; Zhou, K. Characterization of the regenerated cellulose films in ionic liquids and rheological properties of the solutions. *Materials Chemistry and Physics*. **2011**, *128*(1–2), 220–227. <https://doi.org/10.1016/j.matchemphys.2011.02.062>.
- [40] Xia, X.; Yao, Y.; Gong, M.; Wang, H.; Zhang, Y. Rheological behaviors of cellulose/[BMMIM]Cl solutions varied with the dissolving process. *Journal of Polymer Research*. **2014**, *21*(7), 512. <https://doi.org/10.1007/s10965-014-0512-6>.
- [41] Islam, S.; Arnold, L.; Padhye, R. Ionic liquids – recomposting the past and writing the future. *Smartex Res. J.* **2012**, *1*, 72–79.
- [42] Zhang, H.; Wu, J.; Zhang, J.; He, J. 1-Allyl-3-methylimidazolium chloride room temperature ionic liquid: a new and powerful nonderivatizing solvent for cellulose. *Macromolecules*. **2005**, *38*(20), 8272–8277. <https://doi.org/10.1021/ma0505676>.
- [43] Kathirgamanathan, K.; Grigsby, W.-J.; Al-Hakkak, J.; Edmonds, N.-R. Two-Dimensional FTIR as a Tool to Study the Chemical Interactions within Cellulose-Ionic Liquid Solutions. *International Journal of Polymer Science*. **2015**, *9*, 1–9.
- [44] Hameed, N.; Guo, Q. Natural wool/cellulose acetate blends regenerated from the ionic liquid 1-butyl-3-methylimidazolium chloride. *Carbohydrate Polymers*. **2009**, *78*(4), 999–1004. <https://doi.org/10.1016/j.carbpol.2009.07.033>.

Publication III

Javed, K.; Oolo, M.; Savest, N.; Krumme, A. (2018). A Review on Graphene-Based Electrospun Conductive Nanofibers, Supercapacitors, Anodes, and Cathodes for Lithium-Ion Batteries. *Critical Reviews in Solid State and Materials Sciences*.



A Review on Graphene-Based Electrospun Conductive Nanofibers, Supercapacitors, Anodes, and Cathodes for Lithium-Ion Batteries

Kashif Javed, Marco Oolo, Natalja Savest, and Andres Krumme

Department of Materials and Environmental Technology, Tallinn University of Technology, Tallinn, Estonia

ABSTRACT

Electrospinning has recognized as the most versatile and adaptable method for the fabrication of nanofibers. Fiber scientists have extensively introduced original solutions for harvesting and storing energy from nanofibers in order to improve storage capacity and environmental impact of electrospun supercapacitors, anodes, and cathodes. Among these efforts, graphene gained significant interests for researchers, a multifaceted molecule possessing many unique and desirable properties such as high strength, flexibility, optical transparency, and conductivity. This makes graphene as superior as to many other nanomaterials like carbon nanotubes (CNTs) and conductive nanometallic particles. The reported properties and applications of this two-dimensional (2D) structure have opened up new opportunities for the lightweight future devices and systems. This review article aims to present an overview of the advancements in graphene-based electrospun conductive nanofibers, supercapacitors, and graphene-based electrospun anodes and cathodes for lithium-ion (Li-ion) batteries. Details of the electrospinning processes, reduction methods, and electrical properties are discussed to yield insights on how significant improvements can be made in future developments.

Abbreviations: GO: graphene oxide; rGO: reduced graphene oxide; GONRs: graphene oxide nanoribbons; GNS: graphene nanosheets; CNTs: carbon nanotubes; MWCNTs: multi-walled carbon nanotubes; PAN: polyacrylonitrile; DMF: dimethylformamide; PVP: polyvinylpyrrolidone; N_2H_4 : hydrazine; PMMA: poly(methyl methacrylate); PVC/PLGA: polyvinyl chloride/poly(lactic-co-glycolic acid); CNF: carbon nanofibers; ACNF: activated carbon nanofiber; GCNF: graphene-wrapped electrospun carbon nanofibers; ACFs: anisotropic conductive films; PANI: Polyaniline; HCSA: camphor-10-sulfonic acid; PEO: polyethylene oxide; ; G-PBASE: 1-pyrenebutanoic acid, succinimidyl ester functionalized graphene; PVA/ODA-MMT: polyvinyl alcohol/octadecylamine-modified montmorillonites; GO-g-[P(HEMA-g-PCL)]: graphene functionalized poly(2-hydroxyethyl methacrylate)-graft-poly(ϵ -caprolactone); PI-GNR: polyimide composite fibers with graphene nanoribbon; GBEENS: graphene-based electroconductive electrospun nanofibers; KOH: potassium hydroxide; H_2SO_4 : sulfuric acid; CV: cyclic voltammetry; VO: vanadium oxide; V_2O_5 : vanadium pentoxide; $V(C_5H_7O_2)_3$: vanadium acetylacetonate; M-rGO/PA66 medium: medium diameter reduced graphene oxide nanosheets/polyamide-66; PEDOT: poly(3,4-ethylenedioxythiophene); HPCNF: hierarchical porous carbon nanofiber; TEOS: tetraethyl orthosilicate; CNF@PPy: carbon nanofiber/polypyrrole composite materials; Na_2SO_4 : sodium sulfate; GBEAs: graphene-based electrospun anodes; SiNPs: silicon nanoparticles; $SnO_2@C@G$ hNFs: tin dioxide hollow nanofibers coated with carbon and wrapped with GO layer; $CoMoO_4@graphene$: cobalt molybdate/graphene composite; $Si_{60}Sn_{12}Ce_{18}Fe_5Al_3Ti_2$ NFs: silicon-based metallic glass alloy nanofibers; OMTiO₂-rGO-NF: ordered mesoporous titania reduced go nanofibers; $Li_4Ti_5O_{12}$: lithium titanium oxide; CoO: cobalt oxide.

KEYWORDS

Graphene; electrospinning; supercapacitors; nanofibers; lithium-ion batteries

Table of contents

1. Introduction	2
2. What is graphene?	3
2.1. Graphene as nanofiller for electrospinning	4
2.2. Graphene-based electrospun electroconductive nanofibers	4
2.3. Graphene-based electrospun supercapacitors	8

CONTACT Kashif Javed  kashif.javed@ttu.ee

Color versions of one or more of the figures in the article can be found online at www.tandfonline.com/bsms.

© 2018 Taylor & Francis Group, LLC

2.4. Graphene-based electrospun anodes for Li-ion batteries	12
2.5. Graphene-based electrospun cathodes for Li-ion batteries	13
3. Conclusion and future directions	13
3.1. Appropriate dispersion of GO	14
3.2. Reduction of GO-based nanofibers	14
3.3. Stable electrolyte systems for GO-based supercapacitors	14
Disclosure statement	14
References	14

1. Introduction

Nanofibers can be produced by number of methods: examples include by drawing different polymers, template synthesis of nanostructured polymer, phase separation, and self-assembly.^{1,2} However, a unique and versatile technique for producing micro- and nanofibers through an electric field called “electrospinning” has become a ubiquitous method in the field of nanotechnology.^{3–5} The term electrospinning came from electrostatic spinning, which was used more than 60 years ago and the first description of this method was patented in 1902 by J.F. Cooley entitled as “Apparatus for electrically dispersing fluids.” In this patent (US 692631), he designed an apparatus for producing the fibers from the composite fluids through an electrical discharge field.⁶ In brief, electrospinning is a process where a charged jet of polymer solution is spun on a ground collector to produce nanofibers as shown in Figure 1. This is an easy and robust way to produce nanofibers from huge number of different polymers including synthetic polymers, biopolymers, and blends of these polymers.^{1, 7–9} The rising popularity of this method has resulted in fact that over 200 research institutes and universities are studying the electrospinning process and producing different kinds of nanofibers⁷ to explore more potential in this technique.

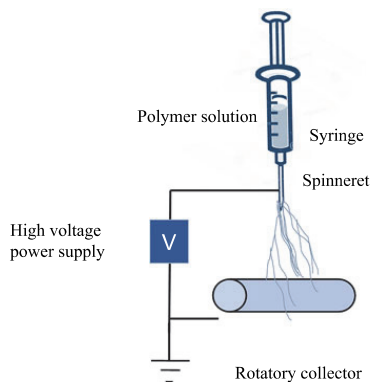


Figure 1. A schematic diagram of electrospinning process.

This century, the number of new fibers that have been electrospun by this process and scientists discovering unique nanofibers that would prove to be breakthroughs in several applications like drug delivery systems, biosensors, solar cells, electronic devices, transparent electrodes, or membrane filtration.^{10–15} In the last 16 years, the contribution of the work in the area of electrospinning presented in Figure 2a with more than 3300 published documents indexed in the Scopus database.

The efforts in electrospinning around the globe in different institutes and research centers (see Figures 2b and 3) clearly beyond doubt that over last 10 years, more than 7000 research papers have been published. So far, electrospinning has been used for the fabrication of one-dimensional (1D) nanofibers¹⁶ from wide range of polymers and each of the nanofiber has

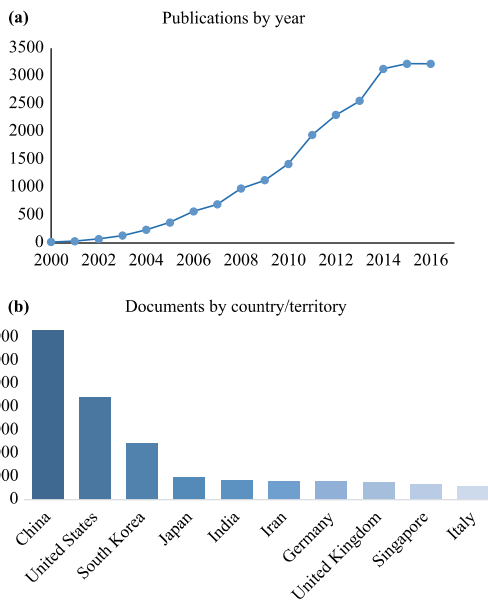


Figure 2. Number of publications by year (a) and electrospinning research around the world in different countries (b), data analysis carried out using the Scopus search with the term “electrospinning” as of December 2016.

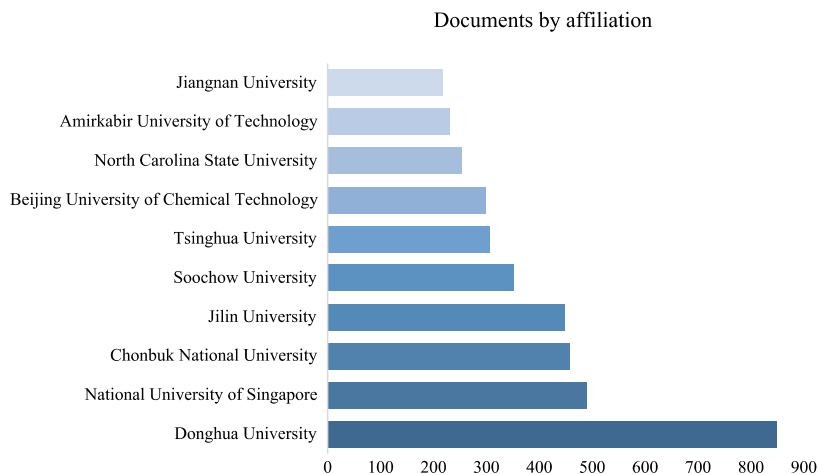


Figure 3. Publication distribution by affiliation data analysis carried out using the Scopus search system with the term “electrospinning” as of December 2016.



Figure 4. Hexagonal structure of graphene.

different chemical and physical properties with a capability of practical significance to be used in advance applications.^{17–22}

For the fabrication of conductive nanofibers, popularity of nanofillers can be categorized into zero-dimensional (0D), 1D, two-dimensional (2D), and three-dimensional (3D)^{23–28} which was commenced with this decade. These nanomaterials enhanced number of properties, for example, optical, mechanical, thermal, and electrical. Among these nanomaterials, graphene (2D nanofiller) shows the best properties across all above-stated types nanomaterials^{29,30} and has many distinct reasons to add into electrospun nanofibers.

In this review article, we present a comprehensive overview on graphene-based electrospun electroconductive nanofibers, supercapacitors, and graphene-

based electrospun anodes (GBEAs) for lithium (Li)-ion batteries including synthesis, fabrication, reduction, and electrical properties. There are many previous review articles on graphene-based nanocomposites, wet-spun fibers, dry-spinning fibers, dry-jet wet-spinning fibers, and their synthesis, performance, and applications.³¹ However, there is no detailed review/study on graphene-based electrospun conductive nanofibers, supercapacitors, anodes, and cathodes for Li-ion batteries. Therefore, in this review paper, we judiciously summarize the recent developments and the fabrication methods of graphene-based electrospun nanofibers in these applications.

2. What is graphene?

The word “graphene” is referred as world first 2D paper like lightweight material.^{32,33} Due to owing multifunctional properties like conductivity, specific capacitance, photocatalytic activity, hydrophobicity, antibacterial, and having high mechanical strength,³⁴ which make graphene far superior than other nanomaterials, graphene is a one-atom-thick sheet of carbon atoms tightly packed into hexagonal structures and looks like a honeycomb lattice as shown in Figure 4. It is the strongest and the thinnest material known to the man, stronger than steel (100–300 times) and lightest (weighing around 0.77 milligrams for 1m²).³⁵ It has been over 13 years now since Geim and Novoselov, two innovative scientists, won the Nobel prize for the discovery of this wondered material “graphene” that triggered a sharp rise in graphene research.^{33,36,37}

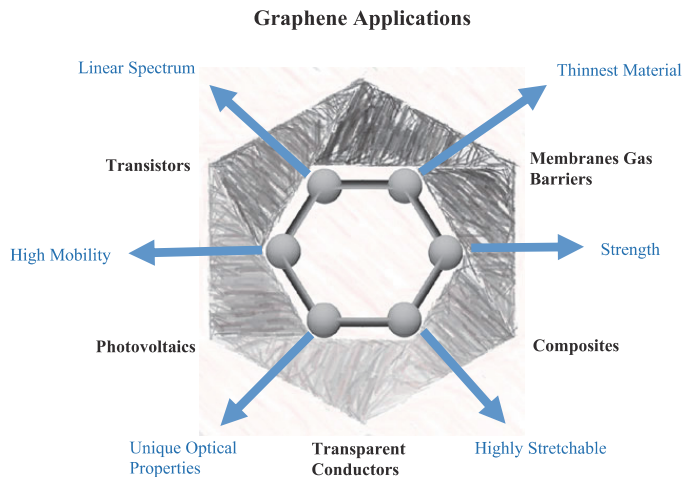


Figure 5. Properties and applications of graphene in different fields.

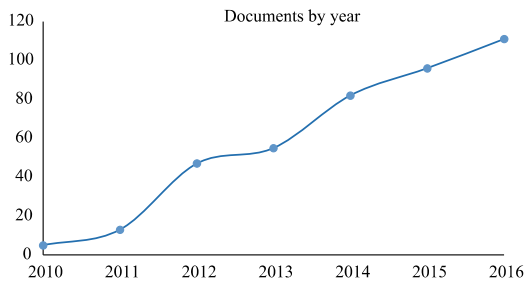


Figure 6. Number of articles published by year using graphene as a nanofiller data analysis carried out using the Scopus search system with the term “graphene electrospinning” from 2010 to 2016.

As seen in [Figure 5](#), there are many practical applications of graphene in science and technology including, but not limited to electronics, spintronic, photonics, and optoelectronics sensors, flexible electronics, energy storage and generation, composites, and biomedical applications.^{38–42}

2.1. Graphene as nanofiller for electrospinning

Graphene, a promising candidate to act as a nanofiller in electrospinning building number of multifunctional properties like mechanical, electrical, and morphological enhancement to achieve desired diameters or porosity of the nanofibers. These characteristics of graphene prove to be a strong nanofiller candidate to potentially revolutionize lightweight nanocomposites. Since graphene was discovered, many types of synthetic and natural polymers were electrospun by this

novel nanofiller which remarkably stimulated the spinning process and have shown dramatic enhancement in the properties of electrospun nanofibers such as mechanical strength, hydrophilicity, conductivity, and thermal stability.^{23,43–57} The loading of graphene in an electrospinning process is a crucial step, which determines the flexibility, chemical affinity, stability, and functionality and consist of two steps: (1) graphene oxide (GO) sheets can incorporate into the polymeric solution by melt mixing, solution blending, or *in situ* polymerization; and (2) electrospun nanofibers were reduced either by chemical method or by annealing under high temperatures, which referred as reduced graphene oxide (rGO) nanofibers. Naturally, GO is an insulator and a poor electrical conductor but when treating with strong reducing agents or treated under high temperatures, most of the conjugated structure of graphene has been restored by removing of oxygen-containing functionalities. However, there are the methods^{58,59} in which reduced graphene can electrospin directly with the polymers. Nevertheless, this will lead inhomogeneous dispersions which might face challenges and difficulties in the continuous electrospinning processes. [Figures 6 and 7](#) give an overview about graphene as a nanofiller in the literatures published from 2010 to 2016.

2.2. Graphene-based electrospun electroconductive nanofibers

Nowadays, enormous advances in graphene-based electroconductive electrospun nanofibers (GBEENs) have been made especially in the field of electronics.

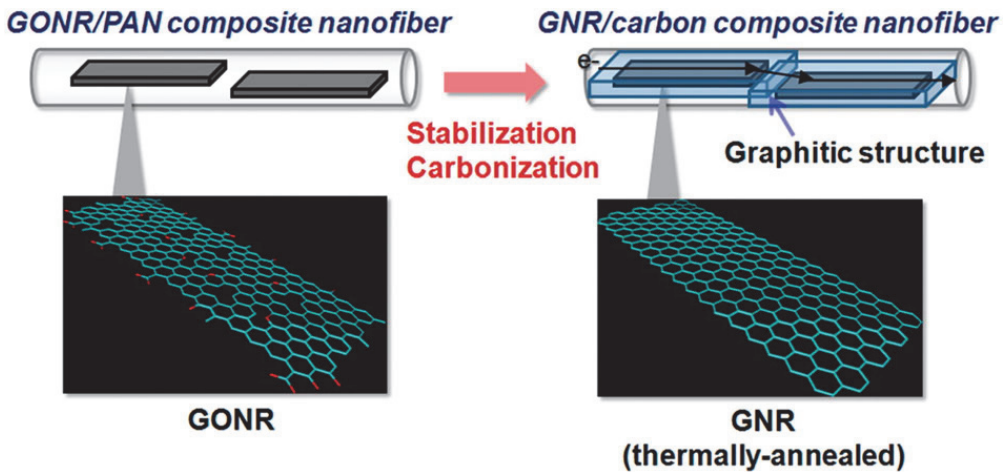


Figure 7. Schematic structures of the GO/PAN nanofiber before and after carbonization as adapted from Matsumoto et al.⁶⁰

Table 1. Summary of graphene-based electrospun hybrid nanofibers.

Electrospinning hybrid materials	Reduction method	Resistivity/conductivity	References
PAN and GONRs	Heated at 1000 °C for 1h	$165.1 \pm 4.3 \text{ Scm}^{-1}$	60
GO, PAN, and PVP	N_2H_4 for 6h	Graphene-PAN 75 Scm^{-1} Graphene-PVP 25 Scm^{-1}	56
PANI/G-PBASE and PMMA	Hydrazine monohydrate at 80 °C for 24h	30 Scm^{-1}	61
PVC/PLGA nanofibers	HI solution (55%) at 100 °C for 1h	10.0 Scm^{-1}	62
RuO_2 /activated carbon nanofiber (ACNF) and G	Heated at 800 °C for 1h	0.59 Scm^{-1}	63
GCNF anchoring of MoS_2	Heated at 800 °C for 2h	0.56 Scm^{-1}	64
Anisotropic conductive film (ACF) ultrasonic spray (S-rGO/ACF)	Heated at 800 °C for 1h	0.42 Scm^{-1}	65
RGO/PAN	Heated at 800 °C for 1h	0.24 Scm^{-1}	58
PAN/ Fe_3O_4 /G	Carbonized at 650 °C for 1h	0.21 Scm^{-1}	66
PAN/PMMA, SbCl_3 , and GO	Heated at 700 °C for 2h	$4.20 \times 10^{-2} \text{ Scm}^{-1}$	67
PANI with camphor-10-sulfonic acid (HCSA)- and polyethylene oxide (PEO)-filled G-PBASE	N_2H_4 heated to 80 24hrs	$9.92 \times 10^{-4} \text{ Scm}^{-1}$	68
PI, GNR, and CNT	HI- H_2O at 98 °C for 10h	$8.3 \times 10^{-4} \text{ Scm}^{-1}$ Parallel $7.2 \times 10^{-1} \text{ Scm}^{-1}$ Perpendicular	69
CNF, Si, and graphene-covered Ni particles	Carbonization at 650 °C for 1h	$9.5 \times 10^{-5} \text{ Scm}^{-1}$	70
PVA/ODA-MMT-poly(MA-alt-1-octadecene)-g-GO	No reduction	$5.91 - 4.42 \times 10^{-5} \text{ Scm}^{-1}$	71
GO-g-[P(HEMA-g-PCL)]/gelatin	Bioreduction	$1.83 \times 10^{-5} \text{ Scm}^{-1}$	72
PANI and PAN with G and GO nanosheets	Ammonia solution at 180 °C for 1h	$1.59 \times 10^{-6} \text{ Scm}^{-1}$	73
GO polyamide 66 (PA66)	0.1 wt.% N_2H_4 and annealing at 350 °C	$8.6 \times 10^3 \text{ } \Omega/\text{sq}$	74
Graphene nanosheet (GNSs) and silver nanoparticles (AgNPs)	NaBH_4 at 100 °C for 24h	$150 \text{ } \Omega/\text{sq}$	75

Compared to traditional metallic wires, graphene-based electroconductive nanofibers are popular materials due to their remarkable properties, such as lightweight, strong mechanical properties, high electrical conductivity, and environmental stability. The precursors for developing graphene-based flexible electrospun conductive nanofibers with polymers such as polyacrylonitrile (PAN), polyvinyl alcohol (PVA), polyvinyl chloride (PVC) nylon, poly(methyl methacrylate) (PMMA), poly(lactic-co-glycolic acid) (PLGA), and poly(vinyl acetate) (PVAc) have been reported in the data provided in Table 1 with

described reduction methods. Graphene employed with polymers has shown improved fiber mechanical and electrical properties. A systematic interaction of graphene with PAN has been reported by Matsumoto.⁶⁰ They prepared graphene oxide nanoribbons (GONRs) by unzipping the multiwalled carbon nanotubes (MWCNTs) with the oxidation process followed by electrospinning with GONRs in PAN/dimethylformamide (DMF) solutions. The electrical conductivity of graphene was greatly improved by thermal reduction (see Table 1; a highest conductivity was achieved, i.e., 165.10 Scm^{-1}). The conductivity of

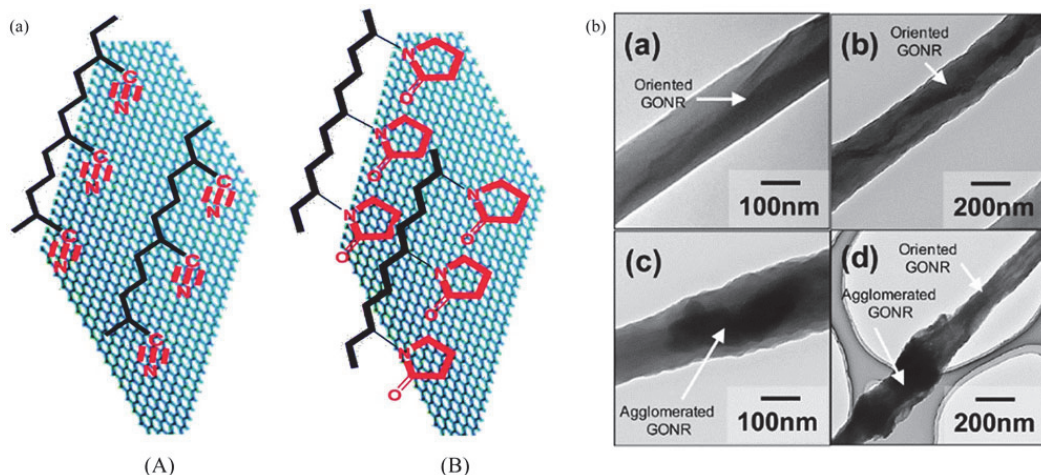


Figure 8. Proposed interactions of (a) graphene sheets with (A) PAN and (B) PVP adapted from Wang et al.⁵⁶ and typical TEM images of (b) the as-spun GONR/PAN composite nanofibers contain (a,b) 0.5 wt % and (c,d) 5 wt % GONR.⁵⁰

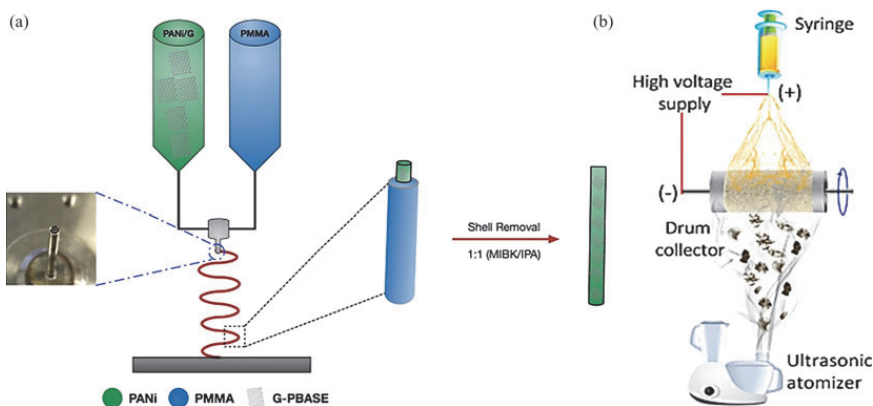


Figure 9. Schematic fabrication of (a) PANI/G-PBASE/PMMA nanofibers by coaxial electrospinning for obtaining neat PANI/G-PBASE nanofibers adapted from Moayeri and Aji⁶¹ and schematic illustration (b) of the electrospinning process adapted and reproduced and coupled with ultrasonic spraying as adapted from Wang et al.⁶⁵

the nanofibers is very much dependent on the reduction strategy and on the sheet-to-sheet interdependence inside the fibers which has well explained by the same work⁶⁰, that is, the schematic graphitic structure of graphene sheets inside the interior of nanofibers with the fabrication and carbonization process (illustrated in Figure 7.). The main challenges for obtaining graphene-based electrospun nanofibers are the improvement of the dispersion, alignment, and appropriate loadings of GO within the polymer matrix. The improvement in rheological characteristics with the different loading levels of graphene is fully understandable by the SEM images of Matsumoto study. Nanofibers with lower wt.% fractions distributed

rather homogeneously than that of GONRs with higher amounts of GONRs, agglomeration phenomenon appeared, and flexural strength gradually decreased with the excessive addition of graphene. Loaded down graphene, a better contributing factor has created smooth structural formations of nanofibers (see Figure 8). Besides thermal reduction, several attempts have been made in chemical reduction of GBEENs and were resurfaced by many researchers. Wang et al. described the chemical reduction of GBEENs for the recovery of precious conductive networks of graphene. A novel composite network of GO sheets with PAN and polyvinylpyrrolidone (PVP) nanofibers has been developed by using hydrazine as

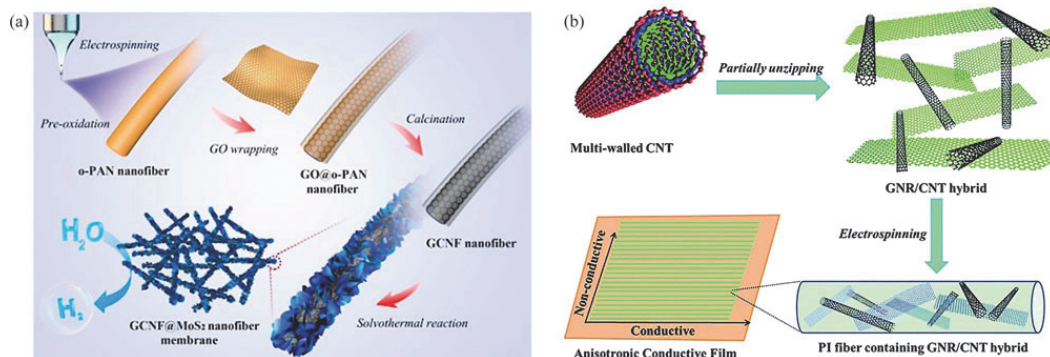


Figure 10. Schematic route for the fabrication of (a) free-standing anisotropic electrically conductive PI-GNR/CNT films adapted from Liu et al.,⁶⁹ where GNR/CNT used as a hybrid nanofiller and (b) schematic electrospinning process for the preparation of GCNF@MoS₂ hybrids as adapted from Gu et al.⁶⁴

reducing agent (N₂H₄).⁵⁶ With this methodology, striking results have been obtained, and the problem of easy curvature of graphene sheets can be thoroughly dissolved with enhanced conductivities, for example, 75 Scm⁻¹ with graphene-PAN and 25 Scm⁻¹ with graphene-PVP (see Table 1).

The governing parameter for the properties of graphene-based electrospun nanofibers is the interaction with the polymer matrix, which has an impact on the usage of a chemical treatment at the surface of the nanofiller. This phenomenal influence was highlighted in the schematic interactions of PVP and PVA with graphene sheets reported in Figure 9.⁵⁶ Table 1 summarized that the fibers, which have been treated under high temperatures, significantly improve the conductivity in comparison with that of the nanofibers reduced by the chemical methods. This might be due to huge removal of the oxygen functionalities from the surface of GO, that is, attached to the interior of an aromatic domain in GO by restoring sp² graphene networks that significantly improved the conductivity of the nanofibers by the thermal reduction process.

Functionalization of metal ions with GBEENS could intensify the conductivity of the nanofibers which can be performed by a mixing process of Ag, Ni, Ru, Si, and Sn along with the electrospinning precursors and there are innumerable reports in the literature for the successful fabrication of these ions as listed in Table 1. In most cases, GBEENS have been used as the backbone materials, in incorporation with electro-active materials, including conductive polymers and metal oxides such as RuO₂, Co₃O₄, and MnO₂ to achieve ultrahigh values of conductivity.⁷⁶⁻⁷⁸ The addition of RuO₂ and MoS₂ in GBEENS has limited their applications where high conductivity of the nanofibers is

needed due to the fact that very low free ion transportations have offered conductivities between 0.59S/cm and 0.56S/cm, respectively.^{63,64} The schematic process of graphene-wrapped electrospun carbon nanofibers (GCNFs)@MoS₂ electrospun nanofibrous membranes has shown in Figure 10b. Compared to unidirectional electrospinning, coaxial electrospinning provides an alternative and effective way of fabricating graphene with conductive polymers such as polyaniline (PANi) with unique core-shell structures. Moayeri and Ajji use this method (see Figure 9a) by utilizing 1-pyrenebutanoic acid, succinimidyl ester (PBASE) with reduced graphene to fabricate conductive nanofibers denoted as PANi/G-PBASE, and the resulted nanofibers have boosted conductivity up to 30S/cm.⁶¹

Fabricating GO is an extremely vital process as it has a large impact on the conductivity of the nanofibers, and therefore makes scientists to explore new methods and techniques for the surface functionalization of the nanofibers with GO to enhance hybrid electrospun fibrous conductivity. In large-scale operations where researchers need to utilize huge quantities of graphene oxide for the industrial production of nanofibers by incorporating of graphene through a mist of GO using an ultrasonic atomizer is the most obvious solution, due to the relative ease in fabricating sufficient amounts of graphene to the desired quality levels. An interesting strategy has followed by Wang et al.⁶⁵ They fabricate conductive nanofibers using electrospinning and ultrasonication simultaneously to dope GO by spraying through an ultrasonic atomizer (see illustrated scheme in Figure 9b) with an achieved conductivity up to the 0.42 Scm⁻¹. Apart from the reduction methods, anisotropic materials and oriented graphene sheets in the interior of nanofibers had a

Table 2. Electrochemical performance of various graphene-based hybrid nanofibers

Electrospinning hybrid materials	Reduction method	Capacitance studies			
		Scan rate (mVs ⁻¹)	Electrolytes	Specific capacitance	References
Graphene oxide/V ₂ O ₅ /PVP	Chemically reduced by PPy	100,75,50,25,10	KOH and H ₂ SO ₄	453.82 Fg ⁻¹	86
Graphene/polypyrrole-coated	Annealed at 850 °C for 1h	2	Na ₂ SO ₄	386.00 Fg ⁻¹	87
Graphene oxide–NG–CNF	800 °C for 2h	1	NaCl solution	337.85 Fg ⁻¹	88
M-rGO/PA66	Hydrazine vapor at 150 °C	10	H ₂ SO ₄	280.00 Fg ⁻¹	89
PAN/PVP in DMF	Carbonized at 850 °C	10	6M KOH	265.00 Fg ⁻¹	90
G/CNF and PAN	Annealed at 800 °C	to 100	KOH	263.70 Fg ⁻¹	91
CNF/graphene/MnO ₂	Carbonized at 900 °C for 1h	50	6 M KOH	225.00 Fg ⁻¹	92
PVA-GO/PEDOT	No reduction carried out	5,10,25,50,100	1 M KCl aqueous	224.27 Fg ⁻¹	93
PAN/GO fiber paper	Hydrazine vapor at 800 °C for 1h	5 to 400	KOH	241.00 Fg ⁻¹	94
MnO ₂ /HPCNF/G	Carbonized for 1h at 800 °C	10 to 100	KOH	210.00 Fg ⁻¹	95
CNF/GNS and GNS/PAN	Hydrazine (80 wt% in water)	5 to 100	KOH	197.00 Fg ⁻¹	96
CNF/G into PAN	Carbonized up to 800 °C	2	Not available	183.00 Fg ⁻¹	97
RuO ₂ /ACNF/graphene composites	Activated at 800 °C for 1h	25	6.0 M KOH	180.00 Fg ⁻¹	63
rGO/thorn-like TiO ₂ nanofiber (TTF)	Reduced at 180 °C for 6h	5,10,20,30,50,70,100	1 M Na ₂ SO ₄	178.00Fg ⁻¹	98
GNW–carbon nanotube (CNT)–PAN	CVD at 1500 °C	10	H ₂ SO ₄	176.00 Fg ⁻¹	99
GO/PANI/PVDF	No reduction carried out	10,20,40,60,80,100	H ₂ SO ₄	170.63 Fg ⁻¹	100
GO and PAN	Carbonized at 1000 °C for 1h	25	KOH	146.62 Fg ⁻¹	101
TEOS, graphene, and PAN	Heated at 800 and 1000 °C	25	KOH	144.79 Fg ⁻¹	102
Graphene in PAN/PMMA	Heated at 1000 °C for 1h	25	KOH	128.00 Fg ⁻¹	103
GO and CNTs embedded in PAN	Heated at 800 °C for 30 min	100	0.5 M Na ₂ SO ₄	120.00 Fg ⁻¹	104

greater influence on the conductivity, for example, contrastive conductivity in different directions by the graphitic hierarchical architecture structures of GO. This feature definitely contributed to the unidirectional transmission of electrons; hence, different conductive networks constructed from cross-linked graphene in both parallel and perpendicular directions. The phenomenon was well described by the Liu et al. who investigated the anisotropic behavior of GO by polyimide–graphene nanoribbons (PI-GNR) and carbon nanotubes (CNTs) by demonstrating two different electrical conductivities, for example, in parallel direction of $8.3 \times 10^{-2} \text{ Scm}^{-1}$ and $7.2 \times 10^{-8} \text{ Scm}^{-1}$ in the perpendicular direction (see a schematic diagram of electrospun PI-GNR/CNT nanofibers presented in Figure 10a).⁶⁹ The prospective of electrospinning is capable of delivering flexible electrodes for the new-generation printable/wearable electronics and can be an encouraging nanocomposite in the developments of high-performance energy storage devices.

2.3. Graphene-based electrospun supercapacitors

In this decade, graphene-based electrospun electroconductive nanofibers (GBEENs) are in high demand for nanocomposites in supercapacitors as they eliminate the binding with the improvements in compaction of graphene structures. It can be a next-generation energy storage material due to number of multifunctional properties like high surface area (a single graphene sheet is 2630 m²/g), flexibility, ultra-thin, chemical stability, and low cost.^{75, 79,80}

Supercapacitors are broadly divided into two different classes: electrochemical double layer capacitors (EDLCs), energy storage involving non-Faradaic processes based on the accumulation of electrostatic charged particles at the electrode/electrolyte interface, and pseudocapacitors, that stores energy by Faradaic redox reactions of the electrode.⁸¹ Graphene-based electrospun nanofibers have been researched extensively for EDLCs comparing to pseudocapacitors⁸². Principally, the specific capacitance of a supercapacitor depends on the specific surface area of the electrode which is determined by the porosity of the electrode material. In this scenario, GBEENs are encouraging porous materials for supercapacitors offering high specific area and conductivity.^{83–85} Many scientists have been able to develop supercapacitors by GBEENs that can store 120 F/g to 453 F/g. Data provided in Table 2 recapitulate several methods to develop GBEEN-based supercapacitors. There are numerous attempts to fabricate GBEENs for supercapacitor systems that have been reported by many different polymers including PAN, PANI, PVA, PVP, and PPMA (as shown in Table 2). However, favorable results have been achieved by PVP and PAN as electrospun precursors owing to their high carbon content. Similar efforts have been made with different kinds of electrode materials, that is, Ni, tetraethyl orthosilicate (TEOS), and TiO₂ and MnO₂ incorporated in the electrospinning process. But a fundamental work⁸⁶ with vanadium pentoxide (V₂O₅) showed highest specific capacitance investigated by Thangappan et al. They have used V₂O₅ as an electrode material because of its unique structure, high

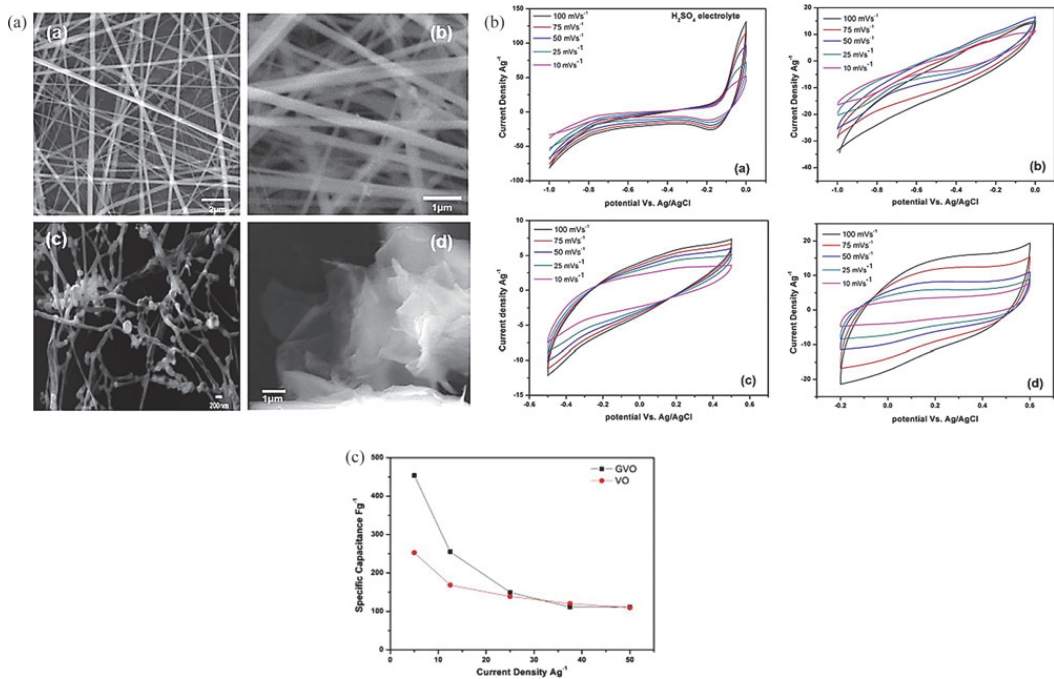


Figure 11. SEM images (a) of pure GVO nanofibers, (a) annealed nanofibers at 350°C and 550°C, (b, c) SEM of pure GO (b) CV curves of graphene and V₂O₅ nanofibers (a, b) in different electrolytes (KOH and H₂SO₄) and CV curves for pure V₂O₅ nanofibers and GO (c, d), and specific capacitance (e) of GVO and VO nanofibers with respect to current densities.⁸⁶

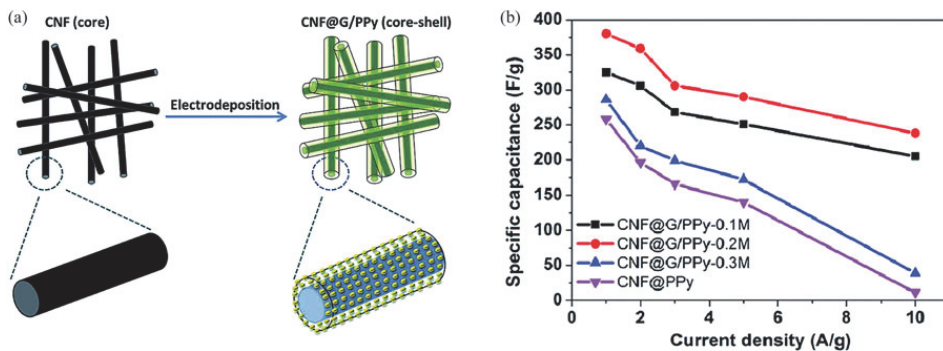


Figure 12. A schematic diagram (a) of the core shell fiber structure and specific capacitance (b) with respect to current density for the CNF@PPy and CNF@G/PPy core-shell electrodes as adapted from Gan et al.⁸⁷

capacity, ease in preparation, and moderate electrical conductivity.¹⁰⁵ Vanadium acetylacetonate, GO, and PVP were used as core electrospun hybrid materials to fabricate graphene oxide/vanadium pentoxide (GVO) nanofibers. Embedded GVO electrospun fibrous mats in a three-electrode cell demonstrated an impressive specific capacitance, that is, 453.824 Fg⁻¹ (see Figure 11).

Although several attempts have been made with graphene-based electrospun supercapacitors by making various combinations of electrolytes, the results concluded that potassium hydroxide (KOH) provides better capacitance due to its ionic conductivity (for 6 M, a maximum value of 0.6 S cm⁻¹ at 25 °C) as compared to the electrolytes, that is, Na₂SO₄, H₂SO₄, KCl, and NaCl mentioned in Table 2. This was confirmed

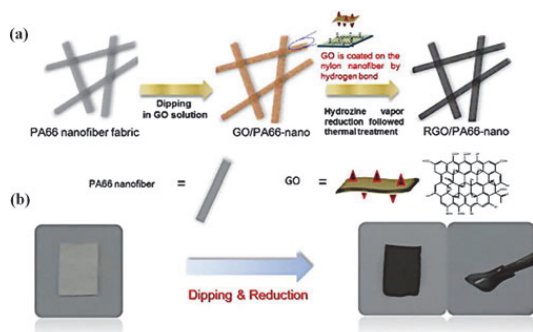


Figure 13. The schematic route of rGO/PA66 nanofabric (a) photographs of PA66 nanofibers and RGO/PA66 nanofabric (b) as adapted from Wang et al.⁸⁹

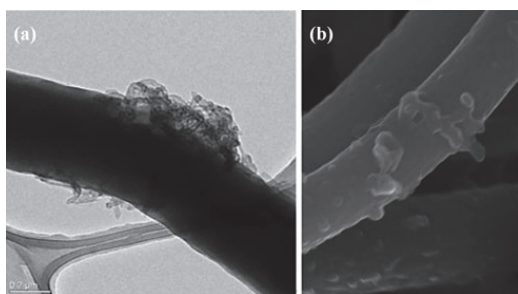


Figure 14. TEM (a) and HRSEM (b) images of GO-CNT/CNF.¹⁰⁴

by capacitance behavior, that is, H_2SO_4 that did not produce ideal cyclic voltammetry (CV) curves as seen in Figure 12; hence, no charging and discharging process take place; therefore, proving KOH is an ideal electrolyte with graphene-based electrospun supercapacitors.

In abovementioned electroactive materials, MnO_2 has materialized as one of the brightest candidates due to its low cost, high electrochemical activity, and eco-friendly nature. The combined characteristics of MnO_2 and graphene have high relevance in many application areas especially in fabricating electrodes for supercapacitor applications. However, intrinsically offered bad electrical conductivity (10^{-5} – 10^{-6} S/cm).⁹² A designed electrospinning process of MnO_2 -containing hierarchical porous CNF/graphene ($\text{MnO}_2/\text{HPCNF}/\text{G}$) was investigated by Lee⁹² with a specific capacitance of 210 F g^{-1} at a current density of 1 mA cm^{-2} . To improve the electrochemical properties of GBEENS, various modifications have been carried in the annealing process, which significantly improve the porosity the nanofibers. As noticed by Thangappan et al., before annealing process, GBEENS exhibited diameters ranging from 200 nm to 300 nm,

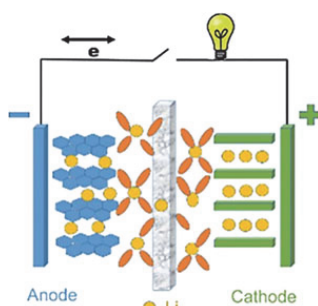
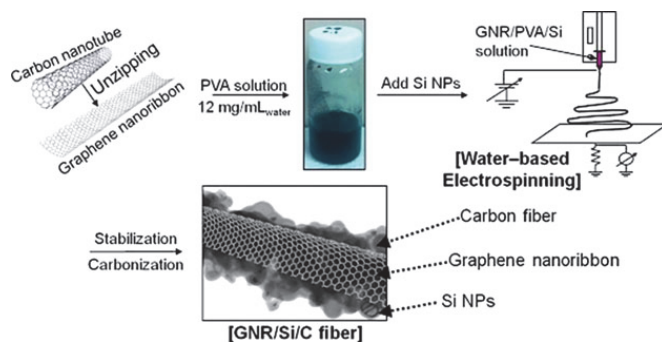


Figure 15. Schematic representation of Li-ion battery (LIB) as adapted from Pampal et al.⁸²

which was influenced by annealing on a decreasing diameter to 90–150 nm as seen in Figure 12. This was attributed to the difference in thermal expansion by the incompatibility of GO and V_2O_5 resulting in the initiation of residual stress and breakage by losing the smooth morphology of the electrospun nanofibers. Combination of graphene with conductive polymers such a polypyrrole (PPy) coated on an electrospun CNF composite surface via a facile electrodeposition method is a promising candidate for pseudocapacitors. This distinctive core-shell structure for high-performance supercapacitors was discovered by Gan et al.⁸⁷ The fabrication method was described in two steps. Initially, the CNF was fabricated via electrospinning from PAN/DMF solutions; second, nanofibers were coated by electrodeposition of graphene/PPy. Benefiting from these features of interwoven and porous structure of the electrospun CNF improved the conductivity and electrochemical performance of the supercapacitor. The overall process of the core shell fiber structure and dependence of specific capacitance on a current density are shown in Figure 12 (reported specific capacitance 386 F g^{-1}).

Table 3. Typical results and state-of-the-art graphene-based electrospun hybrid Li-ion batteries anodes.

Electrospinning hybrid materials	Reduction method	Capacitance studies		References
		Capacity fade%	Specific capacity	
GNRs, MWCNT, and Si/C nanofibers	Carbonized at 900 °C for 5h	94% after 100 cycles	1800 mA h/g	114
SnO ₂ @C@G hNFs	Annealed at 500 °C for 2h	82% after 50 cycles	1600 mA h/g	115
PEO, Si, G, and C denoted as Si-G-C	Heated 1000 °C for 1h	95% after 200 cycles	1344 mA h/g	116
SINPs wrapped by graphene	Carbonized at 900 °C for 5h	85% after 200 cycles	1191 mA h/g	117
GCNF hierarchical WS ₂ /GCNF hybrid	Carbonized at 950 °C for 2h	95% after 100 cycles	1128.21 mA h/g	118
Graphene and encapsulated Co ₃ O ₄ nanotubes	Calcined at 600 °C for 2h	96.1% after 80 cycles	961 mA h/g	119
Si/CNF/GO	Carbonized at 650 °C for 1h	91% after 50 cycles	872 mA h/g	53
PAN/Fe ₂ O ₃ /G	Carbonized at 650 °C for 1h	81.8% after 105 cycles	826 mA h/g	66
rGO in PAN and ZnO nanoparticle	Carbonized at 800 °C for 2h	80% after 100 cycles	815 mA h/g	120
CoMoO ₄ @graphene nanofibers	Carbonized at 450 °C for 2h	80% after 200 cycles	735 mA h/g	121
CoO-graphene-carbon nanofiber	Heated at 650 °C for 2h	After 352nd cycle	690 mA h/g	122
Si and graphene-covered Ni particles	Carbonization at 650 °C for 1h	81% after 70 cycles	600 mA h/g	70
SnO ₂ @G	Calcined at 450 °C for 2h	60% after 120 cycles	591.9 mA h/g	123
Si ₆₀ Sn ₁₂ Ce ₁₈ Fe ₅ Al ₅ Ti ₂ NFs@rGO	Carbonized to 700 °C for 2h	99.9% after 2000 cycles	569.77 mA h/g	124
NiSe ₂ +rGO)-C polyacrylonitrile-polystyrene	Carbonized at 450 °C for 3h	93% after 100 cycles	468 mA h/g	125
SnO ₂ nanorods and graphene sheets	Carbonized at 500 °C	86 % after 50 cycles	467 mA h/g	126
FeSe ₂ @GC-rGO	Carbonized at 500 °C for 3h	82% after 150 cycles	412 mA h/g	127
Antimony-carbon-graphene fibrous	Calcined at 600 °C	98% after 100 cycles	274 mA h/g	128
Graphene-TiO ₂ nanofibers	Heat-treated at 500 °C for 1h	85% after 200 cycles	217 mA h/g	129
OMTiO ₂ -rGO-NF	Heat-treated at 500 °C for 2h	85.3% after 500 cycles	212 mA h/g	130
TiO ₂ -G nanofibers	Carbonized at 450 °C for 1h	84% after 300 cycles	150 mA h/g	131
Graphene-oxide-wrapped Li ₄ Ti ₅ O ₁₂	Annealing at 700 °C for 4h	99% after 100 cycles	110 mA h/g	132
Graphene and conductive Li ₄ Ti ₅ O ₁₂	Calcined at 550 °C for 3h	91% after 1300 cycles	101 mA h/g	133

**Figure 16.** A route for water-based electrospun GNR/Si/C fibers as adapted from Kim et al.¹¹⁴

Impregnation into rGO of a nanofiber fabric (PA66) is a distinct methodology (Figure 13) in the development of graphene-based electrospun supercapacitors. To avoid the aggregation of GO, dipping or coating with ultrahigh mass loading of GO is favorable for electrochemical properties and can be achieved by the simplicity of this method (reported specific capacitance 280.00 Fg⁻¹).⁸⁹

Interfaces between GO and a conductive polymer such as a thiophene derivative poly(3,4-ethylenedioxythiophene) (PEDOT) that possesses a conductivity (300–500 S cm⁻¹) compared with other thiophene derivatives have been fabricated by two integrated methods, that is, electrospinning and electrodeposition. As PEDOT has a large potential window, a good thermal and chemical stability low band gap of 1–3 eV represents the key for successful and great charge mobility that can produce instantaneous

electrochemical kinetics.^{106,107} This hybrid nanocomposite without reducing GO proclaimed a specific capacitance up to 224.27 Fg⁻¹.⁹³ Template hierarchical porous carbon nanofibers (HPCNFs) embedded with graphene are excellent materials to employ in the EDLCs, but they do not satisfy the requirements for commercial application because of their complex preparation, poor electrochemical performance (128.00 Fg⁻¹ as seen in Table 2), and relatively high cost. Moreover, ultra-micropores have accessible pathways to rather small ions (K⁺ and OH⁻) in carbon materials for EDLCs.¹⁰³ Similarly, GO-CNT/CNF electrospun nanofibers present a twine morphology and a rough surface exhibited diameter enlarged to 700 nm. CNT is an inflexible and has a highly curved structure and it could not be embedded in the CNF, resulting in the rough surface of the nanofiber (see Figure 14) strongly influenced

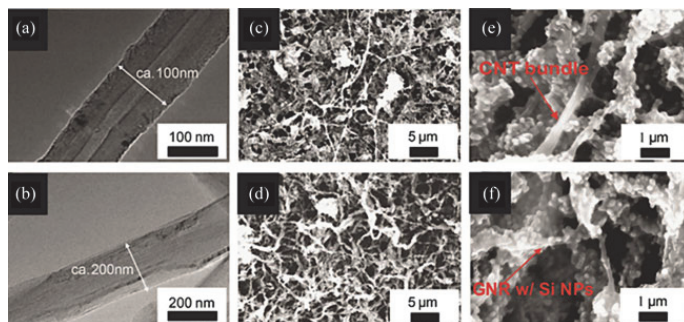


Figure 17. TEM images of carbon nanotubes and unzipped graphene nanoribbons (a,b), low magnification SEM of CNT/Si/C fibers and GNR/Si/C fibers (c,d), and high magnification SEM images of CNT/Si/C and GNR/Si/C fibers (e,f) as adapted from Kim et al.¹¹⁴

the performance of the supercapacitor attributed to 120 Fg^{-1} .¹⁰⁴

2.4. Graphene-based electrospun anodes for Li-ion batteries

At present, Li-ion battery (see schematic Figure 15) electrode materials are usually based on powder materials which may lead to the occurrence of large volume stability during cycling life resulting in the poor performance and cyclability.⁸² Surface modification with carbonaceous materials has been reported by many researchers to improve the battery performance. Among these, major developments have been addressed in GBEAs for Li-ion batteries by attracting considerable attention because of wide range of applications in smart electronics such as laptops, cameras, and mobile phones.^{108–112} Graphene is an attractive candidate with ordinary morphological characteristics, high surface area exceeding $2600 \text{ m}^2/\text{g}^{-1}$, variable density, and high porosity. These characteristics plunges the length of Li^+ diffusion pathways, thus enhances the power capability. In addition, graphene offered high theoretical capacity of 744 mA h g^{-1} for Li^+ storage.¹¹³ GBEAs for Li-ion batteries are considered as one of the most promising storage systems against the hydrogen fuel cell. These doped or blended nanofibers have been considered as an excellent electrode/separator in Li-ion batteries. The enhanced characteristics of graphene-based electrospun nanofibers arise from the integration of compound characteristics which can impart unique morphologies and structures in nanofibers. Several engineering-oriented studies with the materials including SnO_2 , CoMoO_4 , OMTiO_2 , $\text{Li}_4\text{Ti}_5\text{O}_{12}$, TiO_2 , CoO , and ZnO were utilized as hybrid materials for the fabrication of graphene-based electrospun Li-ion anodes (see Table 3).^{66,114–117} GBEA composites merged advantages by

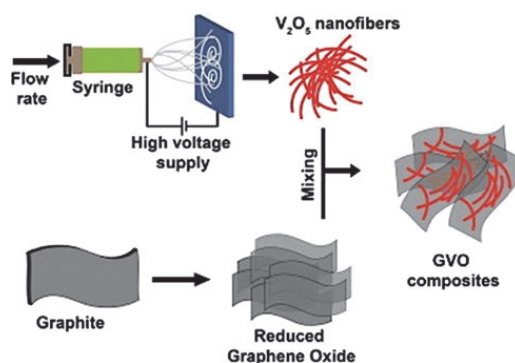


Figure 18. Schematic illustration for fabrication of GCO nanofiber composite as adapted from Pham-Cong et al.¹³⁸

incorporating these materials leading to long-life cyclic stability, mechanical strength, and good electric conductivity.

The detailed electrospinning process, reduction methods, fabrication, and electrical properties of GBEAs for Li-ion batteries are shown in Table 3. Silicon functionality has considered to be excellent candidate since it has been proven as a favorable material for the development of Li-ion batteries with a theoretical capacity of 3579 mA h/g at a room temperature.¹³⁴ A fundamental research work by Kim et al.¹¹⁴ demonstrated highest specific capacitance (up to 1800 mA h/g) by unzipped GNRs from MWCNTs with the help of hexadecyl functionalization process, the comprehensive procedure using water as a solvent for GNR/PVA/Si electrospun nanofibers (see Figure 16). Furthermore, inclusion of other active anodic materials, interesting and efficacious nanostructures can obtain with improved cycling life. Thus, it creates reversible capacity retention, and rate capability of the anodes. Research activities toward improving the ionic and electronic transport properties of titanium have

contributed greatly in last few years. One such approach by electrospun TiO_2 nanofibers containing graphene has reported a high reversible capacity (150 mA h g^{-1}) with 84% retention after 300 cycles¹³¹. Graphene as well as CoO/C electrospun nanofibers were discovered to control the growth of CoO, nucleation during heat treatment, an agreement of a defective fiber structure formation by unhomogenized distribution of graphene sheets and CoO particles. These defects provided better Li^+ storage and thus enhanced the capacity and cycling stability (690 mA h g^{-1} after 352 cycles).¹²³

Reduced graphene also found to electrospun unique hollow core-shell nanofibers with ZnO nanoparticle as cores and rGO/C as shells. In spite of a high initial irreversible capacity loss, rGO core-shell nanofibers offered a specific capacity up to 815 mA h g^{-1} (80% retention after 100 cycles). Through the combination of SnO_2 and graphene, interesting structures have been reported in which high specific capacity of SnO_2 was maintained for more cycles by the presence of graphitic structures. Freestanding SnO_2 /graphene with an additional graphene coating and freestanding SnO_2 /G film from SnO_2 fibers have both been proposed (reported specific capacitance $591.9, 467 \text{ mA h/g}$, respectively).^{123, 126} Another combination of high capacity and stability can be obtained from Si/graphene electrospun nanofibers, and the interconnected graphene sheets buffer the volume proliferation of Si during cycling and thus donate to the anode a better cycling stability (872 mA h/g , 91% after 50 cycles)⁵³ Furthermore, the morphology of the fibers could be controlled by changing the particle size and the dispersion of the Si particles in the fibrous structure ensuring strong interfacial interactions between Si and graphene sheets was highlighted by Kim et al.¹¹⁴

Opposed to CNT/Si/C electrospun nanofibers, GNR/Si/C nanofibers showed better morphology due to their open structure, flexibility, and better dispersion (see Figure 17d). It was suggested that graphene nanopallets proved to be a better nanofiller for reinforcing Si/C fibers, that is, Si nanoparticles evenly distributed throughout the nanofibers, while bundles of silicon nanoparticles (SiNPs) can be observed in CNT/Si/C (see Figure 17e,f).¹¹⁴

2.5. Graphene-based electrospun cathodes for Li-ion batteries

To date, very few attempts have been made in graphene-based electrospun cathodes by improving rate capability and cycling stability of 2D nanostructures.

Minimizing the Li^+ ion transport gap and increasing the number of active sites have been developed.^{135–137}

Two-dimensional rGO nanosheets with high specific area greatly improve the conductivity of the electrospun nanofibers that conquer the side reaction at high voltage in Li-ion batteries cathodes. Reduced electrospun of GO and V_2O_5 nanowires (NWs) (100% after 300 cycles 225 mAh g^{-1}) is considered to control the volume expansion of the active materials during the charge/discharge process, since the structure may assist the migration of lithium ions between the active material and electrolyte.¹³⁸

A schematic electrospinning process of rGO and V_2O_5 NWs is shown in Figure 18. Direct electrospinning or with a combination of lithium-rich manganese followed by sol-gel to encapsulate graphene contained CNFs. This process has researched by very few scientists; an electrospun cathode with reduced GO as 3D hierarchical architectures giving a specific capacitance (145 mAh g^{-1} with retention up to 73.6% after 100 cycles)^{139,140} can further be improved by exploring new materials and methods.

3. Conclusion and future directions

Graphene, as the “mother” of all other allotropes of carbon, has proven a promising nanofiller in electrospinning by owing extraordinary multifunctional properties, for example, conducting, electronic, and physicochemical. In this review, we have provided a comprehensive overview of the developments in graphene-based electrospun nanofibers in the creation of conductive nanofibers, supercapacitors, anodes, and cathodes for the Li-ion batteries including major past progress, technical issues, and nanostructured material developments. Moreover, several methods and advanced characterization techniques involved in the fiber chemistry have been discussed, providing a better understanding of the mechanisms between the fiber structure and electrical properties. Graphene-based electrospun nanofibers that are one dominant type of nanocomposite as a supercapacitor, anode, and cathode in Li-ion batteries have shown promising performances with high capacity, enhanced rate capability, and long-term cycle stability. The application of graphene-based nanofibers as nanocomposites, facilitating easy pathways for ion/electron transport in Li-ion batteries by offering the advantage of a versatile design of nanocomposite. Electrolytes also play a critical role in solving the problems of specific capacity; for example, KOH significantly enhances the Coulombic efficiency and the stability of a supercapacitor. In this regard, KOH

found to be a beneficial electrolyte for the graphene-based electrospun supercapacitors. Despite the considerable advancement achieved during the past few decades, it will still be a long way to go in future and more efforts should be directed toward nanoscience research and approaches. This can lead to viable high-performance smart electronics with a future prospect as upcoming hybrid materials that can replace conventional conductive fibers, Li-ion electrodes, and supercapacitors. The efforts for developing high-performance-based electrospun nanocomposites can be generalized as follows.

3.1. Appropriate dispersion of GO

A well-dispersed form of GO inside polymeric matrix, accountable for uniform distribution of graphene sheets inside nanofibers, is a complicated process. GO stability on the solution-phase manipulation is a critical point controlling the morphologies of the nanofibers. In this context, the solubility of GO with an appropriate loading, sonication, or mechanical mixing needs to be redesigned by exploring new solvent systems with sufficient contact. Poor connection between the insulating GO and the electrical conductor can result in inactive regions, leading to low anodic and cathodic conductivity and low capacity supercapacitors.

3.2. Reduction of GO-based nanofibers

The reduction of GO-based nanofibers is definitely a key process and reducing GO-based nanofibers with high-quality still remains a challenge. Several scientific experiments have been proposed; each of them has advantages and limitations. Different reduction strategies solely by chemical or heat treatments have been followed to transform the effect of the final performance of the nanofibers or devices composed of GO-based nanofibers. Although optimized results have been achieved by thermal annealing of the nanofibers but to achieve flawless rGO is difficult to reach by chemical reduction which can improve further research efforts and should continuously be carried out to find new methods for the future improvements in the reduction of GO-based nanofibers.

3.3. Stable electrolyte systems for GO-based supercapacitors

The current liquid electrolyte is far away from fulfilling the demands of the practical utility of graphene-based nanofibers in supercapacitors and in Li-ion batteries because of the side reactions among electrolyte

solvents. A well-covenanted electrolyte needs to have reliability as well as compatibility with graphene-based electrospun nanofibers; therefore, further research on suitable combinations or novel electrolytes can be focused.

Disclosure statement

No potential conflict of interest was reported by the authors.

Funding

This research did not receive any specific grant from funding agencies in the public, commercial, or not-for-profit sectors.

References

1. S. Ramakrishna, *An Introduction to Electrospinning and Nanofibers*, World Scientific Publishing Co Pte Ltd, National University of Singapore (2005).
2. A. Kumar and M. Deka, *Nanofiber Reinforced Composite Polymer Electrolyte Membranes*, InTech (2010).
3. A. S. Nain, J. C. Wong, C. Amon, and M. Sitti, *Appl. Phys. Lett.* **89**(18), 183105 IntechOpen Limited, London, United Kingdom (2006).
4. D. Almecija, D. Blond, J. E. Sader, J. N. Coleman, and J. J. Boland, *Carbon* **47**(9), 2253–2258 (2009).
5. J. S. Jeong, J. S. Moon, S. Y. Jeon, J. H. Park, P. S. Alegaonkar, and J. B. Yoo, *Thin Solid Films* **515**(12), 5136–5141 (2007).
6. J. F. Cooley, Google Patents US692631 (1902).
7. N. Bhardwaj and S. C. Kundu, *Biotechnol. Adv.* **28**(3), 325–347 (2010).
8. J. D. Schiffman and C. L. Schauer, *Polym. Rev.* **48**(2), 317–352 (2008).
9. S. Torres-Giner, R. Pérez-Masiá, and J. M. Lagaron, *Polym. Eng. Sci.* **56**(5), 500–527 (2016).
10. N. Patra, M. Cernik, and M. Salerno, *J. Nanomater.* **2016**, 2 (2016).
11. T. J. Sill and H. A. von Recum, *Biomaterials* **29**(13), 1989–2006 (2008).
12. M. Modesti, C. Boaretti, and M. Roso, In *Encyclopedia of Membranes*, E. Drioli and L. Giorno (eds.), Electrospun Nanofibrous Membranes, Springer Berlin Heidelberg, Berlin, Heidelberg, 1–4, (2015).
13. M. Fathy, A. B. Kashyout, J. El Nady, S. Ebrahim, and M. B. Soliman, *Alex. Eng. J.* **55**(2), 1737–1743 (2016).
14. R. Song, X. Li, F. Gu, L. Fei, Q. Ma, and Y. Chai, *RSC Adv.* **6**(94), 91641–91648 (2016).
15. M. Zhu, J. Han, F. Wang, W. Shao, R. Xiong, Q. Zhang, H. Pan, Y. Yang, S. K. Samal, F. Zhang, and C. Huang, *Macromol. Mater. Eng.* **302**(1), 1600353–n/a (2017).
16. Y. Xia, P. Yang, Y. Sun, Y. Wu, B. Mayers, B. Gates, Y. Yin, F. Kim, and H. Yan, *Adv. Mater.* **15**(5), 353–389 (2003).
17. A. Kulkarni, V. A. Bambole, and P. A. Mahanwar, *Polym. Plast. Technol. Eng.* **49**(5), 427–441 (2010).

18. Z.-M. Huang, Y. Z. Zhang, M. Kotaki, and S. Ramakrishna, *Compos. Sci. Technol.* **63**(15), 2223–2253 (2003).
19. M. Maccioni, E. Orgiu, P. Cosseddu, S. Locci, and A. Bonfiglio, *Adv. Mater. Weinheim* **89**(14), 143515 (2006).
20. M. Hamed, R. Forchheimer, and O. Ingnas, *Nat. Mater.* **6**(5), 357–362 (2007).
21. C. Müller, M. Hamed, R. Karlsson, R. Jansson, R. Marcilla, M. Hedhammar, and O. Ingnäs, *Adv. Mater.* **23**(7), 898–901 (2011).
22. I. F. Wahab, S. I. A. Razak, N. S. Azmi, F. N. Dahli, A. H. M. Yusof, and N. H. M. Nayan, *Electrospun Graphene Oxide-Based Nanofibres In Advances in Carbon Nanostructures*, A. M. T. Silva and S. A. C. Carabineiro (eds.), InTech, Rijeka, Ch. 05, (2016).
23. C. Wang, Y. Li, G. Ding, X. Xie, and M. Jiang, *J. Appl. Polym. Sci.* **127**(4), 3026–3032 (2013).
24. X.-M. Sui, S. Giordani, M. Prato, and H. D. Wagner, *Appl. Phys. Lett.* **95**(23), 233113 (2009).
25. S. Costa, E. Borowiak-Palen, M. Kruszyńska, A. Bachmatiuk, and R. J. Kalęńczuk, *Mater. Sci.-Poland.* **26**(2), 433–441 (2008).
26. T. W. Ebbesen, *Phys. Today* **49**(6), 26–32 (1996).
27. S. Sahoo, S. Dhibar, G. Hatui, P. Bhattacharya, and C. K. Das, *Polymer* **54**(3), 1033–1042 (2013).
28. M. I. Katsnelson, *Mater. Today* **10**(1–2), 20–27 (2007).
29. Y. Xu, W. Hong, H. Bai, C. Li, and G. Shi, *Carbon* **47**(15), 3538–3543 (2009).
30. F. Barzegar, A. Bello, M. Fabiane, S. Khamlich, D. Momodu, F. Taghizadeh, J. Dangbegnon, and N. Manyala, *Journal of Physics and Chemistry of Solids* **77**, 139–145 (2015).
31. F. Meng, W. Lu, Q. Li, J.-H. Byun, Y. Oh, and T.-W. Chou, *Adv. Mater. Weinheim* **27**(35), 5113–5131 (2015).
32. K. S. Novoselov, V. I. Falko, L. Colombo, P. R. Gellert, M. G. Schwab, and K. Kim, *Nature* **490**(7419), 192–200 (2012).
33. A. K. Geim and K. S. Novoselov, *Nat. Mater.* **6**(3), 183–191 (2007).
34. C. Soldano, A. Mahmood, and E. Dujardin, *Carbon* **48**(8), 2127–2150 (2010).
35. H. S. Dong and S. J. Qi, *Biosurf. Biotribol.* **1**(4), 229–248 (2015).
36. K. S. Novoselov, A. K. Geim, S. V. Morozov, D. Jiang, Y. Zhang, S. V. Dubonos, I. V. Grigorieva, and A. A. Firsov, *Science* **306**(5696), 666 (2004).
37. A. K. Geim, *Science* **324**(5934), 1530–1534 (2009).
38. Y. Yang, A. M. Asiri, Z. Tang, D. Du, and Y. Lin, *Mater. Today* **16**(10), 365–373 (2013).
39. A. C. Ferrari, F. Bonaccorso, V. Fal'ko, K. S. Novoselov, S. Roche, P. Boggild, S. Borini, F. H. L. Koppens, V. Palermo, N. Pugno, J. A. Garrido, R. Sordan, A. Bianco, L. Ballerini, M. Prato, E. Lidorikis, J. Kivioja, C. Marinelli, T. Ryhanen, A. Morpurgo, J. N. Coleman, V. Nicolosi, L. Colombo, A. Fert, M. Garcia-Hernandez, A. Bachtold, G. F. Schneider, F. Guinea, C. Dekker, M. Barbone, Z. Sun, C. Galiotis, A. N. Grigorenko, G. Konstantatos, A. Kis, M. Katsnelson, L. Vandersypen, A. Loiseau, V. Morandi, D. Neumaier, E. Treossi, V. Pellegrini, M. Polini, A. Tredicucci, G. M. Williams, B. Hee Hong, J.-H. Ahn, J. Min Kim, H. Zirath, B. J. van Wees, H. van der Zant, L. Occhipinti, A. Di Matteo, I. A. Kinloch, T. Seyller, E. Quesnel, X. Feng, K. Teo, N. Rupesinghe, P. Hakonen, S. R. T. Neil, Q. Tannock, T. Lofwander, and J. Kinaret, *Nanoscale* **7**(11), 4598–4810 (2015).
40. H. Jang, Y. J. Park, X. Chen, T. Das, M.-S. Kim, and J.-H. Ahn, *Adv. Mater. Weinheim* **28**(22), 4184–4202 (2016).
41. R. Raccichini, A. Varzi, S. Passerini, and B. Scrosati, *Nat. Mater.* **14**(3), 271–279 (2015).
42. F. Bonaccorso, Z. Sun, T. Hasan, and A. C. Ferrari, *Nat. Photon.* **4**(9), 611–622 (2010).
43. Q. Bao, H. Zhang, J.-x. Yang, S. Wang, D. Y. Tang, R. Jose, S. Ramakrishna, C. T. Lim, and K. P. Loh, *Adv. Funct. Mater.* **20**(5), 782–791 (2010).
44. J. Song, H. Gao, G. Zhu, X. Cao, X. Shi, and Y. Wang, *Carbon* **95**, 1039–1050 (2015).
45. S. Ramazani and M. Karimi, *Polym. Composite.* **37**(1), 131–140 (2016).
46. C. Zhang, L. Wang, T. Zhai, X. Wang, Y. Dan, and L.-S. Turng, *J. Mech. Behav. Biomed. Mater.* **53**, 403–413 (2016).
47. Y. C. Shin, J. H. Lee, L. Jin, M. J. Kim, Y.-J. Kim, J. K. Hyun, T.-G. Jung, S. W. Hong, and D.-W. Han, *J. Nanobiotechnol.* **13**(1), 21 (2015).
48. O. J. Yoon, C. Y. Jung, I. Y. Sohn, H. J. Kim, B. Hong, M. S. Jhon, and N.-E. Lee, *Compos. Part A Appl. Sci. Manuf.* **42**(12), 1978–1984 (2011).
49. X. An, H. Ma, B. Liu, and J. Wang, *J. Nanomater.* **2013**, 7 (2013).
50. H. R. Pant, P. Pokharel, M. K. Joshi, S. Adhikari, H. J. Kim, C. H. Park, and C. S. Kim, *Chem. Eng. J.* **270**, 336–342 (2015).
51. L. Tan, L. Gan, J. Hu, Y. Zhu, and J. Han, *Compos. Part A Appl. Sci. Manuf.* **76**, 115–123 (2015).
52. B. Ardeshirzadeh, N. A. Anaraki, M. Irani, L. R. Rad, and S. Shamshiri, *Mater. Sci. Eng. C Mater. Biol. Appl.* **48**, 384–390 (2015).
53. Z.-L. Xu, B. Zhang, and J.-K. Kim, *Nano Energy* **6**, 27–35 (2014).
54. Y. Y. Qi, Z. X. Tai, D. F. Sun, J. T. Chen, H. B. Ma, X. B. Yan, B. Liu, and Q. J. Xue, *J. Appl. Polym. Sci.* **127**(3), 1885–1894 (2013).
55. H. R. Pant, C. H. Park, L. D. Tijing, A. Amarjargal, D.-H. Lee and C. S. Kim, *Colloids Surf. A Physicochem. Eng. Asp.* **407**, 121–125 (2012).
56. Y. Wang, J. Tang, S. Xie, J. Liu, Z. Xin, X. Liu, and L. A. Belfiore, *RSC Adv.* **5**(52), 42174–42177 (2015).
57. R. Ding, Z. Luo, X. Ma, X. Fan, L. Xue, X. Lin, and S. Chen, *Int. J. Anal. Chem.* **2015**, 7 (2015).
58. Q. Dong, G. Wang, B. Qian, C. Hu, Y. Wang, and J. Qiu, *Electrochimica Acta* **137**, 388–394 (2014).
59. T. Lavanya, K. Satheesh, M. Dutta, N. Victor Jaya, and N. Fukata, *J. Alloys Compd.* **615**, 643–650 (2014).
60. H. Matsumoto, S. Imaizumi, Y. Konosu, M. Ashizawa, M. Minagawa, A. Tanioka, W. Lu, and J. M. Tour, *ACS Appl. Mater. Interf.* **5**(13), 6225–6231 (2013).

61. A. Moayeri and A. Ajji, *Nanosci. Nanotechnol. Lett.* **8**(2), 129–134 (2016).
62. L. Jin, D. Wu, S. Kuddannaya, Y. Zhang, and Z. Wang, *ACS Appl. Mater. Interf.* **8**(8), 5170–5177 (2016).
63. K. S. Yang and B.-H. Kim, *Electrochimica Acta* **186**, 337–344 (2015).
64. H. Gu, Y. Huang, L. Zuo, W. Fan, and T. Liu, *Electrochimica Acta* **219**, 604–613 (2016).
65. G. Wang, Q. Dong, T. Wu, F. Zhan, M. Zhou, and J. Qiu, *Carbon* **103**, 311–317 (2016).
66. B. Zhang, Z.-L. Xu, and J.-K. Kim, *RSC Adv.* **4**(24), 12298–12301 (2014).
67. X. Tang, F. Yan, Y. Wei, M. Zhang, T. Wang, and T. Zhang, *ACS Appl. Mater. Interf.* **7**(39), 21890–21897 (2015).
68. A. Moayeri and A. Ajji, *Synth. Met.* **200**, 7–15 (2015).
69. M. Liu, Y. Du, Y.-E. Miao, Q. Ding, S. He, W. W. Tjiu, J. Pan, and T. Liu, *Nanoscale* **7**(3), 1037–1046 (2015).
70. Z.-L. Xu, B. Zhang, Z.-Q. Zhou, S. Abouali, M. Akbari Garakani, J. Huang, J.-Q. Huang, and J.-K. Kim, *Carbon nanofibers containing Si nanoparticles and graphene-covered Ni for high performance anodes in Li ion batteries.* *RSC Adv.* **4**(43), 22359–22366 (2014).
71. Z. M. O. Rzaev, K. Salimi, U. Bunyatova, S. Acar, B. Salamov, and M. Turk, *Mater. Sci. Eng. C Mater. Biol. Appl.* **61**, 257–268 (2016).
72. B. Massoumi, F. Ghandomi, M. Abbasian, M. Eskandani, and M. Jaymand, *Appl. Phys. A* **122**(12), 1000 (2016).
73. M. Matin, S. Masoud, H. Shadie, Z. Soheila, R. Parviz, V. Manouchehr, and H. Simzar, *Biomed. Mater.* **11**(2), 025006 (2016).
74. H. Yuan-Li, B. Avinash, T. Hsi-Wen, Y. Ying-Kui, Y. Shin-Yi, M. M. Chen-Chi, L. Hong-Yuan, M. Yiu-Wing, and W. Nian-Hau, *Nanotechnology* **22**(47), 475603 (2011).
75. Y.-L. Huang, A. Baji, H.-W. Tien, Y.-K. Yang, S.-Y. Yang, S.-Y. Wu, C.-C. M. Ma, H.-Y. Liu, Y.-W. Mai, and N.-H. Wang, *Carbon* **50**(10), 3473–3481 (2012).
76. R.-R. Bi, X.-L. Wu, F.-F. Cao, L.-Y. Jiang, Y.-G. Guo, and L.-J. Wan, *J. Phys. Chem. C* **114**(6), 2448–2451 (2010).
77. Y. Shan and L. Gao, *Mater. Chem. Phys.* **103**(2–3), 206–210 (2007).
78. L. Yuan, X.-H. Lu, X. Xiao, T. Zhai, J. Dai, F. Zhang, B. Hu, X. Wang, L. Gong, J. Chen, C. Hu, Y. Tong, J. Zhou, and Z. L. Wang, *ACS Nano* **6**(1), 656–661 (2012).
79. M. D. Stoller, S. Park, Y. Zhu, J. An, and R. S. Ruoff, *Nano Lett.* **8**(10), 3498–3502 (2008).
80. X. Mao, T. A. Hatton, and G. C. Rutledge, *Curr. Org. Chem.* **17**(13), 1390–1401 (2013).
81. G. Wang, L. Zhang, and J. Zhang, *Chem. Soc. Rev.* **41**(2), 797–828 (2012).
82. E. S. Pampal, E. Stojanovska, B. Simon, and A. Kilic, *J. Power Sources* **300**, 199–215 (2015).
83. X. Hu, Z. Yan, Q. Li, Q. Yang, L. Kang, Z. Lei, and Z.-H. Liu, *Colloids Surf. A Physicochem. Eng. Asp.* **461**, 105–112 (2014).
84. J. Xu, H. Sun, Z. Li, S. Lu, X. Zhang, S. Jiang, Q. Zhu, and G. S. Zakharova, *Solid State Ion.* **262**, 234–237 (2014).
85. B.-H. Kim, C. H. Kim, K. S. Yang, A. Rahy, and D. J. Yang, *Electrochimica Acta* **83**, 335–340 (2012).
86. R. Thangappan, S. Kalaiselvam, A. Elayaperumal, and R. Jayavel, *Solid State Ion.* **268**, 321–325 (2014).
87. J. K. Gan, Y. S. Lim, A. Pandikumar, N. M. Huang, and H. N. Lim, *RSC Adv.* **5**(17), 12692–12699 (2015).
88. Y. Liu, X. Xu, T. Lu, Z. Sun, D. H. C. Chua, and L. Pan, *RSC Adv.* **5**(43), 34117–34124 (2015).
89. Y.-S. Wang, S.-M. Li, S.-T. Hsiao, W.-H. Liao, P.-H. Chen, S.-Y. Yang, H.-W. Tien, C.-C. M. Ma, and C.-C. Hu, *Carbon* **73**, 87–98 (2014).
90. A. Moayeri and A. Ajji, *J. Nanosci. Nanotechnol.* **17**(3), 1820–1829 (2017).
91. Z. Zhou and X.-F. Wu, *J. Power Sources* **222**, 410–416 (2013).
92. D. G. Lee, Y. A. Kim, and B.-H. Kim, *Carbon* **107**, 783–791 (2016).
93. M. A. A. Mohd Abdah, N. A. Zubair, N. H. N. Azman, and Y. Sulaiman, *Mater. Chem. Phys.* **192**, 161–169 (2017).
94. Q. Xie, S. Zhou, S. Wu, Y. Zhang, and P. Zhao, *Appl. Surface Sci.* **407**, 36–43 (2017).
95. D. G. Lee and B.-H. Kim, *Synth. Met.* **219**, 115–123 (2016).
96. Z. Tai, X. Yan, J. Lang, and Q. Xue, *J. Power Sources* **199**, 373–378 (2012).
97. Q. Dong, G. Wang, H. Hu, J. Yang, B. Qian, Z. Ling, and J. Qiu, *J. Power Sources* **243**, 350–353 (2013).
98. T.-W. Kim and S.-J. Park, *J. Colloid Interf. Sci.* **486**, 287–295 (2017).
99. H.-C. Hsu, C.-H. Wang, S. K. Nataraj, H.-C. Huang, H.-Y. Du, S.-T. Chang, L.-C. Chen, and K.-H. Chen, *Diam. Relat. Mater.* **25**, 176–179 (2012).
100. A. Rose, N. Raghavan, S. Thangavel, B. Uma Maheswari, D. P. Nair, and G. Venugopal, *Mater. Sci. Semicond. Process.* **31**, 281–286 (2015).
101. B.-H. Kim and K. S. Yang, *J. Ind. Eng. Chem.* **20**(5), 3474–3479 (2014).
102. S. Y. Kim, K. Yang, and B.-H. Kim, *Electrochimica Acta* **137**, 781–788 (2014).
103. B.-H. Kim, K. S. Yang, and J. P. Ferraris, *Electrochimica Acta* **75**, 325–331 (2012).
104. H.-C. Hsu, C.-H. Wang, Y.-C. Chang, J.-H. Hu, B.-Y. Yao, and C.-Y. Lin, *J. Phys. Chem. Solids* **85**, 62–68 (2015).
105. T. Kudo, Y. Ikeda, T. Watanabe, M. Hibino, M. Miyayama, H. Abe, and K. Kajita, *Solid State Ion.* **152–153**, 833–841 (2002).
106. R. Balint, N. J. Cassidy, and S. H. Cartmell, *Acta Biomater.* **10**(6), 2341–2353 (2014).
107. Z. Feng, D. Mo, W. Zhou, Q. Zhou, J. Xu, B. Lu, S. Zhen, Z. Wang, and X. Ma, *New J. Chem.* **40**(3), 2304–2314 (2016).
108. G. Cui, Y.-S. Hu, L. Zhi, D. Wu, I. Lieberwirth, J. Maier, and K. Müllen, *Small* **3**(12), 2066–2069 (2007).
109. Y. G. Guo, Y. S. Hu, W. Sigle and J. Maier, *Adv. Mater.* **19**(16), 2087–2091 (2007).

110. H.-X. Ji, X.-L. Wu, L.-Z. Fan, C. Krien, I. Fiering, Y.-G. Guo, Y. Mei, and O. G. Schmidt, *Adv. Mater. Weinheim* **22**(41), 4591–4595 (2010).
111. X. Ji, K. T. Lee, and L. F. Nazar, *Nat. Mater.* **8**(6), 500–506 (2009).
112. G.-Z. Wei, X. Lu, F.-S. Ke, L. Huang, J.-T. Li, Z.-X. Wang, Z.-Y. Zhou, and S.-G. Sun, *Adv. Mater. Weinheim* **22**(39), 4364–4367 (2010).
113. C. N. R. Rao, U. Maitra, and H. S. S. R. Matte, *Synthesis, Characterization, and Selected Properties of Graphene*, In *Graphene*, Wiley-VCH Verlag GmbH & Co. KGaA, 1–47, (2012).
114. Y. S. Kim, G. Shoorideh, Y. Zhmayev, J. Lee, Z. Li, B. Patel, S. Chakrapani, J. H. Park, S. Lee, and Y. L. Joo, *Nano Energy* **16**, 446–457 (2015).
115. D. Pham-Cong, J. Y. Kim, J. S. Park, J. H. Kim, J.-P. Kim, E.-D. Jeong, J. Kim, S.-Y. Jeong, and C.-R. Cho, *Electrochim. Acta* **161**, 1–9 (2015).
116. X. Zhou and Y.-G. Guo, *J. Mater. Chem. A* **1**(32), 9019–9023 (2013).
117. L. Fei, B. P. Williams, S. H. Yoo, J. Kim, G. Shoorideh, and Y. L. Joo, *ACS Appl. Mater. Interf.* **8**(8), 5243–5250 (2016).
118. L. Zhang, W. Fan, and T. Liu, *Nanoscale* **8**(36), 16387–16394 (2016).
119. D. Li, Q. Lu, E. Guo, M. Wei, Z. Xiu, and X. Ji, *J. Sol-Gel Sci. Technol.* **82**(1), 75–84 (2017).
120. Shilpa, B. M. Basavaraja, S. B. Majumder, and A. Sharma, *J. Mater. Chem. A* **3**(10), 5344–5351 (2015).
121. J. Xu, S. Gu, L. Fan, P. Xu, and B. Lu, *Electrochim. Acta* **196**, 125–130 (2016).
122. M. Zhang, F. Yan, X. Tang, Q. Li, T. Wang and G. Cao, *J. Mater. Chem. A* **2**(16), 5890–5897 (2014).
123. J. Zhu, G. Zhang, X. Yu, Q. Li, B. Lu, and Z. Xu, *Nano Energy* **3**, 80–87 (2014).
124. J.-W. Jung, W.-H. Ryu, J. Shin, K. Park, and I.-D. Kim, *ACS Nano* **9**(7), 6717–6727 (2015).
125. J. S. Cho, S. Y. Lee, and Y. C. Kang, *Sci. Rep.* **6**, 23338 (2016).
126. S. Jiang, B. Zhao, R. Ran, R. Cai, M. O. Tade, and Z. Shao, *RSC Adv.* **4**(18), 9367–9371 (2014).
127. J. S. Cho, J.-K. Lee, and Y. C. Kang, *Sci. Rep.* **6**, 23699 (2016).
128. K. Li, D. Su, H. Liu, and G. Wang, *Electrochim. Acta* **177**, 304–309 (2015).
129. Y. Yeo, J.-W. Jung, K. Park, and I.-D. Kim, *Sci. Rep.* **5**, 13862 (2015).
130. S. Chattopadhyay, S. Maiti, I. Das, S. Mahanty, and G. De, *Adv. Mater. Interf.* **3**(23), 1600761-n/a (2016).
131. X. Zhang, P. Suresh Kumar, V. Aravindan, H. H. Liu, J. Sundaramurthy, S. G. Mhaisalkar, H. M. Duong, S. Ramakrishna, and S. Madhavi, *J. Phys. Chem. C* **116**(28), 14780–14788 (2012).
132. J. Kim, J. Y. Kim, D. Pham-Cong, S. Y. Jeong, J. Chang, J. H. Choi, P. V. Braun, and C. R. Cho, *Electrochim. Acta* **199**, 35–44 (2016).
133. N. Zhu, W. Liu, M. Xue, Z. Xie, D. Zhao, M. Zhang, J. Chen, and T. Cao, *Electrochim. Acta* **55**(20), 5813–5818 (2010).
134. M. N. Obrovac and L. Christensen, *Electrochem. Solid St. Lett.* **7**(5), A93–A96 (2004).
135. V. Aravindan, J. Sundaramurthy, P. Suresh Kumar, Y.-S. Lee, S. Ramakrishna, and S. Madhavi, *Chem. Commun. (Camb.)* **51**(12), 2225–2234 (2015).
136. S. Kalluri, W. K. Pang, K. H. Seng, Z. Chen, Z. Guo, H. K. Liu, and S. X. Dou, *J. Mater. Chem. A* **3**(1), 250–257 (2015).
137. S. Kalluri, K. H. Seng, Z. Guo, H. K. Liu, and S. X. Dou, *RSC Adv.* **3**(48), 25576–25601 (2013).
138. D. Pham-Cong, K. Ahn, S. W. Hong, S. Y. Jeong, J. H. Choi, C. H. Doh, J. S. Jin, E. D. Jeong, and C. R. Cho, *Curr. Appl. Phys.* **14**(2), 215–221 (2014).
139. D. Ma, Y. Li, M. Wu, L. Deng, X. Ren, and P. Zhang, *Acta Mater.* **112**, 11–19 (2016).
140. O. Toprakci, H. A. K. Toprakci, L. Ji, Z. Lin, R. Gu, and X. Zhang, *J. Renew. Sustain. Ener.* **4**(1), 013121 (2012).

Appendix B

- B. I. CA-[BMIM]Cl-GO solution conductivity.
- B. II. Porosity and conductivity analysis.
- B.III. CA-[BMIM]-Cl membranes conductivity analysis.

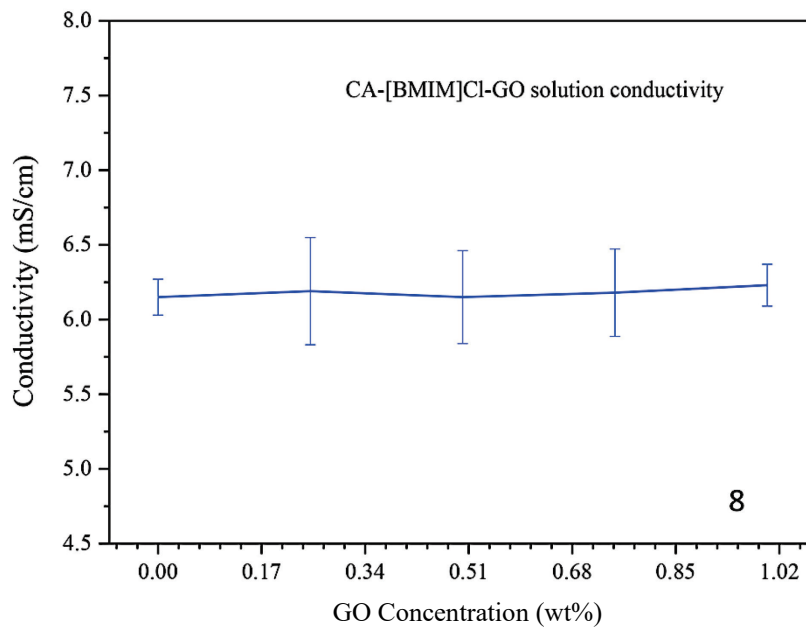


Figure 1. CA-[BMIM]Cl-GO solution conductivity.

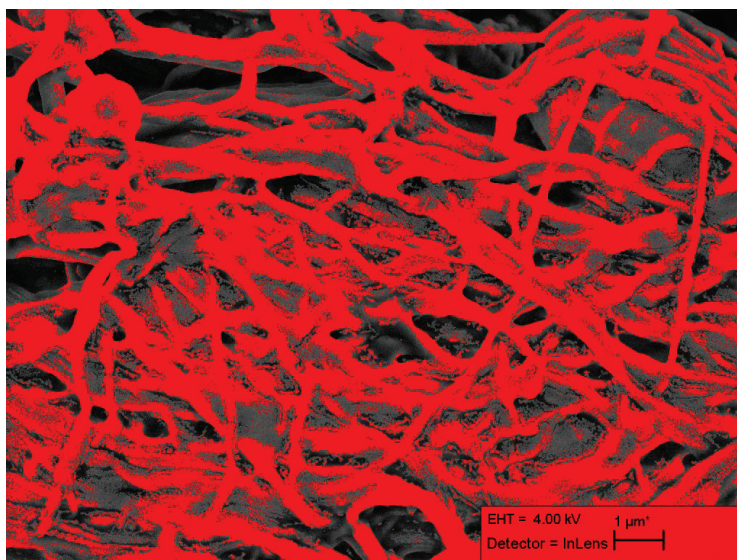


Figure 2. Image of the nanofibers to analyse their porosity, using a local thresholding method.



Figure 3. Experimental validation of the conductivity using a lab scale method (prior to adding GO).

Curriculum vitae

Personal data

Name: Kashif Javed
Date of birth: 02.04.1984
Place of birth: Punjab, Pakistan
Citizenship: Pakistan

Contact data

E-mail: kashif.javed@taltech.ee, kashif.javed@gmx.com

Education

2015–2019 PhD, Tallinn University of Technology, Chemical and Materials Technology, Estonia.
2011–2014 Master of Textile Engineering Jiangnan University, School of Textiles and Clothing, China
2003–2007 B.E. Textiles, Synthetic Fiber Development & Application Center, Karachi Pakistan,
2001–2003 HSSC (Pre-Engineering), Govt. College for Boys, Gojra, T.T.Singh, Pakistan
1999–2001 SSC (Science), Govt. Islamia High School for Boys, Gojra, T.T.Singh, Pakistan

Language competence

English	Fluent
Chinese	Fluent
Urdu	Native speaker
Punjabi	Native speaker
Arabic	Basic speaker
Estonian	Beginner

Professional employment

30.09.2007–30.04.2011	Assistant Merchandiser Franco Mfg. Inc. Co. USA Liaison Office Faisalabad Pakistan
-----------------------	---

Defended Thesis

Master Thesis “Development of flexible and electrically conductive natural fibers by graphene”, Jiangnan University, Wuxi, Jiangsu China
Supervisor: Professor Wang Chaoxia

Elulookirjeldus

Isikuandmed

Nimi: Kashif Javed

Sünniaeg: 02.04.1984

Sünnikoht: Punjab, Pakistan

Kodakondsus: Pakistani

Kontaktandmed

E-post: kashif.javed@taltech.ee, kashif.javed@gmx.com

Hariduskäik

2015–2019 PhD, Tallinna Tehnikaülikool, Keemia- ja materjalitehnoloogia, Eesti

2011–2014 MSC, Master of Textile Engineering, Jiangnan University, School of Textiles and Clothing, Hiina RV

2003–2007 BSC, Textiles, Synthetic Fiber Development & Application Center, Karachi, Pakistan

2001–2003 Keskharidus, Govt. College for Boys, Gojra, T.T.Singh, Pakistan

1999–2001 Põhiharidus, Govt. Islamia High School for Boys, Gojra, T.T.Singh, Pakistan

Keelteoskus

Inglise keel – Kõrgtase

Hiina keel – Kõrgtase

Urdu – Emakeel

Punjabi – Emakeel

Araabia – Kesktase

Eesti - Algtase

Teenistuskäik

30.09.2007–30.04.2011 Müügiassistent, Franco Mfg. Inc. Co. USA
Liaison Office Faisalabad, Pakistan

Kaitstud väitekirjad

Magistritöö "Development of flexible and electrically conductive natural fibers by graphene", Jiangnan University, Wuxi, Jiangsu, Hiina RV

Juhendaja: Professor Wang Chaoxia